Fatigue Crack Propagation and Cyclic Deformation in Ferritic Stainless Steel Single and Bicrystals(Dissertation_全文)

AUTHOR(S):

Kaneko, Yoshihisa

Fatigue Crack Propagation and Cyclic Deformation in Ferritic Stainless Steel Single and Bicrystals

Yoshihisa KANEKO

1998

Fatigue Crack Propagation and Cyclic Deformation in Ferritic Stainless Steel Single and Bicrystals

A Thesis Submitted to Kyoto University

for the requirements of
the Degree of Doctor of Engineering

By
Yoshihisa KANEKO

1998

CONTENTS

Chapter 1

Introduction

The word "fatigue" has become a widely accepted terminology in engineering vocabulary for the damage and failure of materials under cyclic loading. The fatigue fracture sometimes occurs in engineering use and can induce an unexpected accident in machinery and structure. In order to prevent the serious fatigue failure and improve the fatigue strength, it appears necessary to deepen our knowledge about the fatigue phenomena still more, although numerous studies have been performed up to the present. Fatigue of materials is a branch of research that provides a wide variety of complex processes for scientific investigation. The fatigue phenomena involve a lot of factors such as mechanics, metallugy and chemistry. Associated with these factors, the fatigue processes are developed often in several modes including creep fatigue, thermomechanical fatigue, corrosion fatigue etc. Most of failures in structural component can be attributed one of the above fatigue process. With a view to establishing a design standard against cyclic loading, many investigations have been aimed to the characterization of fatigue behavior in terms of stress amplitude – fatigue life (S–N) curves and the concept of fatigue endurance. The estimation of the fatigue strength by the S–N curve and endurance limit is probably enough in designing the engineering component. However, it should be desirable to understand the microstructural aspects of the fatigue process. The research of this kind certainly provides some insights into essential mechanism of the fatigue. Such fatigue experiments had been started in the early 20th century [1]. It was shown that slip bands developed in many grains of the polycrystalline materials broadened with the propagation of fatigue deformation and let to the formation of the cracks.

A fatal fatigue fracture results from propagation of a fatigue crack. With an evolution of fracture mechanics, many attempts were made to characterize the propagation of fatigue crack in terms of stress intensity factor. It has been established that the stress intensity factor range uniquely determines the propagation of fatigue cracks. This relationship is important in predicting the fatal fracture and still is a mainstream

even in recent research field of the fatigue crack propagation. Besides this approach based on the fracture mechanics, the mechanism of the fatigue crack growth has been examined from different points of view. The relationship between crack growth rate and striation spacing became central to the development various theories for fatigue crack growth. For the further evolution of the crack growth theories, the fatigue cracking process from initiation to final rupture has been divided into stages. Forsyth [2] showed in the fatigued aluminum that the fatigue crack propagation is composed from Stage I and Stage II. In the literature, the nucleated fatigue crack started to propagate not perpendicular to loading axis but with a certain inclination (Stage I) and subsequently propagated almost perpendicular to the loading axis (Stage II). The inclined Stage I fatigue crack has been experimentally [3] and theoretically [4] interpreted to result from shear decohesion of the developed slip band. This model for Stage I crack implies an importance of crystallographic orientation. Stage II crack is a primary propagation mode for ductile materials. Laird *et al* [5] proposed the crack blunting model for Stage II crack in fully-reversed fatigue, assuming plastic blunting and re-sharpening of crack tip. Thereafter, the alternate slip model for Stage II crack was proposed by Neumann [6,7]. This model involves the alternate slip activities of two different slip systems at crack tip. The validity of this model was examined by in-situ SEM observation of crack tip slip deformation obtained on copper [8] and Fe-Si [9] single crystals. As reviewed in above, validness of the single crystal study is widely recognized to investigate the fundamental aspects of the fatigue crack growth.

The fatigue life of materials has conventionally been estimated using the S–N curve in designing. However, because this estimation includes statistical aspect, we usually have to set a fatigue strength of material at a lower stress than that obtained in the S–N curve. This method can result in a large and heavy machinery. Hence, it is desirable to find a method that predicts the fatigue cracking before failure at a condition where the material is subjected to critical stress level. For

such an efficient designing, it is necessary to understand a detail of fatigue fracture process. However, the estimation of fatigue strength based on the S–N curve does not take account of the fatigue process including the development of dislocation structure induced by cyclic deformation. To appreciate the detail of the fatigue process, the fatigue studies have been performed in view of metallugy.

In 1950s, the concept that plastic strain amplitude is responsible for fatigue damages was established by Coffin [10]. This is the most widely used approach for the strain-based characterization of fatigue. In view of this approach, we should pay attention to dependence of the internal fatigued substructure on the plastic strain amplitude. In the past four decades, substantial progress has been made in understanding of cyclic deformation and crack initiation mechanism in fatigue owing to advance in microscopy. Thompson *et al* [11] reported the slip band where deformation is concentrated in fatigued metals persistently reappeared at the same sites during cycling even after specimen surface layer was removed. They called these surface markings "persistent slip band (PSB)". The dislocation structure of the PSB was extensively studied using transmission electron microscope for copper at several conditions and was found to consist of "ladder-like" structure [12–18]. This ladder dislocation structure consists of arrays of dislocation dipolar walls, which have 0.03–0.25μm in thickness and a spacing of about 1.3μm for the copper. The cyclic hardening property, that has studied mainly in copper single crystals oriented for single slip, is governed also by the formation of the PSBs. Cyclic hardening behavior is characterized by the plastic strain amplitude: the cyclic saturation stresses are divided into three stages depending on the plastic strain amplitude [19]. The cyclic stress-strain curve of the copper single crystals shows "plateau" domain where the saturation stress is independent of plastic strain amplitude. At the plateau domain, the PSBs are generated within the specimens. The PSBs can accommodate larger plastic strain amplitude than matrix [20]: the plastic deformation during fatigue is localized at the PSBs. Such a PSB suffering large

cyclic deformation was found to be a preferred site for fatigue crack initiation, which was examined in detail using single crystal specimens [21–23].

The fatigue fracture in smooth body must be preceded by crack initiation. In view of the accumulated knowledge about the relationship between the PSB and fatigue crack initiation, the crack initiation is preceded further by the formation of the PSB. Therefore, if we can obtain a method that detects the formation of the PSBs, the prediction of fatigue crack initiation can be achieved. This method can be useful for the efficient designing of the mechanical components. Since a shape of stress-strain curve under monotonic deformation is sensitive to internal dislocation process, one can consider that hysteresis loop shape under cyclic deformation also reflect the internal dislocation state. Dynamic behavior such as strain burst [24–29] which is peculier to fatigue should be responsible to the dislocation structure produced by cyclic deformation. Because the ladder-like dislocation structure of the PSB, dislocation process within the PSB should be significantly different from the matrix. This difference can affect to cyclic response which is evaluated with hysteresis loop shape. Mughrabi [20] showed significant changes of hysteresis loop shape during cyclic deformation of copper single crystals revealing the PSB formation. At almost the same time, Abel [30] could successfully correlate the hysteresis loop shape with the various fatigue stages of copper single crystals by measuring the Bauschinger energy parameter β_E. In Abel's model, the first PSB nucleates at local maximum of the β_E value. Similar relationship between the PSB nucleation and hysteresis loop shape has been reported in copper single crystals by other researchers [31,32]. On the basis of the relationship between the PSB nucleation and the change in hysteresis loop shape reviewed briefly in above, the detection of the local β_E maximum can be a decisive method for the prediction of fatigue crack initiation. This is because the local β_E maximum always precedes to fatigue crack initiation if the cracks are nucleated at developed PSBs. Since this

kind of loop shape change has been found in polycrystals [33–36], there is a prospect that the prediction method based on the change in the β_E value is applicable for engineering structural materials.

Usual polycrystalline materials contain a lot of grain boundaries (GBs). Due to the dislocation blockage effect of the GB, flow stress of the polycrystalline material increased with decreasing average grain size (Hall–Petch relation): the GB contribute to the strengthening of the material. However, several phenomena such as high-temperature sliding, corrosion, stress-corrosion cracking occurs locally at the GB. These phenomena certainly degrade performance of the material. Accordingly, the GB possesses the strong and week points. The GBs play complicated role also in fatigue. The propagating fatigue cracks have shown retardation at the GB [37–40]. In this sense, it can be said that the GB enhances resistance to fatigue crack growth. On the other hand, preferential fatigue cracking along the GB has been reported in fatigue [41–46]. The crack growth rate along a general boundary was significantly faster than that within a grain on αCu-Al alloy bicrystals [47]. Hence, the GB shows dual effect [48] on the fatigue cracking. Incidentally, the GB-related phenomena depends strongly on the character of the GBs [49–53]. The coherent twin boundary of f.c.c. metals and alloys has been known to possess strong resistance against such GB phenomena. This should be because the coherent twin boundary has a stable interfacial structure, which has been observed directly by the transmission electron microscope [54,55]. However under fatigue deformation, the coherent twin boundary with the stable structure has unexpectedly been a preferential site for fatigue cracking [56–58]. As reviewed in above, many factors such as GB structure, compatibility between adjoining grains, preferential chemical reaction at GB can be connected closely with the GB fatigue cracking. In order to clarify the effect of the GBs on the fatigue cracking, a well-defined experiment that cancels the many factors seems required like a bicrystal study.

Although steels which are typical engineering material contain

b.c.c. structure, abovementioned fundamental studies on fatigue have been carried out primarily on f.c.c. metals such as the copper. Hence, there still exist a lot of unknown fatigue fundamental mechanisms for the b.c.c. crystals. The b.c.c. crystals show wider variety of deformation mode than the f.c.c. metals as follows. (1) The slip lines observed at surface are wavy. (2) In monotonic tensile tests, Stage 0 in the stress-strain curve has been found in niobium [59,60] and tantalum [61] single crystals. (3) The crystal is easily deformed by mechanical twinning and fractured by cleavage along {100} plane at lower temperature [62–65]. (4) The yield stresses along {112} plane are different between tension and compression [66]. The small number of studies in b.c.c. single and bicrystals can be attributed to the following reasons. (a) Because the phase diagram of the steel contains γ-loop, austenite phase begins to precipitate in ferrite matrix or *vice-versa* during cooling in producing the single crystals by Bridgman method. (b) Melting points of the b.c.c. crystals such as tungsten and molybdenum are very high for the production by the Bridgman method.

For these reasons, we decided to produce the Fe-30%Cr single crystals (ferritic stainless steel) using Bridgman method. The melting point of the material is relatively low (about 1510°C). The present study deal with following themes using the ferritic stainless steel crystals.

(i) The orientation dependence of monotonic tensile deformation in single crystals

(ii) The orientation dependence of fatigue crack propagation in single crystals

(iii) Change in cyclic stress-strain response in single crystals at several plastic strain amplitudes.

(iv) Effect of the GBs on propagation path of fatigue crack and on the retardation of fatigue crack at the GB.

(v) Interfacial fatigue cracking at mechanical twin boundaries.

References

1. S.Suresh, *Fatigue of Materials*, Cambridge University Press, Cambridge, (1991), 2
2. P.J.E.Forsyth, *Acta Metall.*, **11** (1963), 703.
3. A.J.McEvily, Jr. and R.C.Boettner, *Acta Metall.*, **11** (1963), 725.
4. K.Tanaka and T.Mura, *Acta Metall.*, **32** (1984),1731.
5. C.Laird and G.C.Smith, *Phil.Mag.*, **7** (1962), 847.
6. P.Neumann, *Acta Metall.*, **17** (1969), 1219.
7. P.Neumann, *Acta Metall.*, **22** (1974), 1167.
8. P.Neumann, *Acta Metall.*, **22** (1974), 1155.
9. H.Vehoff and P.Neumann, *Acta Metall.*, **27** (1979), 915.
10. L.M.Coffin, *Trans.American Soc.Mech.Eng.*, **76** (1954), 931.
11. N.Thompson, N.J.Wadsworth and N.Louat, *Phil.Mag.*, **1** (1956), 113.
12. E.E.Laufer and W.N.Roberts, Phil.Mag., **14** (1966), 67.
13. H.Mughrabi, K.Hert adn F.Ackermann, *In Fatigue Mechanism*, ed.by J.T. Fong, ASTM STP 675, 69.
14. J.M.Fenney and C.Laird, *Phil.Mag.*, **31** (1975), 339.
15. L.Buchinger, S.Stanzel and C.Laird, *Phil.Mag.* A, **50** (1984), 275.
16. F.Ackermann, L.P.Kubin, J.Lepinoux and H.Mughrabi, *Acta Metall.*, **32** (1984), 715.
17. R.Wang and H.Mughrabi, *Mater.Sci.Eng.*, **63** (1984), 147.
18. Bao-Tong Ma and C.Laird, *Mater.Sci.Eng.*, **102** (1988), 247.
19. H.Mughrabi, *Mater.Sci.Eng.*, **33** (1978), 207.
20. A.T.Winter, *Phil.Mag.*, **29** (1974), 719.
21. Z.S.Basinski and S.J.Basinski, *Scripta Metall.*, **18** (1984), 851.
22. A.Hunsch and P.Neumann, *Acta Metall.*, **34** (1986), 207.
23. Bao-Tong Ma and C.Laird, *Acta Metall.*, **22** (1989), 1155.
24. P. Neumann, *Z. Metallkde.*, **59** (1968) 927.

25. R. Neumann and P. Neumann, *Scripta Metall.*, **4** (1970) 645.

26. M. P. E. Desvaux, *Z.Metallkde.*, **61** (1970), 206.

27. A. Abel, M. Wilhelm and V. Gerold, *Z. Metallkde.*, **70** (1979), 577.

28. S. I. Hong, C. Laird, *Mater. Sci. Eng.*, **A124** (1990), 183.

29. X. Hu, H. Margolin, X. Duan, S. Nourbakhsh, *Mater. Sci. Eng.*, **A157** (1992), 181.

30. A.Abel, *Mater.Sci.Eng.*, **36** (1978), 117.

31. D.E.Witmer, C.Laird and G.C.Farrington, *Acta Metall.*, **35** (1987), 1911.

32. J.Polák, J.Helesic and K.Obrtík, *Mater.Sci.Eng.*, **A101** (1988), 7.

33. J.Polák, K.Obrtlík and J.Helesic, *Mater.Sci.Eng.*, **A132** (1991), 67.

34. J.Polák, K.Obrtlík, M.Hájek and A.Vasek, *Mater.Sci.Eng.*, **A151** (1992), 19.

35. J.Polák, K.Obrtlík and M.Hájek, *Fatigue Fract.Engng.Struct.*, **17** (1994), 773.

36. A.Vinogradov, Y.Kaneko, K.Kitagawa, S.Hashimoto, V.Stolyarov and R.Z.Valiev, *Scripta Mater.*, **36** (1997), 1345.

37. J.Lankford, *Fatigue Fract.Eng.Mater.Struct.*, 8 (1985), 161.

38. C.Li and T.Bretheau, *Acta Metall.*, **37** (1989), 2645.

39. C.Li, *Metall.Trans.*, **23A** (1992), 3293.

40. Q.Chen and H.W.Liu, *Scripta Metall.*, **28** (1993), 849.

41. L.C.Lim, *Acta Metall.*, **35** (1987), 1653.

42. H.Vehoff, C.Laird and D.J.Duquette, *Acta Metall.*, **35** (1987), 2877.

43. S.Chikwembani and J.Weerman, *Scripta Metall.*, **19** (1985), 1499.

44. S.Chikwembani and J.Weerman, *Metall.Trans*, **20A** (1989), 1221.

45. R.Lombard, H.Vehoff and P.Neumann, *Z.Metallkd,* **78** (1992), 463.

46. A. Vinogradov, T.Mimaki and S.Hashimoto, *Mater.Sci.Eng.*, **A216** (1996), 30.

47. S.Hashimoto, Y.Aoki, Z.Y.Wang and S.Miura, *J.Jpn.Inst.Metal,*

57, (1993), 972.

48. A. Vinogradov, S.Hashimoto and S.Miura, *Scripta Metall.*, **32** (1995), 427.
49. T.Watanabe, M.Yamada, S.Shima and S.Karashima, *Phil.Mag.A*, **40** (1979), 667.
50. G.Hasson, J.-Y.Boos, I.Herbeuval, M.Biscondi and C.Goux, *Surf.Sci.*, **31**(1972), 115.
51. M.Yamashita, T.Mimaki, S.Hashimoto and S.Miura, *Phil.Mag.A*, **63**(1991), 695.
52. M.Yamashita, T.Mimaki, S.Hashimoto and S.Miura, *Phil.Mag.A*, **63**(1991), 707.
53. J.A.Kargol and D.L.Albright, *Metall.Trans.A*, **8** (1977), 27.
54. H.Ichinose and Y.Ishida, *Phil.Mag.*, **43** (1981), 1253.
55. K.L.Merkle, *Interface Science*, **2** (1995), 311.
56. R.C.Boettner, A.J.McEvily, Jr. and Y.C.Liu, *Phil.Mag.*, **10** (1964), 95.
57. A.W.Thompson, *Acta Metall.*, **20**(1972), 1085.
58. A.Heinz and P.Neumann, *Acta Metal.Mater.*, **38**(1990), 1933.
59. T.E.Michell, R.A.Foxall and P.B.Hirsh, *Phil.Mag.*, **8** (1963), 1895.
60. G.Taylor and J.W.Christial, *Phil.Mag.*, **15** (1967), 873.
61. T.E.Michell and W.A.Spitzig, *Acta Metall.*, **13** (1965), 1169.
62. D.Hull, *Acta Metall.*, **8** (1960), 11.
63. P.Beardmore and D.Hull, *J.Less-Comm.Metals*, **9** (1965), 168.
64. R.M.Rose, D.P.Ferris and J.Wulff, *Trans.Metall.Soc.AIME*, **224** (1962), 981.
65. R.Priestner and N.Louat, *Acta Metall.*, 11 (1963), 195.
66. S.Takeuchi, E.Furubayashi, T.Taoka, *Acta Metall.*, **15** (1967), 1179.

Chapter II

Orientation Dependence of Fatigue Crack Propagation and Tensile Deformation

2.1 INTRODUCTION

Propagation processes of intragranular fatigue crack along crystallographic planes have been classified essentially into two kinds [1]. One involves the alternate slip activities of two different slip systems around the crack tip. The other kind is grown in a manner of the shear decohesion along a slip plane. Both kinds of the cracking processes have been examined favorably in the single crystal specimens. Fatigue crack growth of typical alternate slip type has been studied in copper [2,3], Fe-Si alloy [4,5] and Fe-Ni-Cr alloy [6] single crystals. On the other hand, the shear decohesion has been found in crack propagation of αCu-Al alloy single crystals [7] and in an initial short crack nucleated at persistent slip band (PSB) of copper single crystals [8-10]. Resistance to fatigue crack growth should be connected closely with these crack growth mechanism.

It is revealed in Ref.2 that cracking morphology of the alternate slip type is very sensitive to the loading axis since symmetrical operation of two slip systems are required for the propagation of this kind. Moreover, geometry of slip systems is associated with fracture surface morphology of the shear decohesion cracking [7]. In view of these facts, it is likely that the process of fatigue crack propagation is determined partly by the loading axis which affects the operative slip systems around crack tip. In addition to the orientation of the loading axis, geometry of the fatigue crack is characterized by a crystallographic orientation of crack growth direction: we should take account of both the loading axis and growth direction in estimating the orientation dependence of fatigue crack propagation.

The deformation of b.c.c. metals, which we employed in the present study, is considerably complicated than that of f.c.c. metals. The b.c.c. crystals often show a wide variety of deformation and fracture behavior such as wavy slip, mechanical twinning and cleavage fracture. In particular, the difference in the slip system from the f.c.c. metals —— where the abovementioned mechanisms of fatigue crack growth

were investigated primary —— can complicate the understanding of the crack growth process in the b.c.c. metals. For these reasons, it appears desirable to investigate the orientation dependence of both the monotonic deformation mode and the fatigue crack growth. These simultaneous systematic study of orientation dependence can provide some insights into the nature of the fatigue crack growth.

In the present study, the orientation dependence of monotonic deformation and fatigue crack propagation have been investigated in the Fe-30%Cr alloy single crystals. We paid our attention to different orientation dependence of strength between monotonic deformation and fatigue crack propagation. Resistance to fatigue crack propagation was discussed in terms of the geometrical relationship between operative primary slip and broad surface of the specimen.

2.2 EXPERIMENTAL PROCEDURE

Single crystals were grown by the Bridgman method in an argon gas atmosphere from a material of an Fe-30%Cr alloy. Chemical composition of the material used is presented in Table 2-1. Sheet specimens and compact tension (CT) specimens were cut from the single crystals by a spark cutter as illustrated in Fig.2-1. A polycrystalline CT specimen with an average grain diameter of 0.5mm was also prepared. A chevron type notch was introduced to the CT specimens to achieve a crack initiation at lower cyclic load. A broad surface direction (x-axis) on both sheet and CT single crystal specimens was fixed to be [1 1 0]. Tensile direction (z-axis) of the specimens was oriented to be from [0 0 1] to [1 $\bar{1}$ 0] via [1 $\bar{1}$ 1]. The orientations of the specimens will be indicated by an angle ϕ between [0 0 1] to the loading direction in the present thesis. The broad surfaces of the specimens were mechanically and electrolytically polished to obtain mirror-like surface. In order to measure a crack length of the CT specimens, scratch marks parallel to the loading direction were introduced on both surfaces at an interval of 0.1mm.

To obtain fundamental aspects of orientation-dependent deformation of the Fe-30%Cr alloy single crystals, the monotonic tensile tests on the sheet specimens were performed in air at room temperature using an Instron-type testing machine. Thereafter, fatigue crack propagation tests were carried out on the CT specimens in a servo-hydraulic machine. A triangular load wave was applied to the CT specimens at a frequency of 1Hz. Load amplitude was gradually raised from the beginning of the experiments at a constant load ratio of 0.1 ($= P_{min} / P_{max}$). After a nucleation of a fatigue crack was detected, a further experiment was continued at the constant load amplitude. During the fatigue experiments, the crack lengths of both top and reverse surfaces were measured with optical microscopes.

Resistance to fatigue crack growth of materials is estimated usually by the relationship between crack growth rate and stress intensity

factor range. However, the stress intensity factor may not give accurate stress field around crack tip for an elastically anisotropic material such as the present Fe-30%Cr crystal, because an elastically isotropic material is assumed for the stress intensity factor. For this reason, we used "energy release rate" in order to estimate the resistance to fatigue crack growth instead of the stress intensity factor. The energy release rate g is calculated from "compliance method" which is given by Eq.2-1.

$$g = \frac{P^2}{2b}\frac{d\lambda}{dl} \qquad (2\text{-}1)$$

where P is the applied load, b is the specimen thickness, l is the crack length and λ is the compliance ($\lambda = u/P$; u is the opening displacement at loading point of the CT specimen). To calculate the λ value, the displacement u was measured with an MTS clip-on gauge. According to the theory of the liner fracture mechanics, the energy release rate is proportional to a square of the stress intensity factor. Thus, the relationship between crack growth rate dl/dN and energy release rate range Δg ($=g_{max}-g_{min}$) can provide crack growth property of materials.

Table 2-1 Chemical composition of the material used (wt.%)

C	Si	Mn	P	S	Cu
0.0028	0.010	<0.005	0.0005	0.0019	<0.001
Ni	Cr	Al	O	N	Fe
<0.001	30.09	<0.001	0.0004	0.0158	bal.

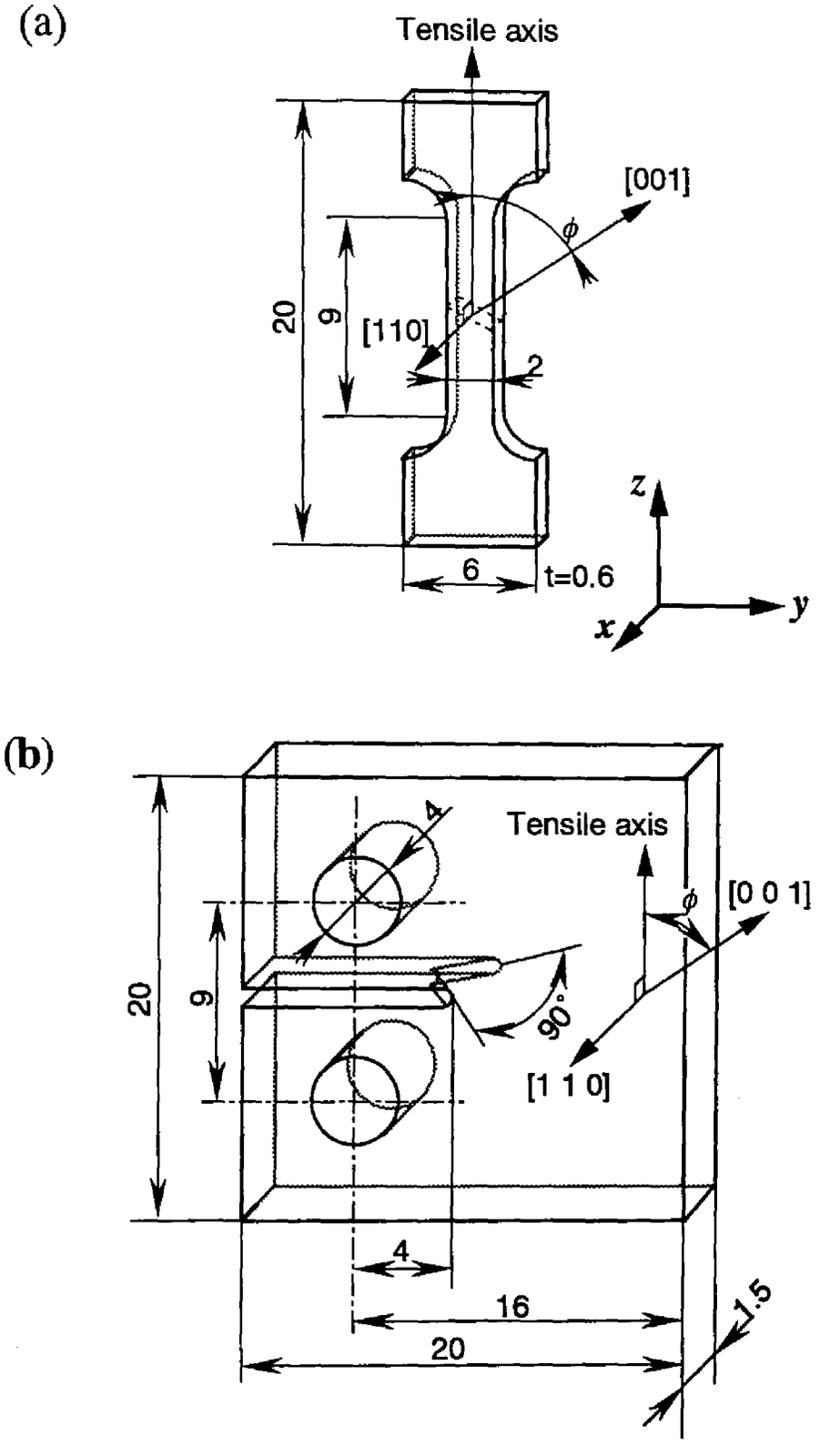

Fig.2-1 Schematic illustration of (a) strip specimen and (b) CT specimen of Fe-30%Cr alloy single crystals.

2.3 RESULTS

2.3.1 *Orientation dependence of deformation and fracture behavior in monotonic tensile straining*

Typical stress-strain curves of the sheet specimens are presented in Fig.2-2. The present specimens showed wide varieties of deformation and fracture behavior at room temperature. All the specimens having [0 0 1] tensile axis were fractured by cleavage at room temperature (293K) although the cleavage fracture did not occur at 323K. This kind of the cleavage fractures in b.c.c. single crystals have been found in the tungsten at room temperature [11], the iron [12] and the Fe-Si alloy [13-15] at 77K. The cleavage fracture observed at the room temperature should be related to lower mobility of dislocations because a ductile-brittle transition temperature of high-chromium ferritic stainless steel has been reported to exist around a room temperature [16]. The disappearance of cleavage fracture at 323K (Fig.2-2) can be understood from the increase in the dislocation mobility. Strain hardening rates depended strongly on the tensile axis as seen in the figure. The specimen having [1 $\bar{1}$ 1] tensile axis deformed at the highest hardening rate. In contrast, little hardening was observed at [2 $\bar{2}$ 1] tensile axis. The specimens having [1 $\bar{1}$ 2] or [1 $\bar{1}$ 0] axis showed intermediate hardening rates. Stress drops due to mechanical twinning were sometimes accompanied by the monotonic deformations (for example, the [1 $\bar{1}$ 2] tensile axis in Fig.2-2). Typical morphologies of the fractured specimens under tensile deformation are shown in Fig.2-3. Fracture modes were divided roughly into cleavage fracture ([0 0 1] axis in the figure) and ductile fracture. For the latter case, the fracture morphologies could be classified into two kinds. One is "chisel edge" fracture occurring in between [1 $\bar{1}$ 1] and [1 $\bar{1}$ 0] (the [2 $\bar{2}$ 1] tensile axes in the figure). The other kind is observed in the tensile axes from [1 $\bar{1}$ 3] to [1 $\bar{1}$ 1], resulting in relatively flat fracture surface.

Figure 2-4 shows orientation dependence of yield stress and

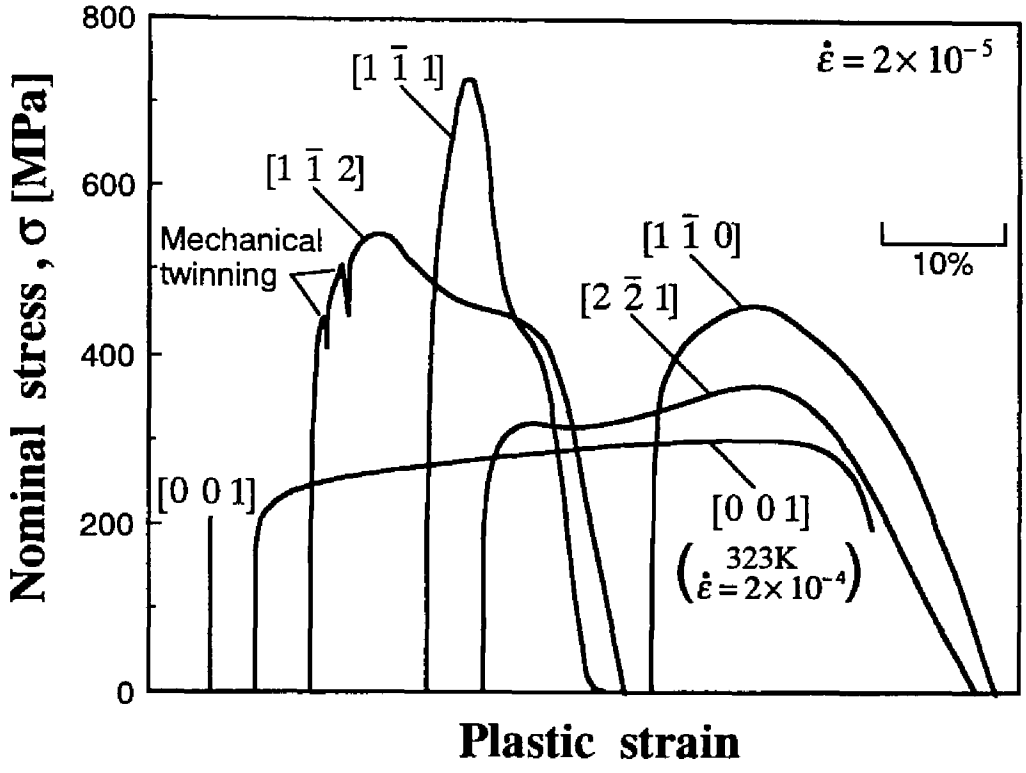

Fig.2-2 Stress-strain curves of Fe-30%Cr alloy single crystals at room temperature at room temparature under an initial strain rate of 2 $\times 10^{-5}s^{-1}$. The specimen having [0 0 1] tensile axis was cleaved along the (0 0 1) plane in spite of the ductile fracture at 323K. Stress drops due to mechanical twinning are seen in the specimen having [1 $\bar{1}$ 2] tensile axis.

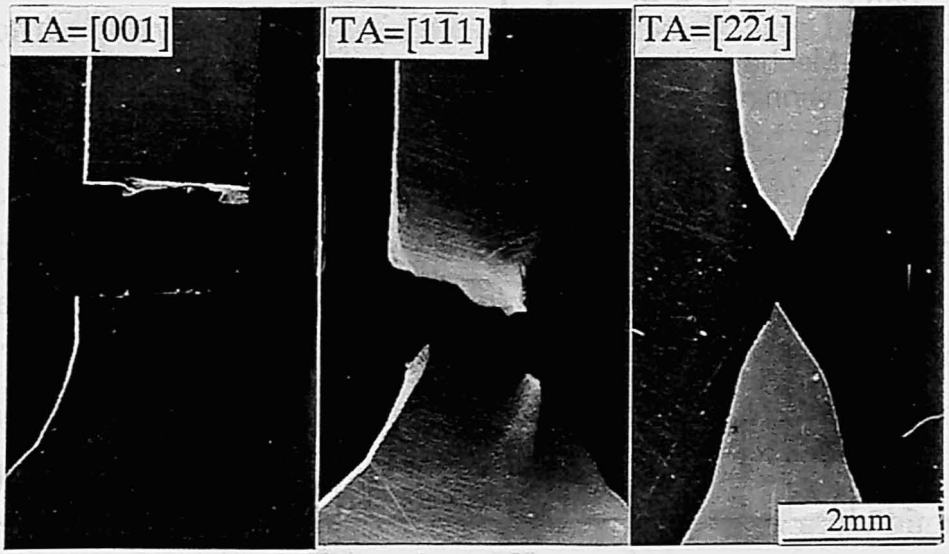

Fig.2-3 Typical fracture morphologies on the monotonic tensile tests.

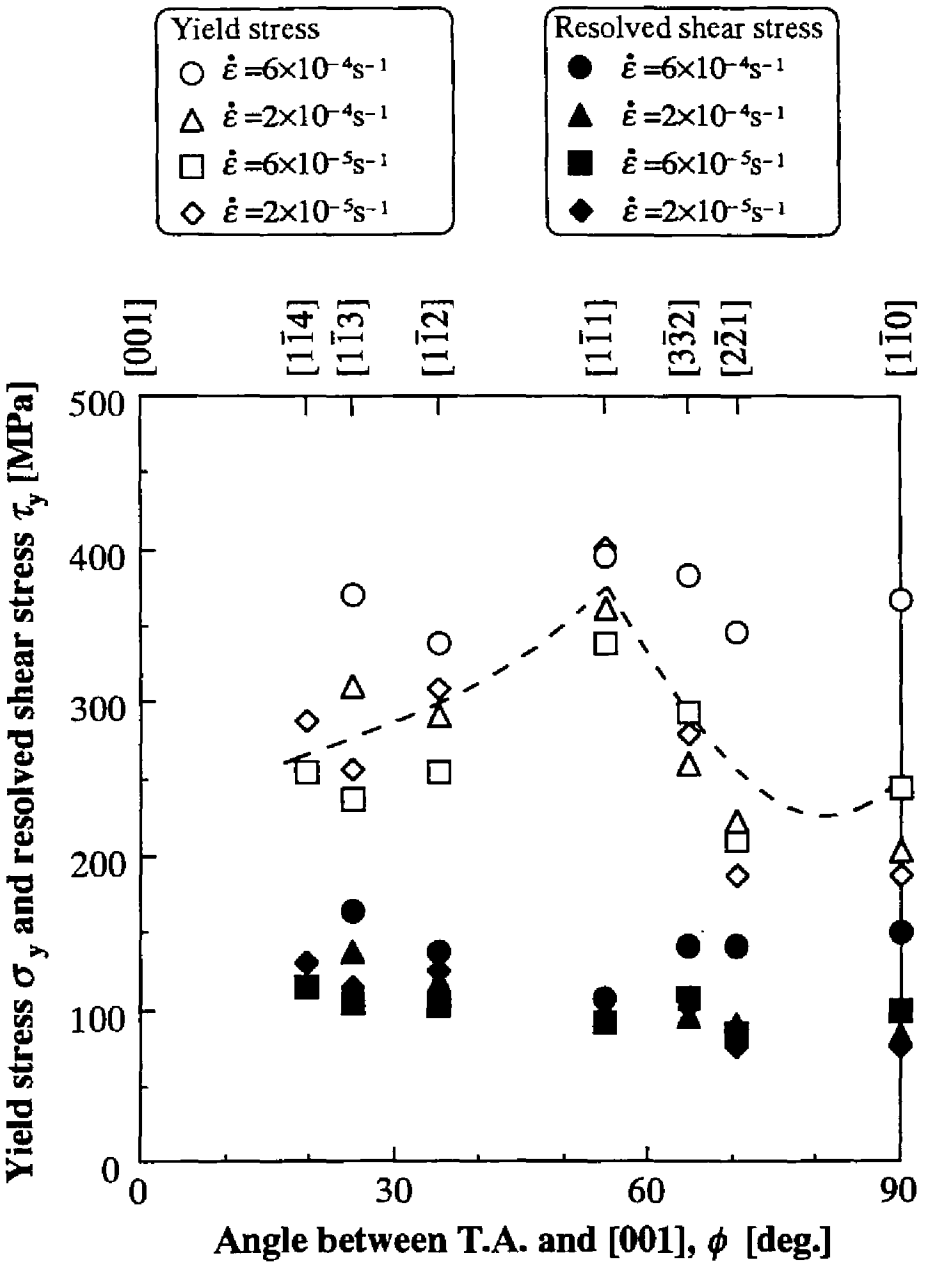

Fig.2-4 Orientation dependences of yield stress and critical resolved shear stress (CRSS) in the strip specimens. The CRSSs at individual strain rates were almost independent of the tensile axis.

critical resolved shear stress (CRSS). Some specimens such as [1 $\bar{1}$ 1] tensile axis in Fig.2-2 showed smooth transition from elastic to plastic deformation in the stress-stain curve: an initial strain hardening rate is very high. In such specimens, it is difficult to specify a yield point from the stress-strain curves. Hence, a stress where appearances of slip lines were observed by the optical microscope is adopted as a yield stress. The yield stresses at [0 0 1] tensile axis were not plotted because the cleavage fractures occurred prior to the plastic deformation. The highest yield stress was attained at the [1 $\bar{1}$ 1] tensile axis at each strain rate tested. The CRSSs were calculated by multiplying the yield stress by the maximum Schmid factor among $\{1\ 1\ 0\}<1\ 1\ 1>$ slip systems, whereas slip deformation in b.c.c. metals and alloys often occurs along several planes containing {1 1 0} and {1 1 2}. This is because the specification of the operated slip system was difficult by means of the broad surface observation if a slip step did not appear at the broad surface. The calculated CRSSs were almost independent of the tensile axis at each strain rate. Hence, it can be said that the Schmid's law is almost applicable for the present specimens.

Orientation dependence of ultimate tensile strength is shown in Fig.2-5. The specimens having the [1 $\bar{1}$ 1] tensile axis also possessed the highest ultimate strength. This is associated with the rapid strain hardening of the [1 $\bar{1}$ 1] tensile axis (Fig.2-2). To indicate the orientation dependence of the mechanical twinning and the cleavage fracture, these are also plotted in the figure.

The cleavage fractures often occurred along (0 0 1) plane at the tensile axes ϕ ranged from 0° to 30°. The orientation- and temperature-dependences of cleavage fracture have been investigated in detail on the iron single crystals [12], where the specimens became easy to be cleaved as the tensile axis was oriented to $<0\ 0\ 1>$ and as the testing temperature decreased. Same orientation dependence of cleavage fracture was also reported in the tungsten [11] and Fe-Si alloy [15] single crystals. This tendency has been understood in terms of the normal stress resolved on {1 0 0} cleavage plane [15]. The present

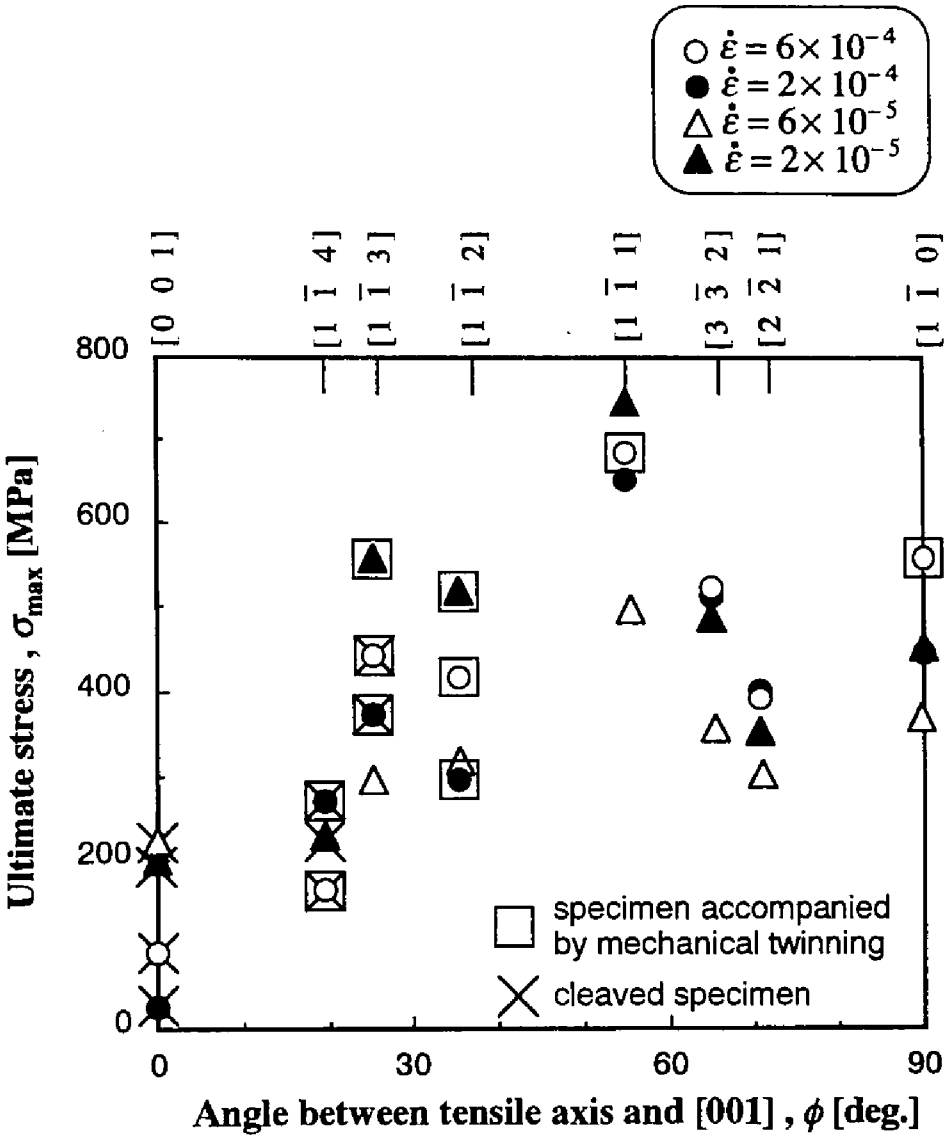

Fig.2-5 Orientation and strain rate dependences of ultimate strength of Fe-30%Cr alloy single crystals. The specimens accompanied by mechanical twinning during deformation are indicated by an open square and those fractured by cleavage are indicated by a cross.

orientation dependence of cleavage fracture agrees well with these results.

The generations of mechanical twins and the resultant stress drops were frequently observed during deformation (the twinned specimens are marked by an open square in Fig.2-5). The occurrence of the mechanical twinning was confirmed by a formation of twin bands having a certain thickness. The mechanical twinning occurred in the early stages of deformation on some specimens having tensile axis from [0 0 1] to [1 $\bar{1}$ 1], and in one specimen of [1 $\bar{1}$ 0] axis. The twinning stresses were of 150 ~ 500 MPa, and these values agreed with the results of a ferritic stainless steel polycrystal [17].

Figure 2-6 are optical micrographs showing the aspects of the broad surface after tensile deformation. The twin bands are seen around the fracture surface of the [0 0 1] and [1 $\bar{1}$ 4] specimens. The specimen having tensile axis from [1 $\bar{1}$ 3] to [1 $\bar{1}$ 1] showed the wavy slip lines, which are characteristic of the deformation of b.c.c. metals. The wavy slip lines appeared along some crystallographic planes such as {1 1 0} and {1 3 4} containing <1 1 1> slip direction. On the other hand, liner slip lines were detected in the specimens having tensile axis from [1 $\bar{1}$ 1] to [1 $\bar{1}$ 0]. Observed from the broad surface, these slip lines were very faint. The specimen having [1 $\bar{1}$ 1] tensile axes showed both of the wavy and liner slip lines. At the specimens showing the liner slip lines, the glide along a primary slip plane does not produce slip steps on the broad surface because the primary slip vector lies parallel to the broad surface. The liner slip lines observed certainly should be due to a slight deviation of the surface plane from (1 1 0).

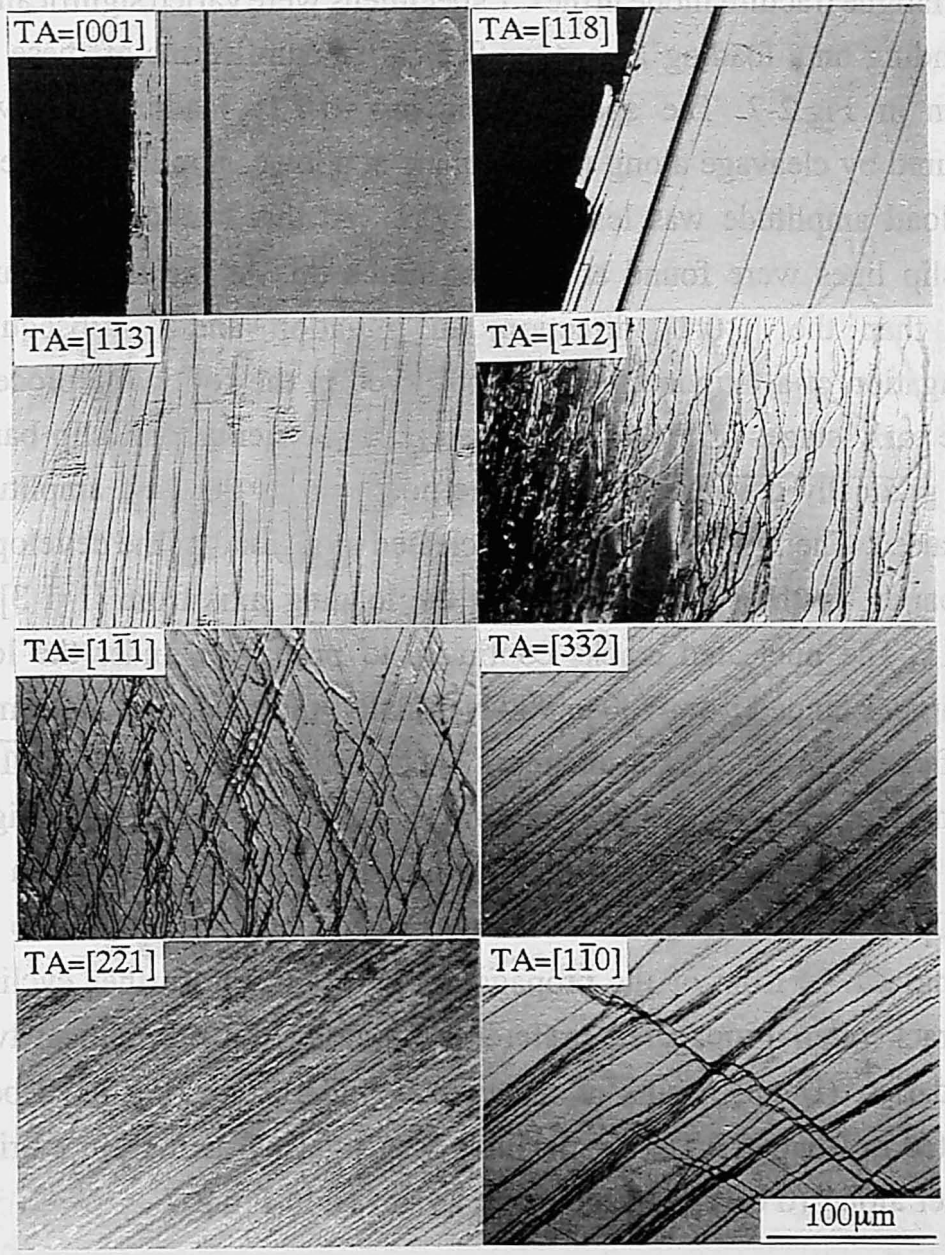

Fig.2-6 Optical photographs showing specimen surfaces after the tensile tests. Wavy slip lines of [111] or [11$\bar{1}$] slip vector were observed at the tensile axes from [1$\bar{1}$3] to [1$\bar{1}$1]. On the other hand, linear slip lines of [$\bar{1}$11] slip vector are could be seen at the tensile axes from [1$\bar{1}$1] to [1$\bar{1}$0]. Double slip of the [$\bar{1}$11] and [1$\bar{1}$1] vectors occured at the [1$\bar{1}$0] tensile axis. The [1$\bar{1}$1] tensile axis showed both of the wavy and the linear slips.

2.3.2 *Basic classification of fracture mode in CT specimens*

A fatigue fracture mode in the CT specimens were varied significantly depending on a loading axis, too. Typical fracture forms of these are shown in Fig.2-7. The specimen having [0 0 1] loading axis was fractured by cleavage along (0 0 1) plane at a lower applied load level (the load amplitude was less than 200N). At this cyclic loading, no any slip lines were found around the notch tip. At the loading axes other than the [0 0 1] direction, an initiation and a subsequent propagation of a fatigue crack was observed in the following process. In the early stages of the fatigue tests on these orientations, slip bands were gradually developed around the notch tip as the load amplitude was raised. The fatigue crack was nucleated along one of the developed slip bands. In the specimens having the loading axis from [1 $\bar{1}$ 3] to [2 $\bar{2}$ 1], The nucleated cracks continued to propagate under the load amplitudes ranged from 700 to 900 N. Finally, the specimens deformed significantly in the ductile manner. The specimen having the [1 $\bar{1}$ 0] loading axis required a higher load amplitude of 1060N for the fatigue crack initiation and propagation. During the crack propagation in the [1 $\bar{1}$ 0] specimen, the mechanical twins were generated parallel to the loading axis in front of the propagating crack. In the further cycling, the crack often propagated preferentially along the mechanical twin boundaries. (Detail results of the twin boundary cracking have been reported in Chapter VI) The specimen was finally fractured in a brittle manner along (0 0 1) cleavage plane as shown in Fig.2-7.

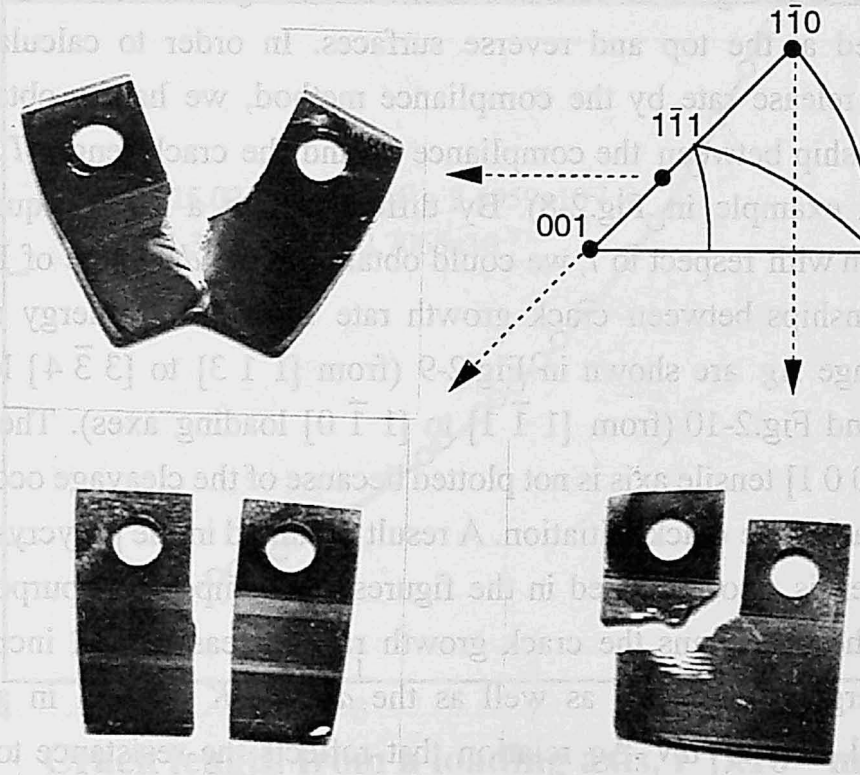

Fig.2-7 Fracture morphlogies of the CT specimens after the crack propagation tests. The specimen having [0 0 1] loading axis was fractured by cleavage without fatigue crack propagation.

2.3.3 *Fatigue crack propagation*

The propagating fatigue cracks observed at specimen surface were usually inclined to the notch direction (x-axis) at certain angles. In the present study, a projected crack length to the x-axis is taken as the crack length l. For the calculation of the energy release rate range Δg and the crack growth rate dl/dN, we averaged the crack lengths observed at the top and reverse surfaces. In order to calculate the energy release rate by the compliance method, we had to obtain the relationship between the compliance λ and the crack length l at first (see an example in Fig.2-8). By differentiating a fitted biquadratic equation with respect to l, we could obtain the $dl/d\lambda$ value of Eq.2-2. Relationships between crack growth rate dl/dN and energy release rate range Δg are shown in Fig.2-9 (from [1 $\bar{1}$ 3] to [3 $\bar{3}$ 4] loading axes) and Fig.2-10 (from [1 $\bar{1}$ 1] to [1 $\bar{1}$ 0] loading axes). The result of the [0 0 1] tensile axis is not plotted because of the cleavage occurring before a fatigue crack initiation. A result obtained in the polycrystalline specimen is also indicated in the figures for comparative purpose. At all of the specimens the crack growth rate increased with increasing the energy release rate as well as the dl/dN-ΔK relation in a usual material. The dl/dN-Δg relation that reflects the resistance to crack growth seemed to depend on the loading axis. In order to estimate the orientation dependence of the resistance to crack growth, we measured the energy release rate range at the dl/dN of 5×10^{-8} m/cycle. Same procedure for comparing the crack growth behavior has been employed in Refs.4 and 6. Figure 2-11 shows the orientation dependence of the energy release rate range at $da/dN = 5\times10^{-8}$ m/cycle. Apparent tendency of the energy release rates can be seen in the figure: the resistance to fatigue crack growth increased as the tensile axes were oriented from [0 0 1] to [1 $\bar{1}$ 0] direction.

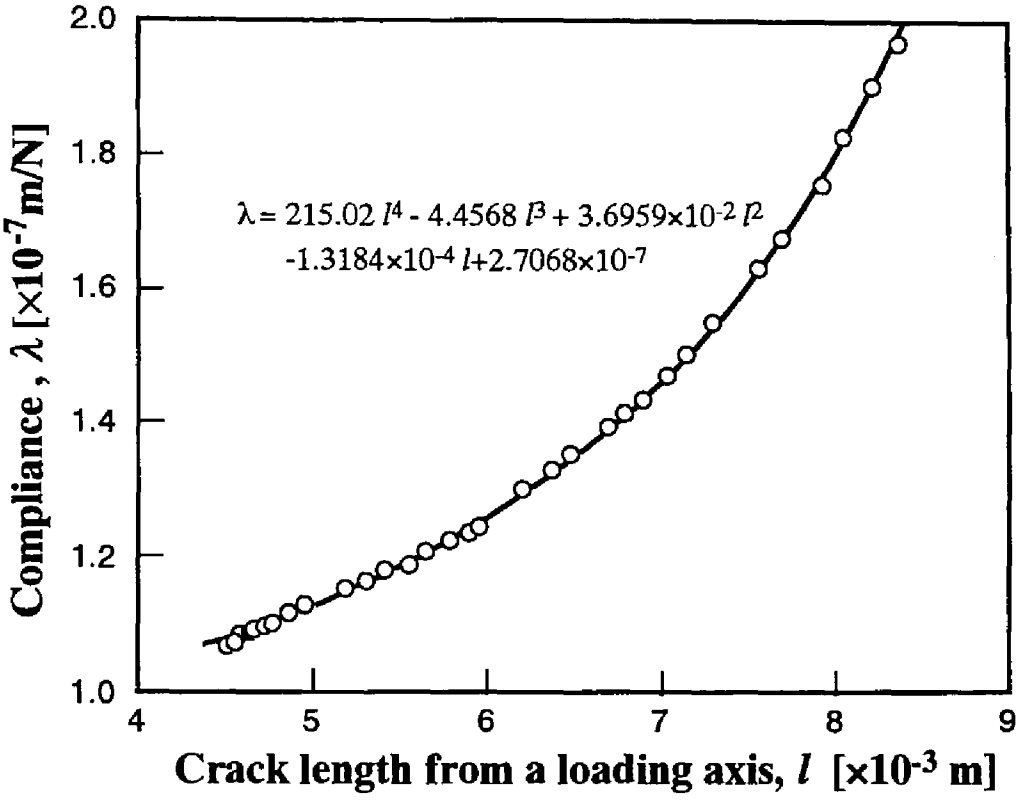

Fig.2-8 A typical relationship between compliance and crack length of a single crystal specimen having [1 $\bar{1}$ 1] tensile axis. The relationship which is curve-fitted by a biquadratic equation indicated.

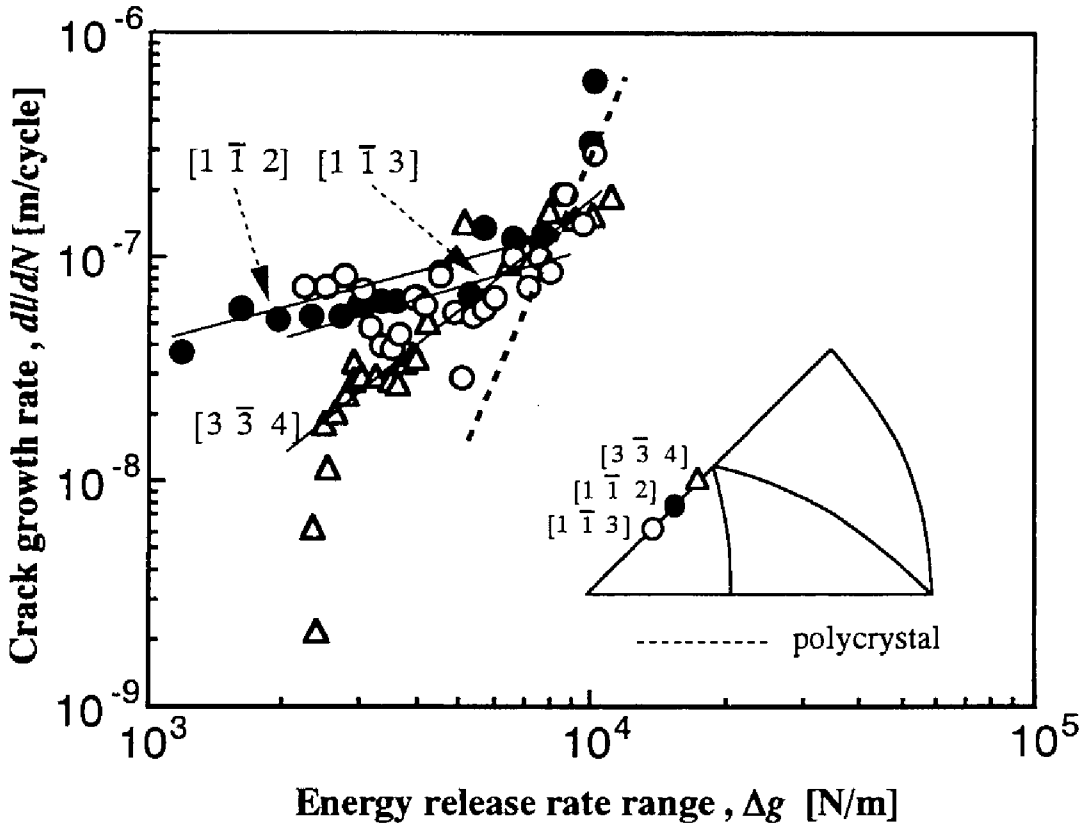

Fig.2-9 Relationship between crack growth rate and energy release rate range in Fe-30%Cr alloy single crystals having [1 $\bar{1}$ 3], [1 $\bar{1}$ 2] and [3 $\bar{3}$ 4] loading axes.

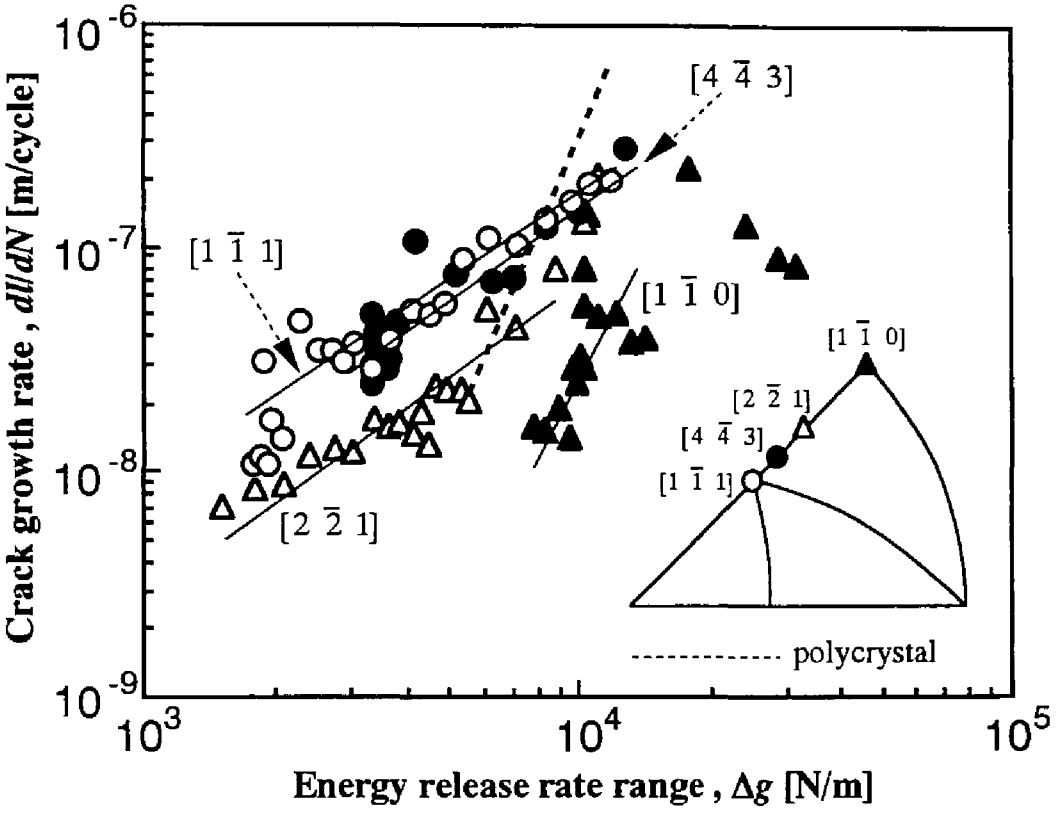

Fig.2-10 Relationship between crack growth rate and energy release rate range in Fe-30%Cr alloy single crystals having [1 $\bar{1}$ 1], [4 $\bar{4}$ 3], [2 $\bar{2}$ 1] and [1 $\bar{1}$ 0] loading axes.

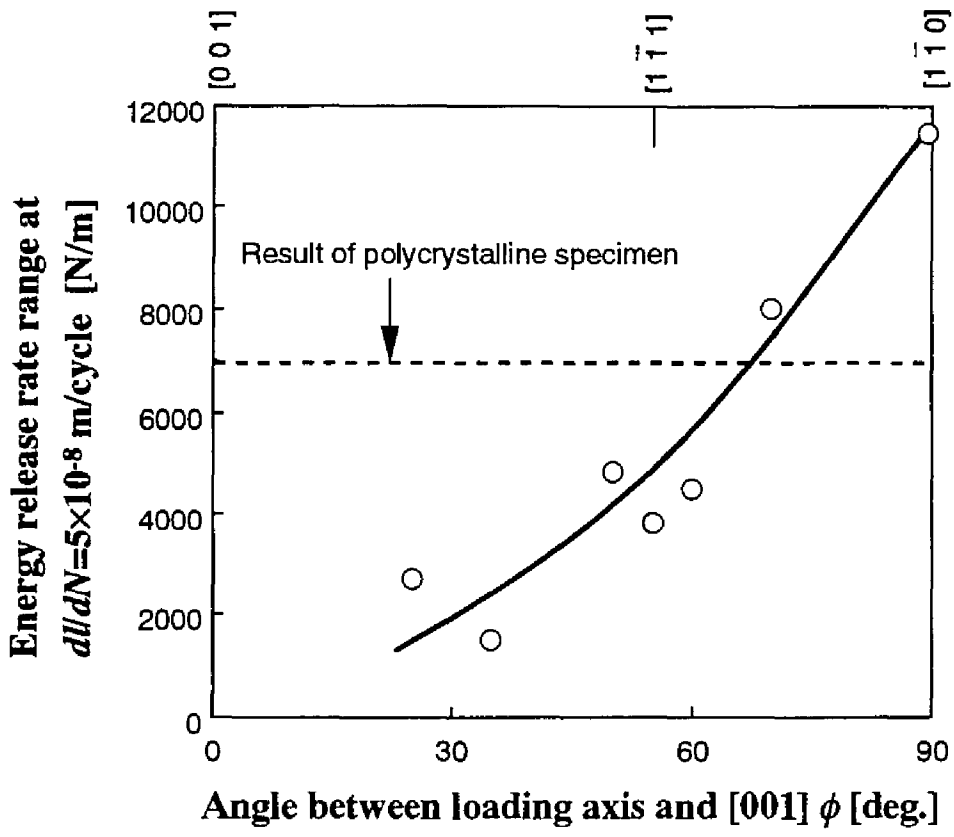

Fig.2-11 Relationship between resistance of fatigue crack growth and loading axes of specimens. The resistance of fatigue crack propagation is estimated by the energy release rate range at the crack growth rate of 5×10^{-8} m/cycle.

2.3.4 *Classification of fatigue crack morphologies*

From the surface observation with the optical microscope, the morphologies of the fatigue cracks could be classified into two kinds. Figure 2-12 shows both kinds of the fatigue crack morphologies. In this paper, we define them as Type A and Type B cracking, respectively. We could discriminate these two kinds from slip lines developed around the crack tips. Type A cracking had the slip lines developed asymmetrically at one side of the cracking plane. The individual slip lines were wavy, which is frequently observed in deformed b.c.c. metals. On the other hand, no developed plastic zone was observed at Type B cracking. In front of the crack tip, one can notice the presence of a straight slip band which is parallel to the crack plane.

Both kinds of the cracks propagated not along a normal plane to loading axis but along certain crystallographic planes that are inclined to notch direction (x-axis). Irrespective of the crack type, their fatigue surfaces had the following crystallographic aspect. The fatigue surfaces contained one of $<1\ 1\ 1>$ directions ——which are slip directions of usual b.c.c. metals and alloys —— from the analyses of the fracture surfaces at least in the region near the broad surfaces.

Figure 2-13 shows fractographic features of Type A and Type B cracking, indicating the apparent difference in the morphology of the fatigue surfaces. It is seen in photograph that the fracture surface of Type A cracking shows the traces extending uniformly to the [1 1 1] direction. The fatigue surfaces of Type A cracks were filled with one of [1 1 1] or [1 1 $\bar{1}$] traces. (At another fatigue surface of Type A cracking, the traces parallel to [1 1 $\bar{1}$] direction, which is crystallographically equivalent to the [1 1 1], were also observed.) On the other hand, many traces arranging parallel to the broad surface are visible on the fatigue surface of Type B cracking. In addition to such parallel traces, we can see several striations that are perpendicular to broad surface.

Cracking paths in some specimens were frequently changed into

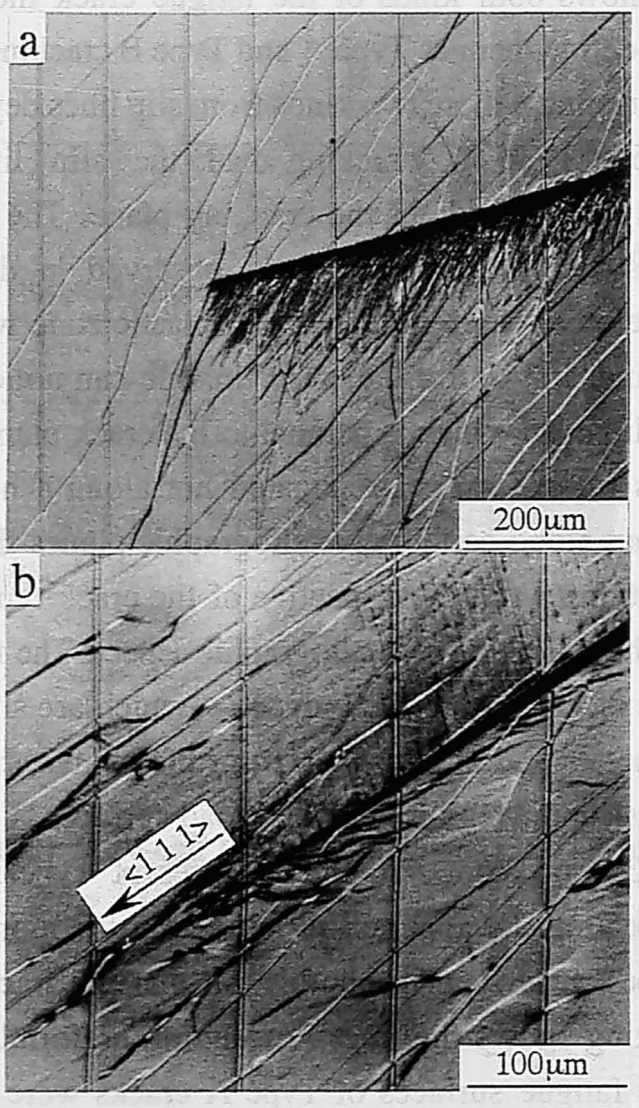

Fig.2-12 Cracking forms observed on the specimen surfaces.One has (a) wavy slip bands developed asymmetrically (Type A cracking), the other has (b) a straight slip band parallel to the cracking plane (Type B cracking). Scratch marks from the top to the bottom whose interval is 100 μm can be seen in the figure.

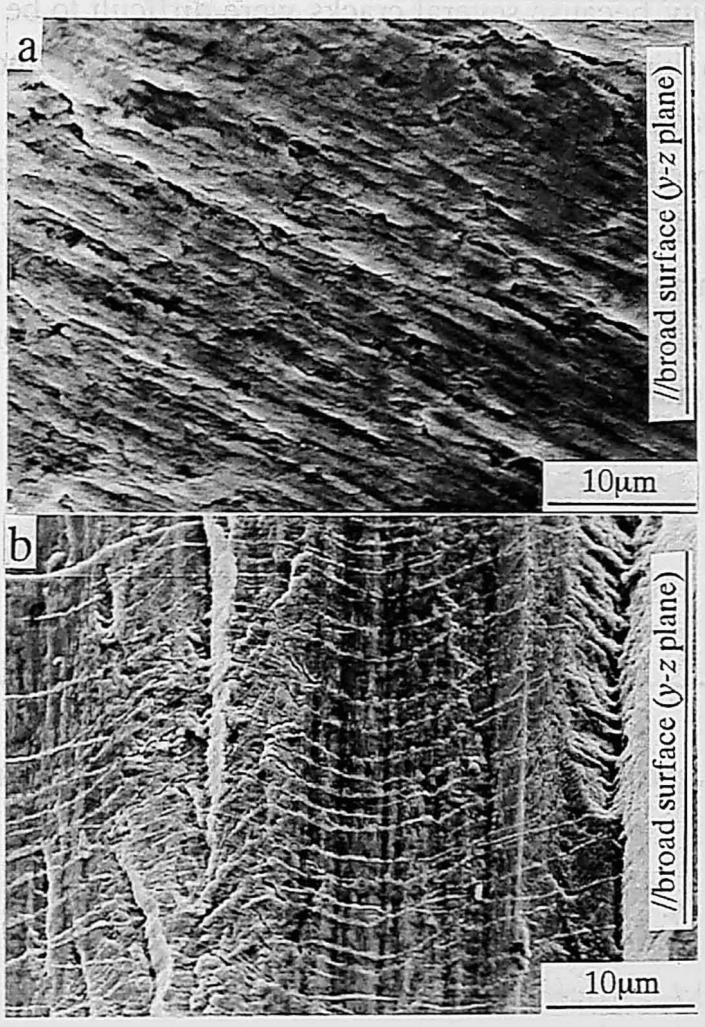

Fig.2-13 SEM photographs showing fractographic features of (a) Type A and (b) Type B crackings.

another crystallographic plane during propagation. At such a corner of the crack path, the cracking type sometimes changed into the other one. Thus, the primary cracks consisted of one or both cracking kinds. Predominant cracking kind was sensitive to the loading axis. Figure 2-14 shows the orientation dependence of the fraction of the both cracking kinds. (It is noted that a sum of the two types is not always unity because several cracks were difficult to be classified into these two kinds.) At the loading axes of [1 $\bar{1}$ 3] and [1 $\bar{1}$ 2], the fatigue cracks propagated in the manner of Type A. On the other hand, Type B cracking was predominant at the loading axes from [1 $\bar{1}$ 1] to [1 $\bar{1}$ 0]. It can be said that the fraction of Type B cracking tends to increase as the loading axis is oriented from [0 0 1] to [1 $\bar{1}$ 0] direction. This orientation dependence is similar to that of the resistance to fatigue crack growth.

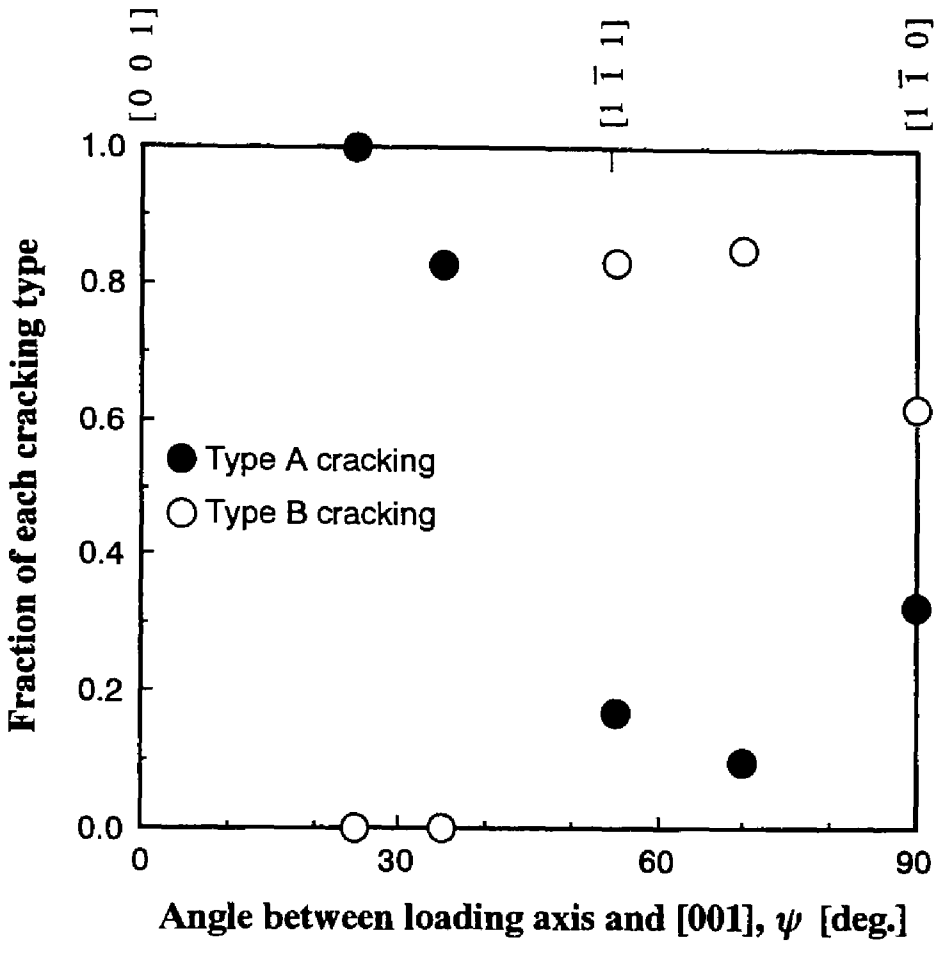

Fig.2-14 Fractions of Type A and Type B crackings occupied in primary cracks. Type A cracking was predominant in the loading axes from [0 0 1] to [1 $\bar{1}$ 1]. In contrast, Type B cracking became predominant in the loading axes from [1 $\bar{1}$ 1] to [1 $\bar{1}$ 0].

4. DISCUSSION

2.4.1 *Morphology of fatigue cracking*

The nature of fatigue cracking along crystallographic planes has been classified into two kinds. One is the decohesion along the slip planes [7–10], and the other is resulted from the alternate slip activities at the crack tip [2] as referred in Section 2.1. For both kinds, the geometry of the fatigue surface is related closely to the operated slip systems. The fatigue crack growth of the slip-plane decohesion must be accompanied by the development of the crack-tip slip band which is common to the cracking plane. In order to produce such a slip band, the slip-plane decohesion model should involve a process of dislocation emission from the crack tip [18,19]. (The dislocation emission of this kind has actually been recognized by the in-situ TEM observation [20].) Hence, the shear-decohesion crack has a crystallographic feature that the resultant cracking plane is parallel to the Burgers vector of the dislocations which are dominantly contained in the slip band. The inclined cracking plane against a loading axis is produced in the shear-decohesion cracking. On the other hand, the alternate slip model gives rise to the cracking plane which is almost perpendicular to the loading axis. In view of the experimental fact that the cracking planes were inclined against the loading axes and contained one of the <1 1 1> directions, the shear decohesion is a plausible cracking mode in the present study. Since the fatigue surface of Type A cracking contained the [1 1 1] or [1 1 $\bar{1}$] direction, the a/2[1 1 1] or a/2[1 1 $\bar{1}$] dislocations contribute to Type A cracking. The activity of a/2[1 $\bar{1}$ $\bar{1}$] dislocations can be applicable for Type B cracking for the same reason.

Now we consider the topography of the fatigue surfaces. A deforming b.c.c. crystal glides to <1 1 1> direction frequently along several slip planes: the cross slips occur along "pencil glide" planes. Under cyclic deformation, the fatigue crack propagates along such pencil glide planes. Many straight traces observed at both kinds suggest that the fatigue

surfaces are composed from shallow hills and valleys. Since these traces were arranged parallel to one of the <1 1 1> directions (Fig.2-13), the decohesion along the pencil glide planes should cause the generation of the straight traces.

In addition to the straight traces parallel to [1 $\bar{1}$ $\bar{1}$] direction, Type B cracking had the curved striations on its fatigue surface. The observation from the broad surface shows that the wake of Type B cracking was accompanied by a large number of indistinct slip bands directed towards [1 $\bar{1}$ 1] direction linearly. These slip bands should be produced by the slip deformation towards [1 $\bar{1}$ 1] direction. It is probable that these [1 $\bar{1}$ 1] slips are operated in order to relax the stress concentration at the crack tip. The thick [1 $\bar{1}$ 1] slip bands formed on the broad surfaces were found to coincide with the striations observed on the fatigue surfaces; the curved striation indicates a front of Type B crack. Accordingly, the propagation direction of Type B cracking can be determined to be [$\bar{1}$ 1 1], for the striations were arranged perpendicular to the [$\bar{1}$ 1 1] direction. On the other hand, the fatigue surface of Type A cracking possessed no any fractographic features indicating the crack growth direction, except for the straight traces parallel to [1 1 1] or [1 1 $\bar{1}$] directions. One can consider that the straight traces of Type A cracking correspond to the crack front. This assumption provides the propagation direction perpendicular to the slip direction: the fatigue crack of Type A is grown by mean of the shear decohesion caused by the "anti-plane (Mode III) shearing".

Since the shear decohesion fatigue cracking involves the slip band formation at crack tip and its subsequent decohesion, the dislocations should be emitted from the crack tip. From the observations and discussion about the fatigue surfaces described in above, the following dislocation emission models can be drawn. Type A cracking should involve the emission of a/2[1 1 1] or a/2[1 1 $\bar{1}$] screw dislocations for producing the slip band, because the crack growth direction is predicted perpendicular to [1 1 1] or [1 1 $\bar{1}$]. For Type B cracking, the crack growth direction parallel to [$\bar{1}$ 1 1] direction gives the emission of

a/2[$\bar{1}$ 1 1] edge dislocations.

Figure 2-15 is SEM photograph showing the specimen surface in the vicinity of the fatigue surface. It is likely that the dislocation process at crack tip is associated closely with the morphology of the fatigue crack. Type A cracks showed the crack-tip wavy slips which were developed asymmetrically. These wavy slips would be resulted from the activities of the screw dislocations because the wavy slip lines in b.c.c. crystals are induced by the motions of screw dislocations cross-slipped into another slip plane. Since these wavy slip bands were originated from the crack tip as seen in Fig.2-15, the dislocation emission from the crack tip is responsible for these characteristic bands around Type A cracking. The asymmetrically developed slip band of Type A crack may be produced by the motions of the emitted screw dislocations which are cross-slipped along highly-sheared slip planes. Hence, the morphology of Type A cracking is consistent with the screw dislocation emission model described in above. On the other hand, such wavy slip bands were absent from the crack tip of Type B cracking. This result also agrees with the edge-dislocation emission model for Type B cracking, because the movement of a/2 [$\bar{1}$ 1 1] edge dislocation can not induce the cross slip trace on the broad surface. Accordingly, the validity of the dislocation emission models for both Type A and B cracking are supported by the observations of the slip band morphology.

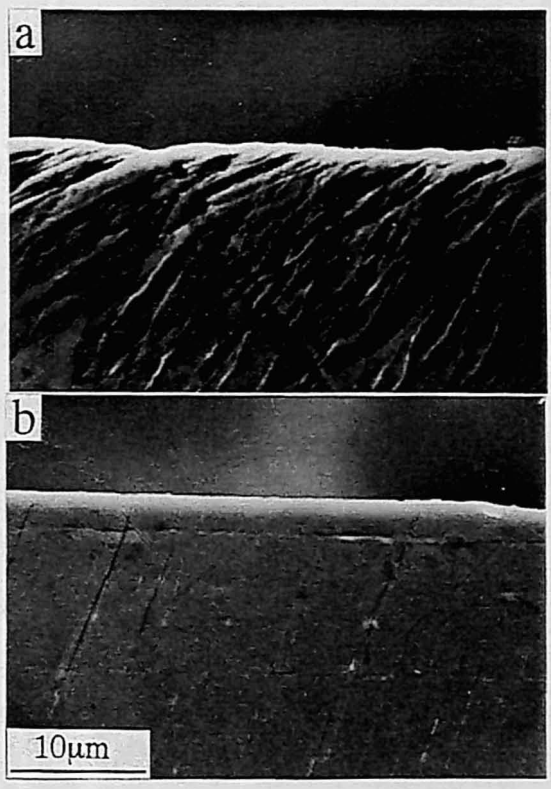

Fig.2-15 SEM photographs showing the specimen surface in the vicinity of the fracture surface in (a) Type A and (b) Type B crackings.

2.4.2 *Resistance to fatigue crack growth*

In view of the discussed model of the dislocation emission, each kind of the fatigue cracks should have individual propagation mechanisms. Hence, the inherent resistance to fatigue crack growth may differ from each other. The present results give following orientation dependence of fatigue crack propagation. (1) The energy release rate at $dl/dN = 5 \times 10^{-8}$m/cycle increased as the loading axis is oriented to [1 $\bar{1}$ 0] direction (Fig.2-11). (2) The composition of the primary crack also changed depending on the loading axis (Fig.2-14): the amount of Type B cracking became large at the loading axes from [1 $\bar{1}$ 1] to [1 $\bar{1}$ 0]. These relationships suggest that the resistance to fatigue crack growth increased with increasing amount of Type B cracking. Accordingly, it is probable that Type B cracking (edge dislocation emission) is more resistant than Type A cracking (screw dislocation emission).

Detail of the crack growth mechanisms that explain the difference in the crack growth resistance is still unclear; we attempt to understand the difference in the crack growth resistance from a view point of a geometrical relationship between a primary slip vector and a free surface in the following way. Figure 2-16 shows fractographic features of both kinds, which are taken at lower magnification. On Type A cracking, the feature of the fatigue surface near the free surface was apparently different from that at the central site. On the other hand, such a difference is unremarkable on Type B cracking. Thus, influence of free surface is recognized just for Type A cracking. Now we consider the slip deformation near the specimen surface. The [1 1 1] and [1 1 $\bar{1}$] slip directions have different geometrical relationship with free surface from the [$\bar{1}$ 1 1] slip direction. The [1 1 1] and [1 1 $\bar{1}$] slips possess a large glide component towards the free surface direction, while the [$\bar{1}$ 1 1] slip does not have it. One can consider that the region close to the free surface would experience more intensive slip activity than the inner site when the operative slip is oriented to the

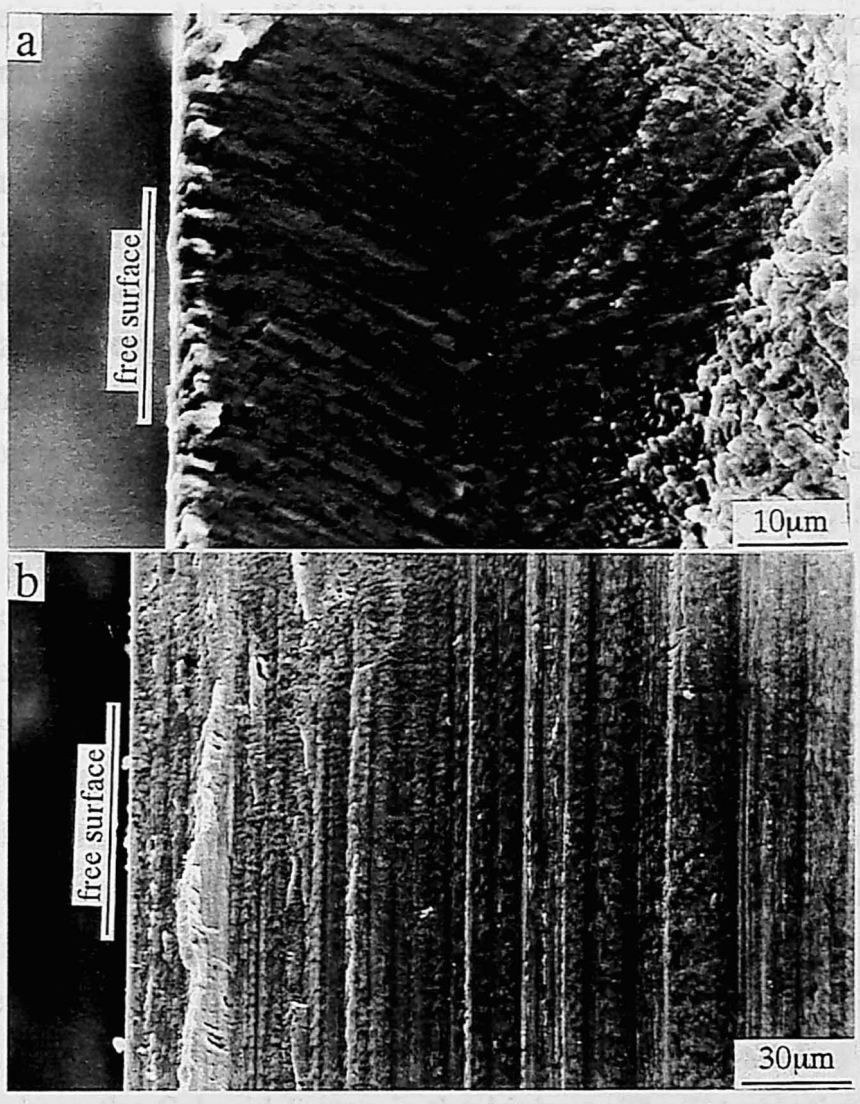

Fig.2-16 Difference in fractographic morphology between the regions close to and distant from free surface at Types A and B crackings. A magnification of (a) is higher than that of (b) by a factor of 3.

free surface because slip deformation towards free surface direction is subjected to no constraint. For this reason, Type A cracking showed the influence of the free surface. On the other hand, the $[\bar{1}\ 1\ 1]$ slip operation may be depressed in comparison with the $[1\ 1\ 1]$ and $[1\ 1\ \bar{1}]$ slips, for the free surface component of slip vector is absent as mentioned in above. Thus, it is possible that the surface region of Type B cracking deformed cyclically at a lower plastic strain amplitude than that of Type A cracking at a same load amplitude if the $[1\ 1\ \bar{1}]$ slip is assumed to contribute to Type B cracking. It has been reported that a crack growth rate depends on the plastic strain amplitude around crack tip rather than on an amplitude of stress intensity factor [21]. Hence, the lower growth rate (i.e., the higher crack growth resistance) of Type B crack is interpretable in terms of the geometrical relationship between the primary slip vector and the free surface.

2.4.3 *Comparison between monotonic deformation and fatigue crack growth*

In the tensile axis close to [0 0 1] direction, both sheet and CT specimens were fractured by cleavage. Hence, it is likely that the orientation dependence of the cleavage fracture is independent of both the specimen shape and the method of loading. However, the orientation dependences of the strengths —— which are estimated by the yield stress and the ultimate tensile strength in the tensile test, and by the energy release rate in the crack propagation test, respectively —— were obviously different between the tensile and fatigue crack propagation tests. Such a difference in the orientation dependence should be ascribed to the strengthening mechanisms of each phenomenon.

The orientation dependence of the yield stress in the Fe-3%Si alloy single crystals [22] has fitted the Schmid law with regard to the {110}<111> slip system, and that of the hardening rate in the iron single crystals [23] has been reported sensitive to the number of operative slip systems. The present results on the tensile deformation agree well with these studies. Thus, it is suggested that the orientation-dependent strength in the monotonic tensile deformation is understood in terms of the conventional Schmid factor and the number of operative slip systems; the orientation of the tensile axis plays an important role on the strengthening.

The fracture surface of fatigue crack was almost parallel to the slip plane where the Schmid factor is the highest. The intersection of the cracking plane with the broad surface corresponds to the observed fatigue crack. Thus, the propagation direction of fatigue crack seems to be determined by the geometry of such a slip plane subjected to severe cyclic shearing. In this sense, the operative slip plane under the monotonic tensile test can give the preferential propagation direction of fatigue crack.

On the contrary, the influence of the multiple-slip operation is

obscure in the crack propagation tests: the fatigue crack tended to propagate along one of the slip bands. Because the shear-decohesion crack of the present study involves the active motion of primary dislocations included in the slip band, the reaction with secondary dislocations may not be connected closely with the process of the fatigue crack propagation. The orientation dependence of work hardening rate, which should be associated with the mode of dislocation reaction under the monotonic deformation, appears to provide little contribution to the orientation dependence of the resistance against fatigue crack propagation.

The morphology of fatigue crack had the following relations to the slip lines observed under the monotonic deformation. Type A fatigue crack was observed in the orientation range in which the wavy slip lines were formed in the monotonic straining. On the other hand, the orientation range of Type B cracking coincided with that of the linear slip lines. In the tensile tests, the Schmid law governed the patterns of slip lines which are related closely to the operative slip vector. Hence, the morphology of the fatigue crack on the (1 1 0) surface —— which was associated with the resistance against fatigue crack growth (Figs.2-11 and 2-14) —— would be predicted also from the Schmid law. Accordingly, whereas the Schmid factor could not provide the resistance against fatigue crack growth directly, the orientation-dependent strength of the CT specimen having the (1 1 0) broad surface could be understood in terms of the distribution of the crack morphologies which are predicted by the Schmid law.

In summary, the strength under the monotonic deformation was governed by the tensile orientation that determines the Schmid factor and the number of the operative slip systems. On the other hand, the orientations of both the tensile axis and the crack propagation direction (or the broad surface plane) should be taken into account to discuss the property of the fatigue crack propagation.

2.5 CONCLUSIONS

From the investigation on the orientation dependences of the tensile deformation and the fatigue crack propagation in Fe-30%Cr alloy single crystals having (110) broad surface, following conclusions are obtained.

1. The monotonic deformation and fracture behaviors were changed depending on the tensile axes and the specimens having [1 $\bar{1}$ 1] tensile axis possessed the highest tensile strength. The specimens having tensile axes close to [0 0 1] were fractured by cleavage even at room temperature.

2. The fatigue cracks were propagated by the decohesion of slip plane. The forms of the fatigue cracks on the surfaces were classified into the cracking with asymmetrical and wavy slip bands and that with coplanar slip band. The former was predominant in the specimens having loading axes from [1 $\bar{1}$ 3] to [1 $\bar{1}$ 1] and the later was predominant in those from [1 $\bar{1}$ 1] to [1 $\bar{1}$ 0]. The screw dislocations with the Burgers vector of [1 1 1] or [1 1 $\bar{1}$] and The edge dislocations with that of [$\bar{1}$ 1 1] or [1 $\bar{1}$ 1] may be emitted from the crack tips on the crackings of each type respectively. The cracking with coplanar slip band is considered to possess higher growth resistance.

3. The resistances of fatigue crack growth were increased as the loading axis approached the direction of [1 $\bar{1}$ 0]. This may be responsible for the changes in the mechanism of the fatigue crack growths.

4. The primary Burgers vectors in the monotonic deformations at each tensile axis were corresponded to those of the emitted dislocations from the predominant crackings.

References

1. A.J.McEvily, Jr. and R.C.Boettner, *Acta Metall.*, **11** (1963), 725.
2. P.Neumann, *Acta Metall.*, **22** (1974), 1167.
3. H.Vehoff and P. Neumann, *Acta Metall.*, **27** (1979), 915.
4. C.E.Richards, *Acta Metall.*, **19** (1971), 583.
5. H.Vehoff and P. Neumann, *Acta Metall.*, **28** (1980), 265.
6. P.Rieux, J.Driver and J.Rieu, *Acta Metall.*, **27** (1979), 145.
7. Sun Ig Hong and C. Laird, *Metall. Trans.*, **22A** (1991), 415.
8. Z.S.Basinski and S.J.Basinski, *Scripta Metall.* **18**(1984), 851.
9. A.Hunsch and P.Neumann *Acta Metall.* **34** (1986), 207.
10. Bao-Tong Ma and C.Laird, *Acta Metall.*, **37** (1989), 325.
11. R.M.Rose, D.P.Ferriss and J.Wulff, *Trans.Metall.Soc.AIME*, **224**, (1962), 981.
12. B.Edmondson, *Proc.Roy.Soc.London*, **264** (1961), 176.
13. D.Hull, *Acta Metall.*, **8** (1960),11.
14. R.Honda, *J.Phys.Soc.Japan*,**16** (1961),1309.
15. R.Priestner and N.Louat, *Acta Metall.*, **11** (1963), 195.
16. W.A.Matejka and R.J.Noth, *J.Test.Eval.* **3** (1975), 199.
17. T. Magnin and F.Moret, *Scripta Metall.*, **16** (1982), 1225.
18. K.Tanaka and T.Mura, *Acta Metall.*, **32** (1984),1731.
19. D.J.Duguette and M.Gell, *Metall.Trans.*, **2** (1971), 1325.
20. S. M. Ohr, *Mater. Sci.Eng.*, **72** (1985), 1.
21. P.Lukás, L.Kunz, Z.Knesl, B.Weiss and R.Stickler, *Mater.Sci.Eng.* **70** (1985), 91.
22. F.W. Noble and D.Hull, *Phil.Mag.*, **12** (1965), 777.
23. A.S. Keh, *Phil.Mag.*, **12** (1965), 9.

Chapter III

Cyclic Stress-Strain Response of Single Crystals Having a (1 1 2) Primary Slip Plane

3.1 INTRODUCTION

It is desirable to predict the fatigue crack nucleation in order to prevent fatigue fractures of structural materials. According to the researches on fatigue crack nucleation [1-3], the PSBs are preferential sites for the fatigue crack initiation. Hence, if we can observe the PSB formation, the prediction of fatigue crack nucleation becomes possible. However, such a direct observation is difficult for the engineering application because the PSBs can be visible using a high-magnification microscopy. Thus, it is desired to find an indirect method to detect the PSBs. One of this method can be achieved by an analysis of cyclic stress-strain response during fatigue [4].

A shape of hysteresis loop is a typical parameter that reflects internal dislocation state. The hysteresis loop shape drastically changes during cyclic deformation especially of copper single crystals where persistent slip bands (PSBs) are formed [5,6]. The hysteresis loop shape has been evaluated by "Bauschinger energy parameter β_E" which is given by Eq.3-1 [7] or "loop shape parameter V_H" [6].

$$\beta_E = \frac{4\sigma_p\varepsilon_{pl} - \oint_{loop} \sigma \, d\varepsilon}{\oint_{loop} \sigma \, d\varepsilon} \qquad (3\text{-}1)$$

where σ_p is the stress amplitude and ε_{pl} is the plastic strain amplitude. (The loop shape parameter is written in the form $V_H = 1/(1+\beta_E)$.) Abel [7] proposed that the beginning of the PSB nucleation stage coincides with the number of cycles where a local β_E maximum is attained. Similar results of the relationship between the hysteresis loop shape and the PSB formation have been reported in copper [8,9] and austenitic stainless steel [4] single crystals. The PSB structure consisting of dipolar walls has also been found in Fe-Cr [10] and Fe-Si [11] alloy single crystals. However, no experiments about the changes of hysteresis loop shape during the cyclic deformation have been reported in the b.c.c. alloy single crystals to the best of our knowledge.

Incidentally, the difference in peak stresses between tension and compression (i.e., stress asymmetry) has been recognized in cyclically-deformed b.c.c. single crystals of molybdenum [12], Fe-26%Cr alloy [13,14] and niobium [15-17]. This characteristic feature was explained by the asymmetric motion of screw dislocations. To obtain another informative parameter about the development process of dislocation structure from the cyclic response, measurement of this stress asymmetry seems to be preferred. This is because the magnitude of the stress asymmetry can reflect a relative contribution of screw dislocation movement to plastic deformation as referred in above.

In the present study, Fe-30%Cr alloy single crystals with a {1 1 2} maximum shear-stressed plane were cyclically deformed under several constant plastic strain amplitudes because the {1 1 2} slip plane was reported to show the highest stress asymmetry [18]. By measuring the various parameters obtained from the hysteresis loop shapes, the present authors attempted to estimate the predominant deformation mechanism under a given plastic strain amplitude. Moreover, a prospect of the crack nucleation prediction was discussed from the view point of the change in the β_E value.

3.2 EXPERIMENTAL PROCEDURE

Single crystals were grown by the Bridgman method from a material of Fe-30wt.%Cr alloy. Single crystal specimens were cut with a spark cutter to have a gauge shape of square 1.5×1.5 mm^2 cross section and length of 4 mm from the single crystals grown. In order to perform the present experiments successfully, we have to take account of the following requirements in choosing the tensile axis: (1) A maximum-resolved-shear-stressed plane must be oriented to be {1 1 2} in order to achieve the highest stress asymmetry. (2) The tensile axis should be distant from < 1 0 0 > direction to prevent the occurrence of {1 0 0} cleavage fracture that is often observed in b.c.c. single crystals [19-22]. (3) A ratio of the Schmid factor of a secondary slip system to that of a primary system is desired to be minimized so as to avoid double slips. For these reasons, we chose the < 1 4 4 > tensile where the (1 1 2)[$\bar{1}$ $\bar{1}$ 1] system has the Schmid factor of about 0.5. A stereographic projection of crystallographic orientation and a schematic illustration of the primary slip system are presented in Fig.3-1. Primary slip vector was oriented to the direction between surface and tensile directions, and thus slip steps will appear at the top surface. The specimens were quenched in water after an annealing at 1373K in vacuum, and then mechanically and electrolytically polished to obtain mirror-like surface.

The cyclic deformation test were carried out in air at room temperature in a servo-hydraulic machine. Strain was measured with a strain gauge that was glued to the reverse side of surface. Due to the limited size of the specimen shape, it is difficult to perfom a strain controlled test at lower amplitudes using an extensometer. For specimen positioning and alignment, Wood's metal was employed to fasten a lower grip. During the experiments, total strain amplitude was automatically adjusted at every half cycle to control plastic strain amplitude. The specimen was cyclically deformed under a constant plastic strain amplitude ε_{pl} ranged from 2×10^{-4} to 1.2×10^{-3} at a

strain rate of $1\times10^{-3}s^{-1}$. Hysteresis loops were recorded into magnet-optical (MO) disks through an analogue-to-digital (A/D) converter of 12-bit resolution in order to analyze the cyclic stress-strain response in detail. During the period corresponding to 10 cycles, signals of stress and strain were sampled and then saved as one data file. Thus, each data file contain sequential at least 9 hysteresis loops (zero strain during tensile straining is taken as a beginning of the hysteresis loop in the present study). We extracted the complete 9 cycles from the data files and then averaged stress amplitudes of the 9 cycles for indication in a cyclic hardening diagram. Same procedure was conducted for calculation of the Bauschinger energy parameter β_E which is used for evaluating the shape of hysteresis loop. A schematic illustraion of the definition of the β_E value is shown in Fig.3-2.

Deformation cycling was interrupted at a cumulative plastic strain of approximately 30. After the fatigue experiments, surface topography was observed with a scanning electron microscope (SEM).

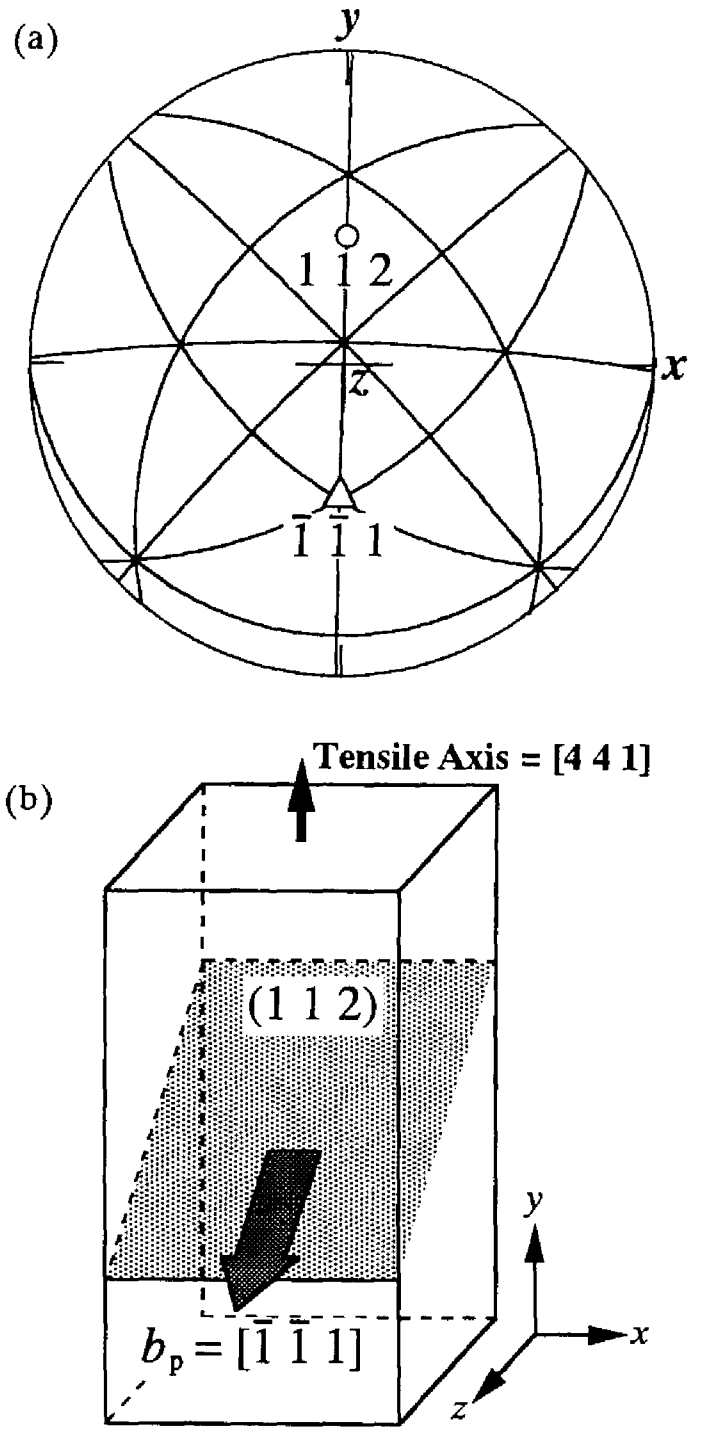

Fig.3-1 A stereographic projection of the specimen orientation and a schematic illustration of the slip geometry.

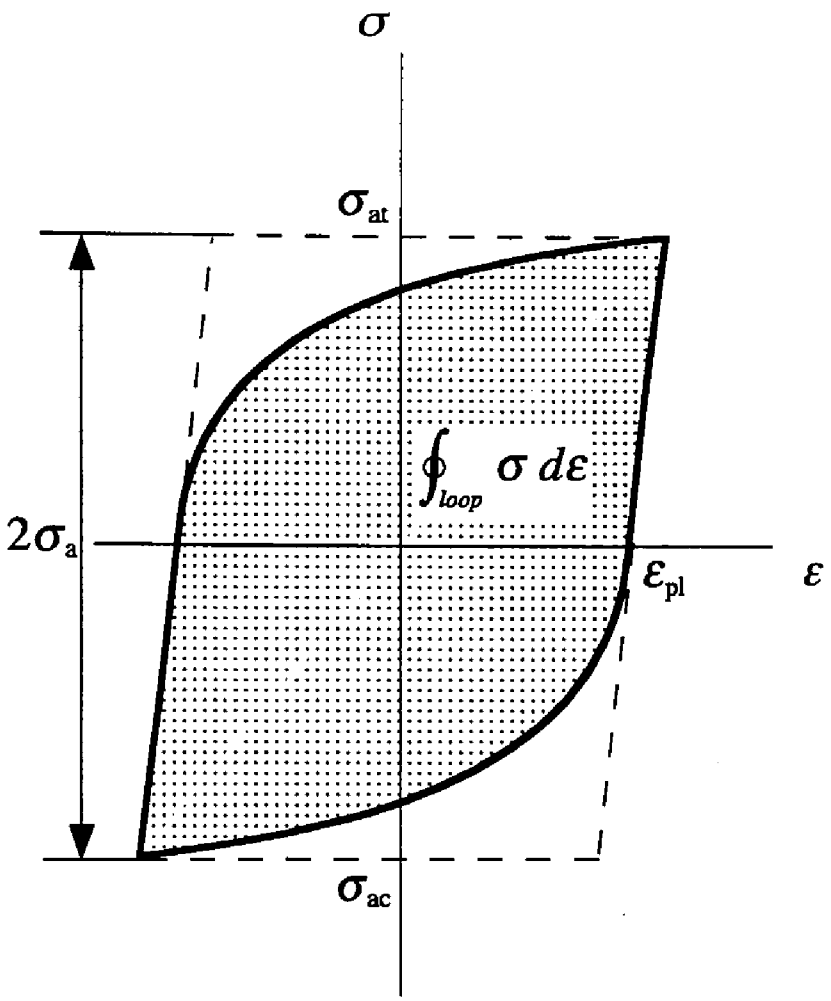

$$\beta_E = \frac{4\sigma_a\varepsilon_{pl} - \oint_{loop} \sigma \, d\varepsilon}{\oint_{loop} \sigma \, d\varepsilon}$$

Fig.3-2 Definition of the Bauschinger energy parameter, β_E.

3.3 RESULTS

3.3.1 *Cyclic Hardening and Stress Asymmetry*

Figure 3-3 shows some hysteresis loops whose shape was changed with cyclic deformation at a constant plastic strain amplitude of 1.2×10^{-3}. We can notice a difference in stress-strain curves between tensile and compressive region with a very careful observation of the hysteresis loop shapes. Figure 3-4 presents the stress amplitudes of both tension σ_{at} and compression σ_{ac} during cyclic deformation tests under various plastic strain amplitudes. The specimens were gradually hardened except for the initial cyclic softening at the ε_{pl} of 5×10^{-4} and at 1.2×10^{-3}. Saturation behavior of the stress amplitudes was ambiguous within the cumulative plastic strain $\varepsilon_{pl,cum}$ up to about 30, unlike usual copper single crystals. This kind of cyclic hardening curve is similar to that obtained in an Fe-13.6%Cr alloy single crystal oriented for single slip [10].

It is noteworthy that the stress amplitudes in tension were always higher than that in compression. The difference between these stress amplitudes changed certainly with cyclic deformation (Fig.3-4). In order to indicate these variations in the stress asymmetry with cycling, we calculated the difference in the stress amplitudes $\Delta\sigma = \sigma_{at} - \sigma_{ac}$, and then normalized the $\Delta\sigma$ value by the mean stress amplitude between tension and compression. Changes in the stress asymmetry during the experiments are shown in Fig.3-5. At the beginning of the experiments, the normalized $\Delta\sigma$ value at $\varepsilon_{pl} = 1.2 \times 10^{-3}$ was lower than those at smaller strain amplitudes. In the early stages, all of the specimens showed continuous decrease in the stress asymmetry with increasing cycles. The stress asymmetry under $\varepsilon_{pl} = 2 \times 10^{-4}$ continued to decrease until an interruption of the experiment, whereas large fluctuations of the normalized $\Delta\sigma$ value were observed. These fluctuations of the stress asymmetry are probably due to frequent occurrences of small strain bursts which have been discussed in Chapter

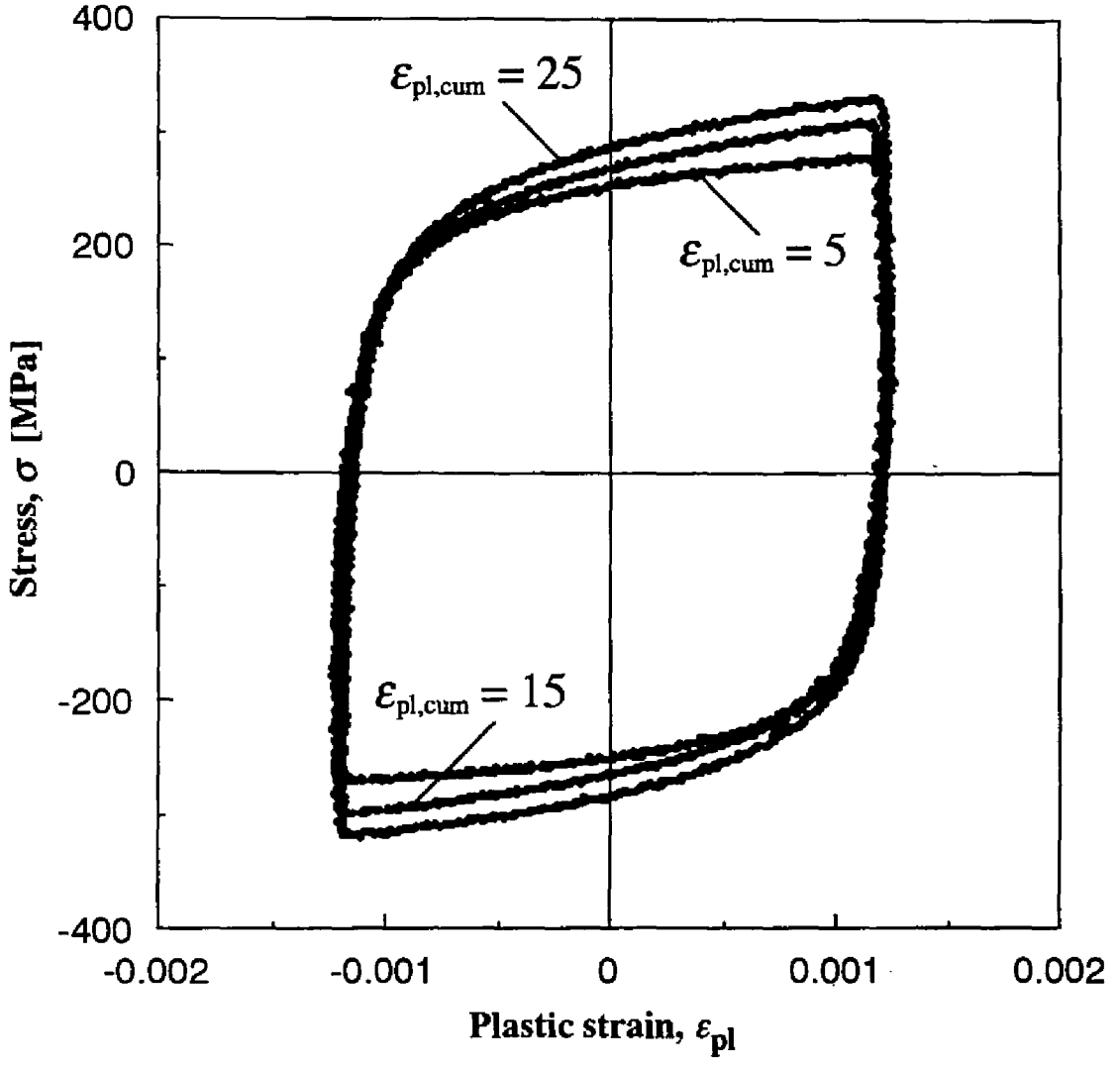

Fig.3-3 Change in hysteresis loop shape during cyclic deformation under a plastic strain amplitude ε_{pl} of 1.2×10^{-3}.

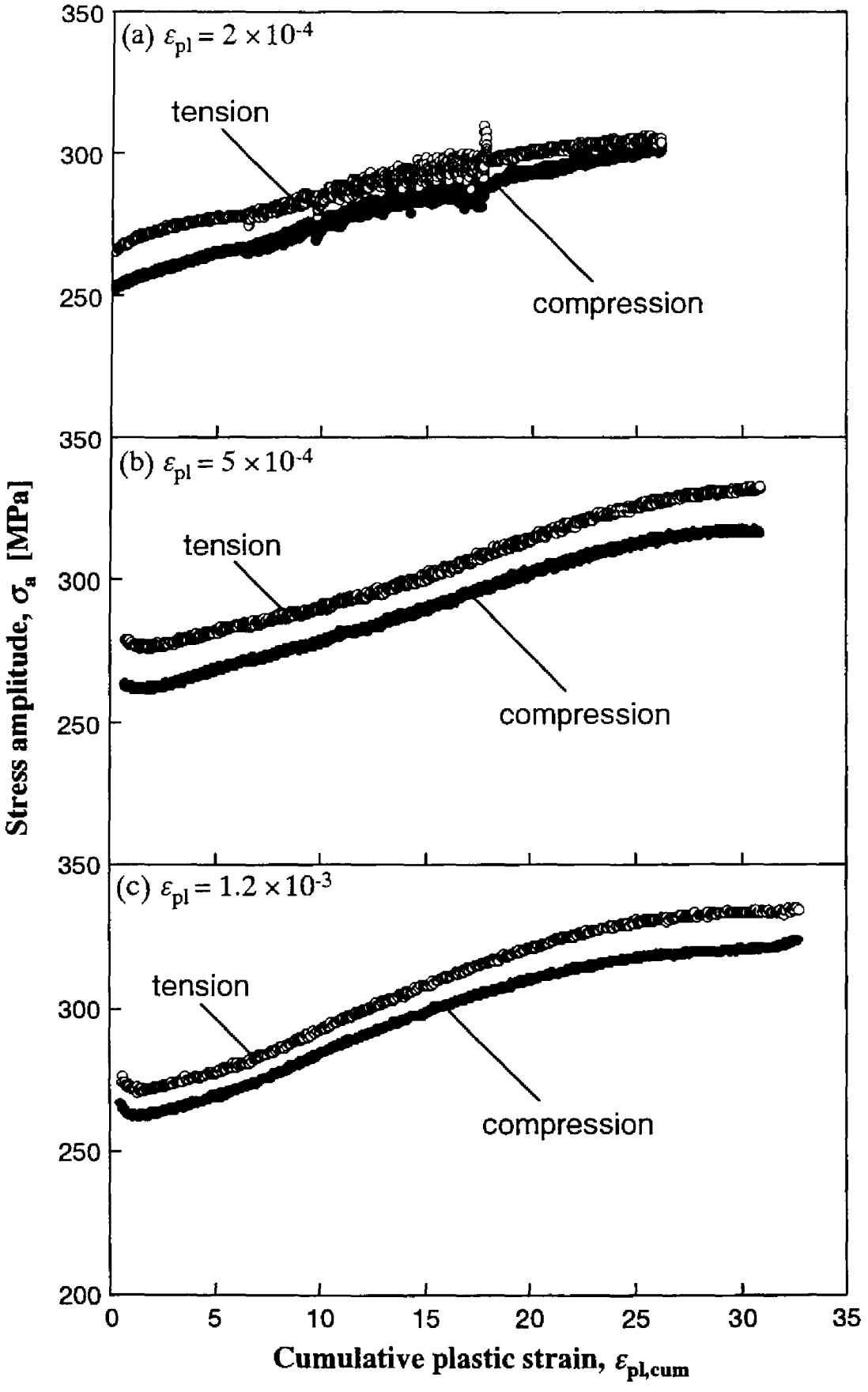

Fig.3-4 Cyclic hardening curves of tensile and compressive regions under several plastic strain amplitudes.

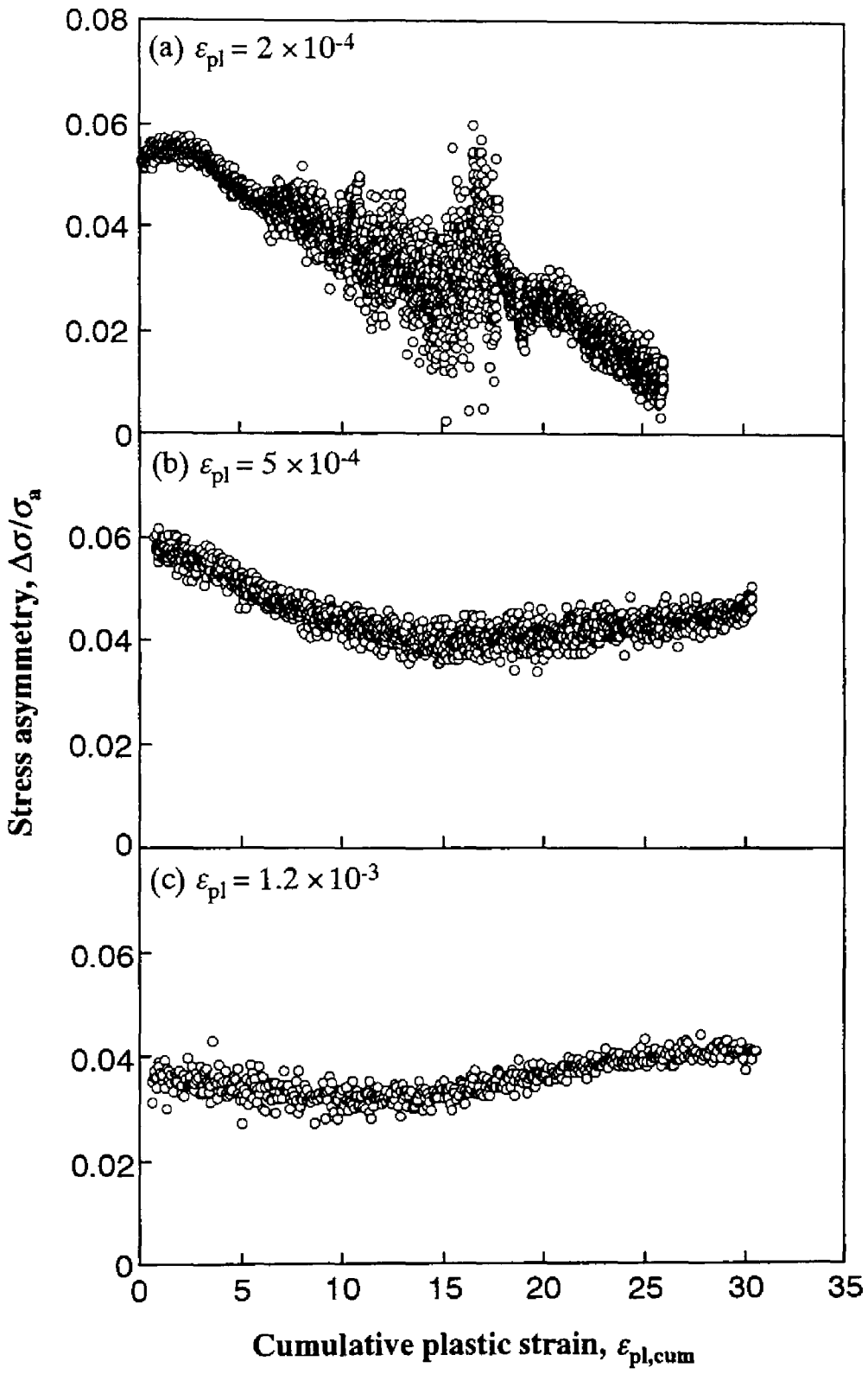

Fig.3-5 Changes in stress asymmetry during cyclic deformation under several plastic strain amplitudes. The stress asymmetry is defined as a difference in peak stresses between tensile and compressive regions, which is normalized by an average peak stress.

IV. The normalized $\Delta\sigma$ value was reduced by a factor of 6 at the cumulative plastic strain amplitude $\varepsilon_{pl,cum}$ of 25, compared with that at the beginning. On the other hand, the stress asymmetry at $\varepsilon_{pl} = 5\times10^{-4}$ became a constant value of approximately 0.04 after the $\varepsilon_{pl,cum}$ of 12. In the experiment at $\varepsilon_{pl} = 1.2\times10^{-3}$, the initial continuous decrease in the $\Delta\sigma$ value seems to be terminated at $\varepsilon_{pl,cum}$ of 10, and then the stress asymmetry began to increase at $\varepsilon_{pl,cum}$ of 15 again.

The strain bursts, which occurred at $\varepsilon_{pl} = 2\times10^{-4}$, were not observed at larger plastic strain amplitudes. These results at the large amplitudes agree with those reported in Cu-Al [23] and Cu-Zn alloy single crystals [24]. The occurrence of the strain burst has been ascribed to the avalanche of dislocations which are pinned by dislocation dipoles [25] or segregated solute atoms [26]. The disappearance of the strain burst at large amplitude has been explained by following two manners. Abel et al [23] proposed that at large amplitude, internal stresses are strong enough to overcome the obstacles which produce discontinuous flow whereas at small amplitude the strain bursts occur. The other model took account of high cyclic hardening at large amplitude. When the friction stress increases as a result of strain hardening to a value close to that of strengthening produced by Zn atom segregation, it would be expected that the strain burst should disappear (Hu et al. [24]). However, there was no significant difference in stress amplitude among the plastic strain amplitudes in the present study. It appears difficult to attribute the strain amplitude dependence of the strain burst to differences in the stresses. One can expect that dislocation structure is different between the given strain amplitude. The Fe-Si alloy single crystals cyclically deformed at a large amplitude ($\Delta\varepsilon_{pl}$=2×10^{-2}) had dislocation bundles containing dislocation loops which are fragmented into small size [27]. Such debris loop can prevent the dissociation of the dislocation dipoles occurring at the strain burst.

3.3.2 *Bauschinger energy parameter*

Figure 3-6~3-8 show the Bauschinger energy parameter β_E during cyclic deformation under several strain amplitudes. A large β_E value means a pointed shape of hysteresis loop. The stress amplitudes were also plotted in the figures for convenience. Strong dependence of the β_E value on the plastic strain amplitude is recognized: the β_E values tend to decrease with increasing plastic strain amplitude. In addition to the strain amplitude dependence, the β_E values of the individual specimens changed obviously during cyclic deformation in the following manners. The β_E values increased continuously with increasing cycles in the early stages of all experiments. In further cycling, characteristic changes of the β_E value were observed in some specimens. The specimen cycled at $\varepsilon_{pl} = 2 \times 10^{-4}$ showed discontinuous increase and decrease in the β_E value. Except for these discontinuous changes, the β_E value continued to increase until the interruption of cycling. The β_E value at $\varepsilon_{pl} = 5 \times 10^{-4}$ continuously increased until very late stage of the experiment, and then became constant at $\varepsilon_{pl,cum}$ of 26 although the stress amplitude was still increasing. In the specimen cycled at $\varepsilon_{pl} = 1.2 \times 10^{-3}$, a local maximum of the β_E value was attained at $\varepsilon_{pl,cum}$ of 15 as indicated by an open arrow. Thereafter, the β_E value continued to decrease. No local maxima attained under such a gradual β_E change were found at $\varepsilon_{pl} = 2 \times 10^{-4}$, and it is ambiguous for $\varepsilon_{pl} = 5 \times 10^{-4}$ that the mentioned constant β_E value at $\varepsilon_{pl,cum}$ of 26 corresponds to the local maximum.

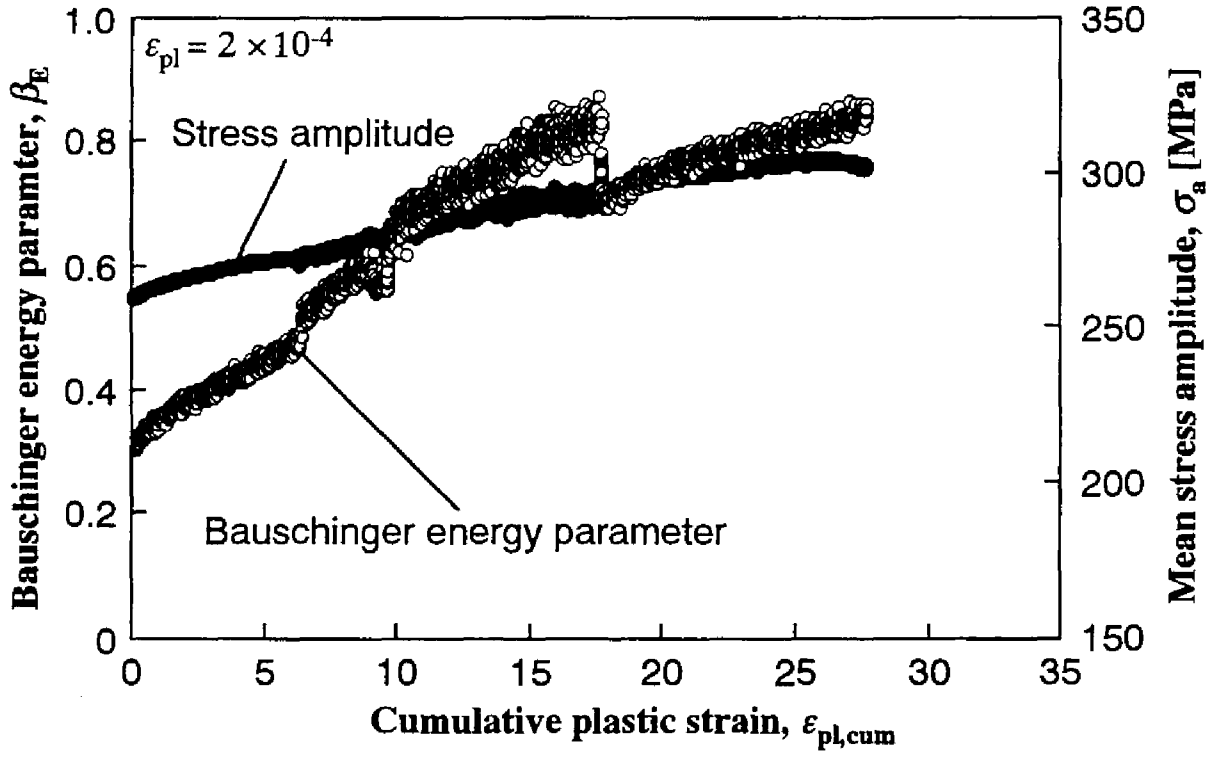

Fig.3-6 Changes in the Bauschinger energy parameter during cyclic deformation at ε_{pl} of 2×10^{-4}. Stress amplitudes are also plotted for convenience.

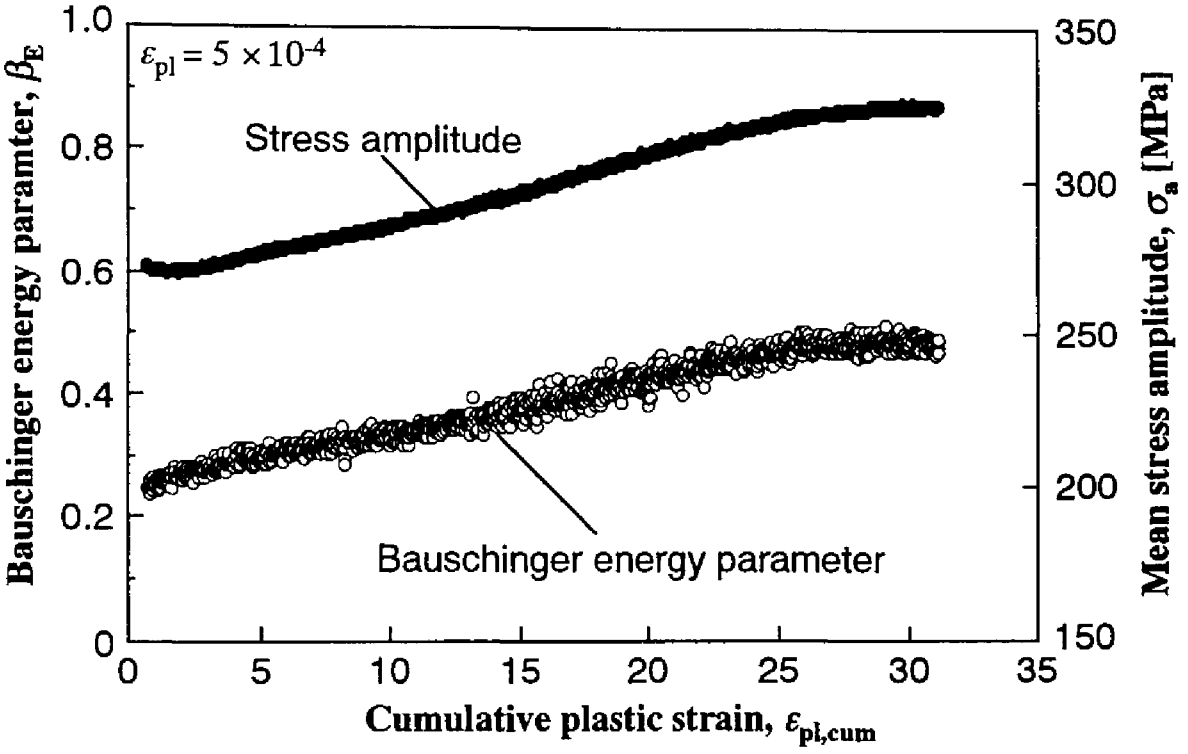

Fig.3-7 Changes in the Bauschinger energy parameter during cyclic deformation at ε_{pl} of 5×10^{-4}. Stress amplitudes are also plotted for convenience.

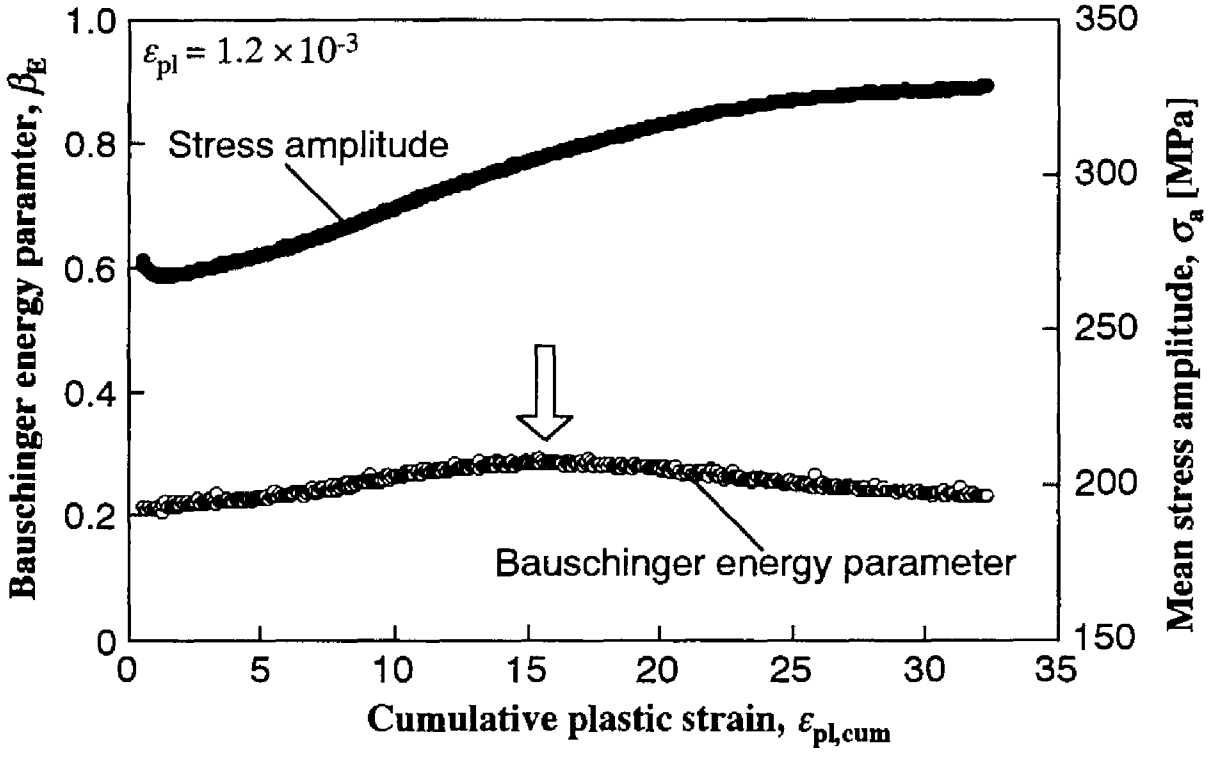

Fig.3-8 Changes in the Bauschinger energy parameter during cyclic deformation at ε_{pl} of 1.2×10^{-3}. Stress amplitudes are also plotted for convenience. An arrow indicates a local maximum of the β_E value.

3.3.3 *Development of slip bands at specimen surface*

Figure 3-9 is the SEM photograph showing the specimen surfaces after the experiments. The specimen surface at $\varepsilon_{pl} = 2 \times 10^{-4}$ is featureless: with the SEM we could not find any development of slip bands which were certainly visible when the optical microscope was used. The slip bands are seen in the specimen fatigued at $\varepsilon_{pl} = 5 \times 10^{-4}$ and 1.2×10^{-3}. Especially at $\varepsilon_{pl} = 1.2 \times 10^{-3}$, a lot of extrusions grown locally at the slip bands are recognized.

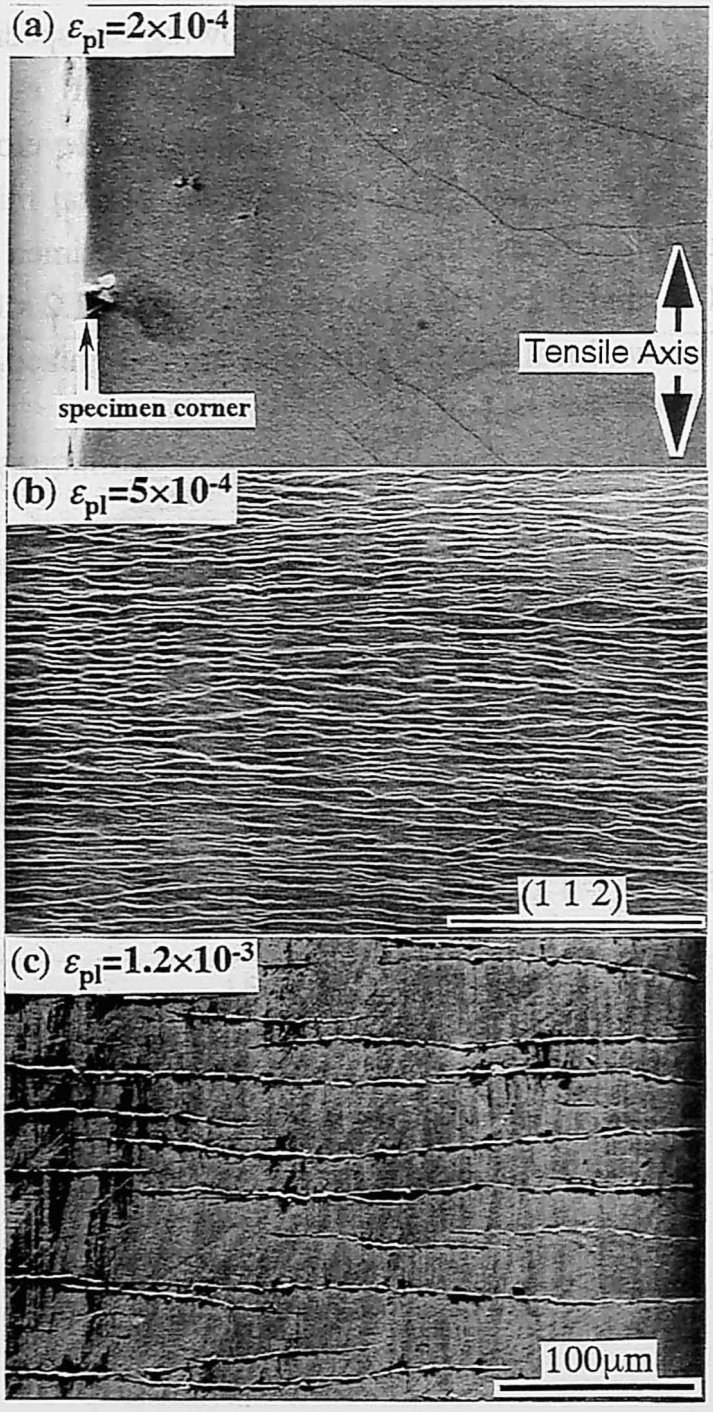

Fig.3-9 SEM photomicrographs showing the aspect of specimen surface after the cyclic deformation tests. Development of extrusions at slip bands is visible at $\varepsilon_{pl}=1.2\times10^{-3}$. Since the photographs of $\varepsilon_{pl}=2\times10^{-4}$ and 5×10^{-4} were taken at higher contrast with compared to that of $\varepsilon_{pl}=1.2\times10^{-3}$, their slip lines are barely recognized.

3.4 DISCUSSION

3.4.1 *Change in the Bauschinger energy parameter during cyclic deformation and its dependence on plastic strain amplitude*

It was found that the β_E values decreased with increasing plastic strain amplitude as shown in Fig.3-6 ~-8. In other words, the reversibility of dislocation motion was reduced at larger strain amplitude, since the β_E value represents a recoverability of stored deformation energy during cyclic deformation [28]. This tendency is compatible with that the β_E value decrease with the amount of pre-strain in single load resersal tests on the low-carbon steels [29]. The decreasing β_E value with increasing plastic strain amplitude was also seen in austenitic stainless steel single crystals fatigued under ε_{pl} of at least less than 5×10^{-4} [4].

The repulsive force between dislocations, which is produced during pre-straining, has been a plausible explanation for the Bauschinger effect observed at a single crystal [28]. In fatigued single crystals, it is likely that a higher back stress is produced with a help of a peculiar structure such as edge dislocation bundles. Now we consider the Bauschinger effect in the present specimen deformed cyclically. It is widely accepted that the cyclic deformation of b.c.c. metals at lower temperature can be characterized by the lower mobility of screw dislocations [30] and by the higher frictional stress of the screw dislocations [13]. At a lower plastic strain amplitude, the relative contribution of edge dislocation motion should be larger because the mobility of edge dislocation is higher than that of screw dislocation. The high mobility of the edge dislocations has actually been observed as a dislocation loop elongated to a direction of the Burgers vector [30]. On the other hand, a larger strain amplitude must require long-distant movements of dislocations including screw component since the referred edge dislocation movements can be stopped at various barriors. Such a screw dislocation movement would be accompanied

by a lot of cross slip and resultant cutting of dislocations. The cross slip of screw dislocations and the cutting of dislocations may not contribute to the back stress resulted from the long-range elastic interaction between dislocations, thus resulting in low recoverability of cyclic deformation. Accordingly, the observed lower β_E value at the larger strain amplitude is attributed probably to the increasing activity of the screw dislocations, since the β_E value represents a recoverbility of stored deforamation energy [28].

The sudden changes in the β_E value, which were observed at $\varepsilon_{pl} = 2 \times 10^{-4}$, may be due to occurrences of huge strain bursts or to activations of new dislocation sources. The β_E value at $\varepsilon_{pl} = 1.2 \times 10^{-3}$ had one local maximum as indicated in Fig.5, whereas the β_E value measured at $\varepsilon_{pl} = 2 \times 10^{-4}$ and 5×10^{-4} increased monotonically until interruption of experiment, except for the sudden changes. The maximum of the β_E value of this kind (or a minimum of the loop shape parameter V_H which is given by $V_H = 1/(\beta_E - 1)$) has also been found in the single crystals of copper [6-9] and of austenitic stainless steel [4,31] and in the polycrystals of copper [33-35] and of austenitic stainless steel [35]. The SEM surface observation after the tests revealed that the extrusions were developed at the slip bands at $\varepsilon_{pl} = 1.2 \times 10^{-3}$, while these extrusions were absent from the specimens fatigued at $\varepsilon_{pl} = 2 \times 10^{-4}$ and 5×10^{-4} until $\varepsilon_{pl,cum}$ of 30. The observed extrusion is a peculiar topology for the PSB. Formation of the PSB structure has been reported also in the Fe-Cr [10] and Fe-Si [11]alloy single crystals, being observed as dipolar wall and cell structure. Hence, the present extrusions can be the PSBs containing the characteristic dislocation structures.

The local β_E maximum has been considered to correspond to the beginning of the PSB formation in copper single crystals [7,8]. This is because a substantial part of flow stress within the PSB is believed to come from a friction provided by obstacles between the walls [36]. Thus, it is probable that the back stress giving rise to the Bauschinger effect is lower within the PSB than that in the matrix. Similar friction

stress within the PSB can be predicted also in the fatigued b.c.c. single crystals. Because the developed extrusions at the slip bands were seen exclusively in the specimens showing the β_E maximum, it is therefore feasible that the local β_E maximum observed at $\varepsilon_{pl} = 1.2 \times 10^{-3}$ coincides with the beginning of the PSB formation as reported in the copper single crystals.

Fatigue crack nucleations were recognized in the specimen at ε_{pl} of 1.2×10^{-3}. Another specimen that was fatigued at ε_{pl} of lower than 1.2×10^{-3} never showed the fatigue crack nucleations within a cumulative plastic strain of at least 30. Aspects of the fatigue cracks observed at surface is presented in Fig.3-10. It becomes apparent that the fatigue cracks were initiated preferentially along the developed slip bands under the present experimental condition. Prediction of such a crack initiation must be significantly important for engineering purposes. If the developed extrusions correspond to the PSBs, it can be proposed that the detection of the β_E maximum leads to the prediction of the fatigue crack initiation [4]. This is because the fatigue crack initiation is preceded by the β_E maximum that coincides with the beginning of the PSB formation. There is a prospect of the prediction of fatigue crack initiation in the ferritic stainless steel by measuring the β_E value, in spite of the fact that the prediction of this kind is difficult from an analysis of the cyclic hardening curve (Fig.3).

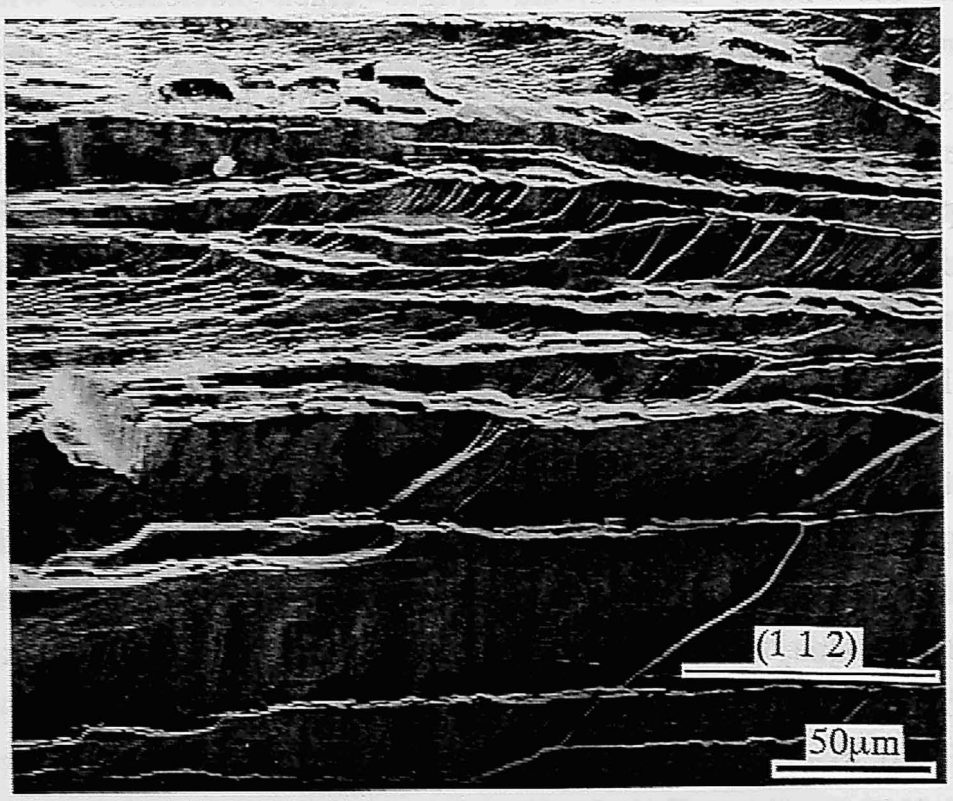

Fig.3-10 Nucleated fatigue cracks along the developed slip bands under a plastic strain amplitude of 1.2×10^{-3}.

3.4.2 *Cyclic response described by stress asymmetry*

It has been established in the Fe-Si single crystals [18] that the yield stress under monotonic deformation is high when an operative {112} plane is sheared to the "anti-twinning" direction in comparison with the yield stress under the "twinning" direction shearing. The difference between tensile and compressive peak stresses also follows this law in the cyclically deformed b.c.c. metals [12,13]. This difference in the stresses has been attributed to the behavior of screw dislocation moving towards opposite directions along the {112} slip plane: the asymmetric yield stress was explained by the different constriction processes of the screw dislocation dissociated on three {112} planes [18,37]. The different Peierls stresses of the screw dislocation sheared to opposite directions along {112} was also calculated using an atomic simulation [38]. The present slip geometry gives the anti-twinning shear on the (1 1 2) primary system when the specimen is strained to tensile direction. Hence, the observed stress asymmetry is consistent with the referred asymmetric motion of the screw dislocation on the (1 1 2) plane.

At the beginning of the experiments, the magnitude of the stress asymmetry at $\varepsilon_{pl} = 1.2 \times 10^{-3}$ was not so high as those at lower plastic strain amplitudes as shown in Fig.3-5. This decrease in the initial stress asymmetry at a larger strain amplitude can be understood in the following manner. A larger strain amplitude requires dislocation movements for longer distance, leading to more frequent occurrences of cross slip of screw dislocations. Hence, the slip planes showing low stress asymmetry may become operative paths for screw dislocations; the screw dislocation movements along the (1 1 2) plane should be reduced relatively. This cross slip of screw dislocation is compatible with both the low stress asymmetry and the low β_E value observed at $\varepsilon_{pl} = 1.2 \times 10^{-3}$.

The stress asymmetry decreased continuously with cycles in the early stage at all of the plastic strain amplitudes tested. Such an initial

decrease in the stress asymmetry must be related to the reduction in relative contribution of the screw dislocation movements along the (1 1 2) plane. This should be because the increase in dislocation density leads to increasing movements of edge dislocations possessing higher mobility, thus resulting in the reduced contribution of screw dislocations.

At the plastic strain amplitudes of 5×10^{-4} and of 1.2×10^{-3}, the initial continuous decreases in the stress asymmetry were terminated during the experiments, being different from the result at $\varepsilon_{pl}=2\times10^{-4}$. Moreover, the stress asymmetry at $\varepsilon_{pl}=1.2\times10^{-3}$ began to increase again at $\varepsilon_{pl,cum}$ of 15. The changes in the deformation mechanism at these cycles can be expected for these experiments. The cessation of the continuous decrease seems inconsistent with the increasing stress amplitude (Fig.3-4) in view of the widely-known relationship that a flow stress is proportinal to the square root of a dislocation density. It is at least plausible that the amount of screw dislocation activities along the (1 1 2) plane did not decrease with increasing stress amplitude after the stress asymmetry became constant.

For the interpretation of this fact, following two posibiliites about the changes in dislocation process can be conceivable. One of the possible changes is the dislocation substructure. Many studies on copper single crystals have established that the cyclic deformation produces the peculiar dislocation structures such as the vein structure and the ladder-like PSB structure [39]. Cyclically deformed Fe-Cr [10] and Fe-Si [11] alloy single crystals have been reported to have similar dislocation bundles. According to these facts, the cyclic deformation at the larger strain amplitude can produce extensive dislocation bundles also in the present ferritic stainless steels. It has been reported that the dislocation bundles contain a number of small prismatic loops in low-cycle fatigue tests on Fe-Si alloy single crystals [27]. Under such a structural state, it is likely that an edge dislocation trapped within the dislocation bundles become less mobile and/or a movement of a free edge dislocation is restricted at the dislocation bundles. Hence, complemental movements of screw dislocations on the {1 1 2} plane

may raise the stress asymmetry again to accommodate an applied plastic strain amplitude.

The other possibility is the change in the frequency of cross slip during the experiment. In the early stage where the mobile dislocation density is low, the long-distance movements of the screw dislocations along the {1 1 2} plane can be accompanied by many cross slips as discussed for the initial lower stress asymmetry at $\varepsilon_{pl} = 1.2 \times 10^{-3}$. A mean amplitude of to-and-fro dislocation movements under cycling would decrease with increasing mobile dislocation density. This can cause the reduction in relative contribution of screw dislocations having lower mobility, thus resulting in the decreased frequency of the cross slip along the planes showing stress asymmetry lower than the (1 1 2) plane.

Some screw dislocations have been observed between the walls of the PSBs in the cyclically deformed copper single crystals, and the movements of these screw dislocations are considered to dominate the plastic deformation of the PSBs [36]. Since the analogous dipolar wall structure was found in the cyclically deformed Fe-Cr alloy single crystals [10], the movement of screw dislocations may play an important role also for the PSB deformation in the present study. On the specimen cycled at $\varepsilon_{pl} = 1.2 \times 10^{-3}$, the number of cycles where the stress asymmetry began to increase coincided almost with the local maximum of β_E value. This correspondence between the stress asymmetry and the β_E value is interpretable by the screw dislocation movement within the PSBs, because the β_E maximum is expected to coincide with the beginning of the PSB nucleation as described in Section 3.4.1.

However, the stress asymmetry became a constant value without the β_E local maximum at $\varepsilon_{pl} = 5 \times 10^{-4}$. In addition, the cessation of decrease in the stress asymmetry at $\varepsilon_{pl} = 1.2 \times 10^{-3}$ preceded to the β_E local maximum. The cessation of the continuous decrease in the stress asymmetry is inconsistent with the increasing β_E value in view of the reffered movements of screw dislocations within the PSBs along the (1 1 2) plane. In this sense, the saturation of the stress asymmetry

at these point can be understood in terms of the reduced frequency of the cross slip. The increasing β_E value that reflects high recoverability of cyclic deformation is compatible with the reduced frequency of the cross slip.

3.5 CONCLUSIONS

From the investigation on the cyclic deformation of the Fe-30%Cr alloy single crystals having (1 1 2) primary slip plane at plastic strain amplitudes ε_{pl} ranged from 2×10^{-4} to 1.2×10^{-3}, we have obtained following conclusions about plastic-strain-amplitude dependence of cyclic deformation behavior.

1. The change in the Bauschinger energy parameter β_E during the experiments depended strongly on the plastic strain amplitude, although the shapes of the cyclic hardening curves were almost the same. At $\varepsilon_{pl}=2\times10^{-4}$ and 5×10^{-4}, the β_E value continued to increase until a cumulative plastic strain of at least about 30, except for the sudden changes observed at $\varepsilon_{pl}=2\times10^{-4}$. On the other hand, the specimen cycled at $\varepsilon_{pl}=1.2\times10^{-3}$ showed a local maximum of the β_E value; this phenomenon is similar to that observed in a copper single crystal containing PSBs.

2. The stress amplitude in tension was always higher than that in compression at all strain amplitudes. This stress asymmetry was consistent with the conventional result that the flow stress under the anti-twinning shear along {112} plane is higher in comparison with the twinning shear. The stress asymmetry was sensitive to the strain amplitude, too. At $\varepsilon_{pl}=5\times10^{-4}$ and 1.2×10^{-3}, the initial continuous decrease —— which can be attributable to the increasing dislocation density —— was terminated during experiments while the stress amplitude was still increasing. It is presumed that these changes are due to the development of the dislocation substructure peculiar to cyclic deformation.

3. The developed extrusions and the fatigue crack initiation along these were found in the specimen at $\varepsilon_{pl}=1.2\times10^{-3}$. Since the β_E maximum probably coincides with the beginning of the PSB nucleation,

the prediction of fatigue crack initiation is expected to be practicable by measuring the β_E value in the present material.

References

1. Z.S.Basinski and S.J.Basinski, *Scripta metall.*, **18** (1984), 851.
2. A.Hunsch and P.Neumann, *Acta metall.*, **34** (1986), 207.
3. Bao-Tong Ma and C.Laird, *Acta metall.*, **22** (1989), 1155.
4. Y. Kaneko, Y. Morita and S. Hashimoto, *Scripta mater.*, **37** (1997), 963.
5. A. T. Winter, *Phil. Mag.*, **30** (1974), 719.
6. H. Mughrabi, *Mater. Sci. Eng.*, **33** (1978), 207.
7. A. Abel, *Mater. Sci. Eng.*, **36** (1978), 117.
8. D. E. Witmer, C. Laird and G. C. Farrington, *Acta metall.*, **35** (1987), 1911.
9. J. Polák, J. Helesic and K. Obrtík, *Mater. Sci. Eng.*, **A101** (1988), 7.
10. B. Šesták, Z. Vicherková, V. Novák, S. Libovický and J. Brádler, *Phys. Stat. Sol.*, **(a)104** (1987), 79.
11. B. Šesták, V. Novák and, S. Libovický, *Phil. Mag. A*, **57** (1988), 353.
12. B. Etemad and F.Guiu, *Scripta metall.*, **8**, 931 (1974).
13. T. Magnin and J. H. Driver, *Mater. Sci. Eng.*, **39**, 175 (1979).
14. T. Magnin, A. Fourdeux and J. H. Driver, *Phys. Stat. Sol. (a)*, **65**, (1981), 301 .
15. M. Anglada and F. Guiu, *Phil. Mag.*, **44**, 499 (1981).
16. M. Anglada and F. Guiu, *Phil. Mag.*, **44**, 523 (1981).
17. F. Guiu and M. Anglada, *Phil. Mag.*, **46**, 881 (1982).
18. S. Takeuchi, E. Furubayashi and T. Taoka, *Acta metall.*, **15** (1967), 1179.
19. D. Hull, *Acta metall.*, **8** (1960), 11.
20. R. Honda, *J. Phy. Soc. Japan*, **16** (1961), 1309.
21. R. M. Rose, D. P. Ferriss and J. Wulff, *Trans. Metall. Soc. AIME*, **224** (1962), 981.
22. P. Beardmore and D. Hull, *J. Less-Comm. Metals*, **9**, 168 (1965).

23. A. Abel, M. Wilhelm and V. Gerold, *Z. Metallkde.*, **70** (1979), 577.
24. X. Hu, H. Margolin, X. Duan and S. Nourbakhsh, *Mater. Sci. Eng.A*, **A157** (1992), 181.
25. P. Neumann, *Z. Metallkde.*, **59** (1968), 927.
26. S.I. Hong and C. Laird, *Mater. Sci. Eng. A*, **A124** (1990), 183.
27. H. Mori, M. Tokuwame and T. Miyazaki, *Phil.Mag.A*, **40** (1979), 409.
28. A. Abel, *Materials Forum*, **10.** 11 (1987).
29. A. Abel and H. Muir, *Phil. Mag.*, **26,** 489 (1972).
30. H. Mughrabi, K. Herz and X. Stark, *Acta metall.*, **24** (1976), 659.
31. Y. Kaneko and S. Hashimoto, *Mater. Sci. Eng.*, **A234-236** (1997), 386.
32. J. Polák, K. Obrtlík and J. Helesic, *Mater.Sci.Eng.*, **A132** (1991), 67.
33. J. Polák, K. Obrtlík, M. Hájek and A. Vasek, *Mater.Sci.Eng.*, **A151** (1992), 19.
34. A. Vinogradov, Y. Kaneko, K. Kitagawa, S. Hashimoto, V. Stolyarov and R. Z. Valiev, *Scripta mater.*, **36** (1997), 1345.
35. J. Polák, K. Obrtlík and M. Hájek, *Fatigue Fract.Engng.Struct.*, **17** (1994), 773.
36. J. M. Finney and C. Laird, *Phil.Mag.*, **31** (1975), 339.
37. B. Šestak and N. Zárubová, *Phys.Stat.Sol.*, **10** (1965), 239.
38. V. Vitek, *Proc. R. Soc. Lond. A*, **352** (1976), 109.
39. S. Suresh, *Fatigue of Materials*, p.43, Cambridge University Press, Cambridge (1991).

Chapter IV

Strain Burst Phenomena in Cyclically Deformed Single Crystals

4.1. INTRODUCTION

It has been recognized that some kinds of single crystal specimens fatigued often show "strain burst" phenomena. These strain bursts were explained by the dissociation of dipoles and subsequent dislocation avalanches [1], and the multiplication of slip bands activated by internal stress field [2]. The burst phenomena were reported in copper [1], aluminum, silver, gold, lead, magnesium, zinc, cadmium [3], αCu-Al alloy [2,4,5] and αCu-Zn alloy [6] single crystals to the best of our knowledge. On the basis of the above dislocation mechanisms, it is also feasible that the strain burst occurs at cyclically-deformed b.c.c. single crystals. Since the dislocation mechanism proposed for the strain burst is a localized and dynamical phenomenon, a direct TEM observation seems to be difficult. Hence, it can be effective to measure several parameters characterizing a cyclic response, for the further understanding of the dislocation mechanism occurring at strain burst.

Cyclically-deformed b.c.c. single crystals often show the "stress asymmetry": the cyclic stress amplitudes in tensile and compressive are different [7-11]. Such a stress asymmetry has been believed to be due to an asymmetric motion of a screw dislocation which is shear-stressed along a {1 1 2} plane [12,13]. Aside from the stress asymmetry, in a series of the strain-controlled experiments [2,5,6], relatively huge changes in the stress amplitude have been regarded as the strain burst. However, it is no wonder that the dipole dissociation, which was proposed for the strain burst, occurs locally within the cyclically hardening materials. Such a microscopic burst occurrence reflecting the dislocation structure is expected to give rise to a certain change in both of stress and plastic strain amplitude. We have actually found out that magnitude of these instabilities varies during experiment in an austenitic stainless steel single crystal [14].

It has been shown that hysteresis loop shape estimated by the Bauschinger energy parameter is related closely to the cyclic deformation process [15]. Likewise, we can image operative dislocations

and dislocation distribution during an experiment by measuring the stress asymmetry and the instability of stress amplitude. In the present study, Fe-30%Cr alloy single crystals (b.c.c. lattice) were cyclically deformed under the plastic strain control. The present authors attempt to understand the structural change with a help of some parameters such as the mentioned stress asymmetry, especially at the huge strain bursts.

4.2. EXPERIMENTAL PROCEDURE

The motion of screw dislocations along the {1 1 2} plane should be attributable to the stress asymmetry as referred in the Section 1. In order to examine the relative contribution of screw dislocations to cyclic plastic deformation, it is desirable to choose a specimen tensile axis that produces a large difference in the stress amplitude between tensile and compressive straining. A specimen having a {1 1 2} <1 1 1> primary slip system may show such a large stress asymmetry [12]. At a tensile axis near <1 4 4> or <1 1 8>, the Schmid factor of the {1 1 2} <1 1 1> system becomes a maximum value. But, b.c.c. single crystals are frequently fractured by cleavage at lower temperature, when the tensile axes are oriented close to <0 0 1> [16-19]. Moreover, a ratio of the Schmid factors between the primary {1 1 2} <1 1 1> system and secondary one is lower at the <1 4 4> tensile axis than that at the <1 1 8>. For these reasons, we employed the <1 4 4> tensile axis; both (1 1 2) normal and $[\bar{1}\ \bar{1}\ 1]$ direction are inclined to the tensile axis at about 45°. The slip geometry of the $(1\,1\,2)[\bar{1}\ \bar{1}\ 1]$ system is illustrated in Fig.4-1. Single crystals were grown by the Bridgman method from an Fe-30wt.%Cr alloy. The specimens were cut from the single crystal to have a gauge shape of square cross section of 1.5×1.5 mm^2 and length of 4 mm. For direct observation of slip step of the $(1\,1\,2)[\bar{1}\ \bar{1}\ 1]$ system, the $[\bar{1}\ \bar{1}\ 1]$ was oriented to a direction between surface axis and tensile axis. The specimens were annealed at 1373K. Surfaces of the specimens were mechanically and electrolytically polished to obtain a mirror-like surface.

The cyclic deformation test was carried out in air at room temperature in a servo-hydraulic machine. Strain of the specimen was measured with a strain gauge that was cemented to the reverse side of surface. In most of conventional cyclic experiments under a constant plastic strain control, a strain rate was very fast at an elastic part of hysteresis loop. Such a fast strain rate can induce the cleavage in b.c.c. alloys [20]. To

avoid this cleavage, the present cyclic deformation tests were performed at a constant total strain rate of $1\times10^{-3}s^{-1}$. Total strain amplitude was automatically regulated at every half cycle in order to maintain the plastic strain amplitude constant. During the experiment, the specimen surface was observed by an optical microscope with a Nomarski differential interferometer.

For the purpose of detailed analysis of the cyclic stress-strain response, hysteresis loops during the test were stored into magneto-optical (MO) disks through an analogue-to-digital (A/D) converter with 12-bit resolution. During the time period corresponding to ten cycles, these signals were recorded as one data file; each data file contained sequential at least 9 hysteresis loops. A sampling rate was determined so as to obtain one hundred data of both stress and strain for each one cycle. We averaged stress amplitudes of the complete 9 cycles for indication in a cyclic hardening diagram. In addition, shape of hysteresis loop was evaluated using the Bauschinger energy parameter β_E which is given by Eq.4-1[15].

$$\beta_E=\frac{4\sigma_a\varepsilon_{pl}-\oint_{loop}\sigma\ d\varepsilon}{\oint_{loop}\sigma\ d\varepsilon} \qquad (4\text{-}1)$$

where σ_a is the stress amplitude of the hysteresis loop and ε_{pl} is the plastic strain amplitude.

For the quantitative estimation of the delicate changes of stress amplitudes, we calculated the standard deviation of the stress amplitude S_σ for each data file from Eq.4-2.

$$S_\sigma=\sqrt{\sum_{i=1}^{n}(\sigma_{a,i}-\bar{\sigma}_a)^2/n} \qquad (4\text{-}2)$$

where $\sigma_{a,i}$ is the stress amplitude of each loops, $\bar{\sigma}_a$ is the mean stress amplitude, and n is the number of the sequential cycles (n=9 in the present study).

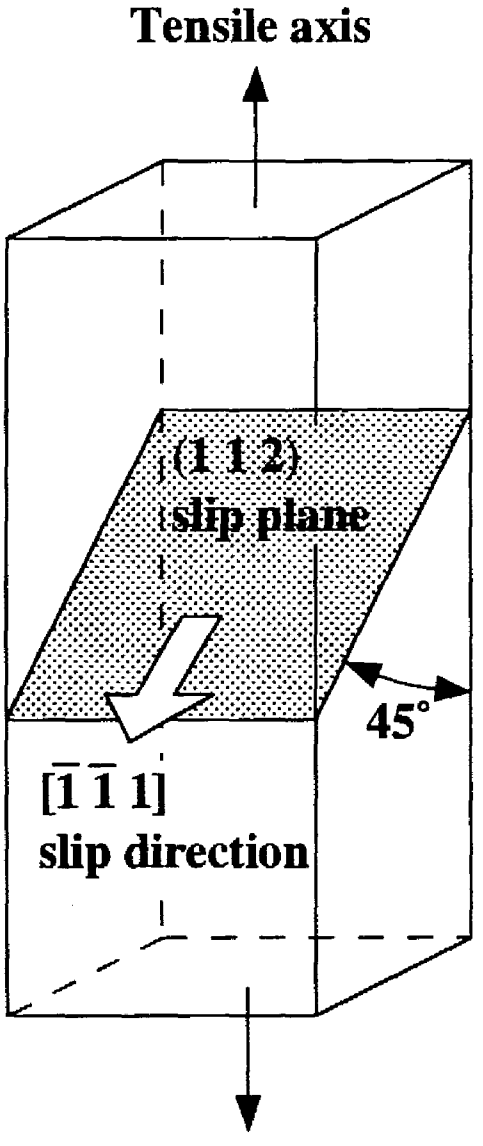

Fig.4-1 Schematic illustration of slip geometry of the specimen tested.

4.3. RESULTS AND DISCUSSION

4.3.1 *Cyclic Hardening, Stress Asymmetry and Bauschinger Energy Parameter*

Figure 4-2 shows cyclic hardening curves of tensile and compressive regions under a constant plastic strain amplitude ε_{pl} of 2×10^{-4}. Stress amplitudes of both tensile and compressive regions seem to increase monotonically with increasing cycles. The hardening curves are similar to those observed in the Fe-13.6%Cr alloy single crystals [21]. However, some sudden reductions in stress amplitude were found as indicated in small windows embedded in Fig.4-2. These stress reductions occurred simultaneously at both tensile and compressive regions. Such a phenomenon of stress reduction is very analogous to the strain bursts which have been found in the αCu-Al [2,5] and αCu-Zn [6] alloy single crystals fatigued under strain control, thus the observed stress reduction occurring in the present Fe-30%Cr alloy can also be taken as the strain burst. A huge burst that can be noticed in cyclic hardening curve like Fig.4-2 was never recognized in the specimens deformed at ε_{pl} of larger than 5×10^{-4}. Hence, we will deal with the results only at $\varepsilon_{pl}=2\times10^{-4}$ in the present paper.

The observation with the optical microscope revealed that distinct slip lines of about twenty in number appeared at the specimen surface from the beginning of the experiment. Most of them were arranged along the (1 1 2) plane as predicted in Section 4.4.2. The number of these slip lines and individual thickness seemed to be unchanged throughout the experiment. With a careful observation of the specimen surface, many diffused slip lines were recognized between the distinct slip bands. However, it was difficult to confirm these development during the experiment using the optical microscope.

The stress amplitudes of tensile region were certainly higher than that of compressive region in the present specimens. It has been established that the yield stress under monotonic deformation [12] and

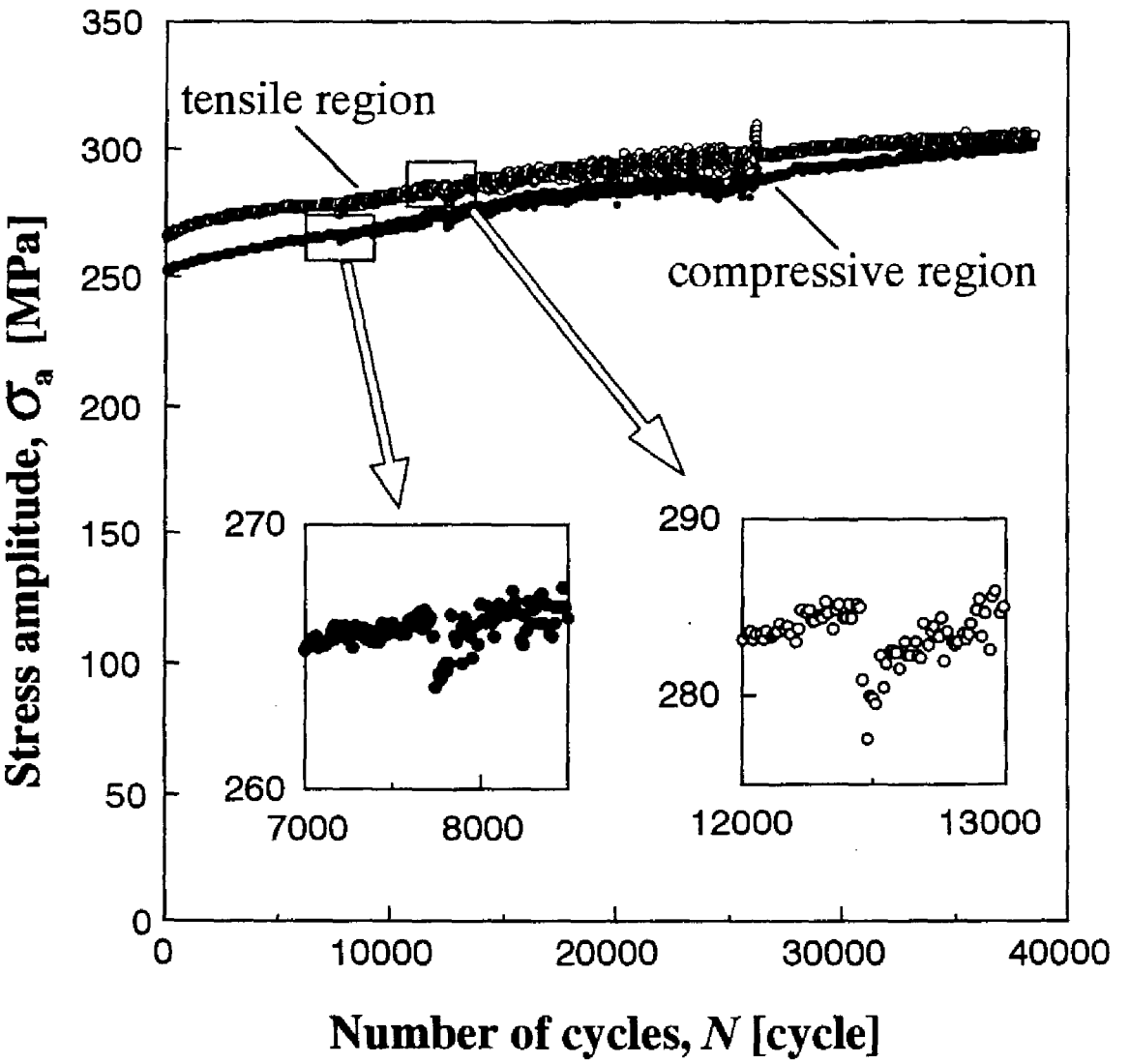

Fig.4-2 Cyclic hardening curves of both tensile and compressive regions under a plastic strain amplitude ε_{pl} of 2×10^{-4}.

the peak stress under cyclic deformation [7] become higher when an operative {1 1 2} plane is sheared to the "anti-twinning" direction, with compared to the stress under the shearing to the "twinning" direction. In the present specimens, tensile axial stress produces the anti-twinning shear on the (1 1 2)[$\bar{1}$ $\bar{1}$ 1] primary system. Therefore, the observed stress asymmetry is consistent with the referred asymmetric motion of a screw dislocation.

Figure 4-3 shows the difference in stress amplitudes between tension and compression, which is normalized by an average stress amplitude of them. An approximate value of the stress asymmetry decreased with increasing cycles, whereas large scatters were locally seen. Such a transition of the stress asymmetry during experiment has not been reported as far as we know. The cyclic hardening in iron single crystals [22] has been attributed to the increase in an internal stress (athermal stress) τ_G which is given by Eq.4-3; the increase in dislocation density $\rho$is believed to cause the cyclic hardening primarily.

$$\tau_G = \alpha G b \sqrt{\rho} \qquad (4\text{-}3)$$

Here α a constant related to dislocation arrangement, G the shear modulus and b the Burgers vector. According to Eq.4-3, the dislocation density of the present specimen must be low in the early stage, where the stress amplitude was low. Now we consider the mobility of dislocations in b.c.c. crystals. Plastic deformation of b.c.c. crystals is characterized partly by lower mobility of screw dislocations at low-temperature regime, where temperature is lower than the "athermal" temperature T_0. For the Fe-26%Cr alloy single crystals, the T_0 was measured to be about 330K at a strain rate of $1\times10^{-3}s^{-1}$ [8]; a room temperature is probably included in the low-temperature regime also of the Fe-30%Cr alloy. The lower mobility of screw dislocations has been found in the form of dislocation loops elongated to a primary slip vector, in both monotonic [23,24] and cyclic deformation [22]. Hence, edge dislocations should move preferentially during plastic deformation.

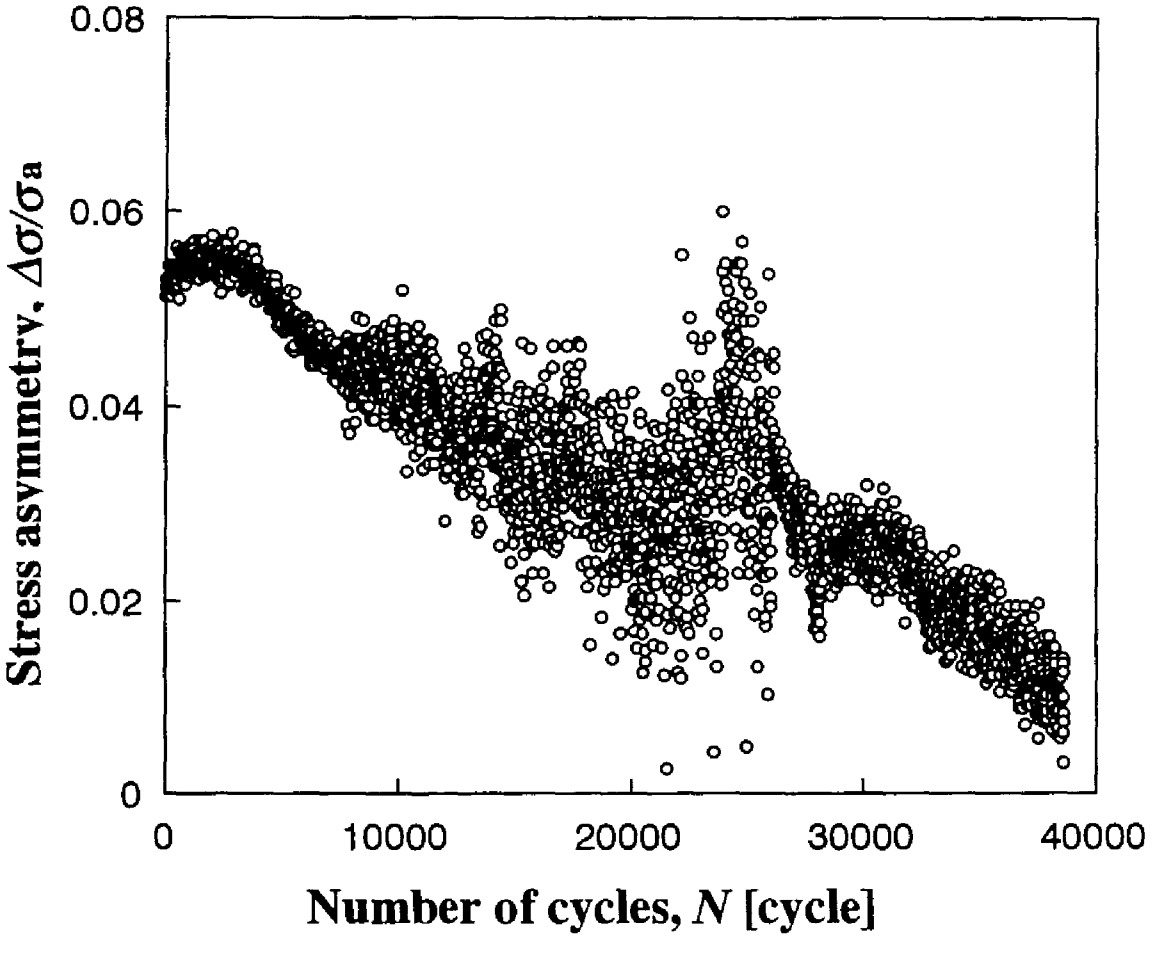

Fig. 4-3 Change in the stress asymmetry during cyclic deformation. The stress asymmetry is defined as the difference in stress amplitude between tensile and compressive regions, which is normalized by an average stress amplitude of them.

However, these movements can be stopped readily at various barriers, because of the increasing elastic interaction between edge dislocations. If the dislocation density is low, each dislocation has to move for longer distance so as to accommodate the applied plastic strain amplitude. In such a situation, contribution of the screw dislocations to plastic deformation should be enhanced. Accordingly, the higher stress asymmetry —— this is associated closely with the screw dislocation motion on {1 1 2} plane —— can be interpreted at the early fatigue stage. On the other hand, the mobile-dislocation density would increase in the later stage of experiment, thus relative contribution of the screw dislocation may be reduced. The decreasing stress asymmetry with cycles can be explained by the decreasing screw dislocation motion.

Change in hysteresis loop shape is estimated using the Bauschinger energy parameter β_E (Fig.4-4). At least three sudden changes (indicated as I, II and III in the figure) appeared during the cyclic deformation test, and were more prominent phenomena than those of stress amplitude described above. The β_E value tends to increase with increasing cycles on the whole except for these sudden changes.

Flow stress of materials can be divided into two contributions; an athermal component τ_G and a thermal component τ^*, from the view point of temperature dependence of yield stress and work hardening [25]. In the cyclic deformation test, the athermal elastic stress τ_G can correlate with a back stress produced by long-range elastic interaction between dislocations, but the thermal stress τ^* should act frictionally. The β_E value represents a recoverability of stored deformation energy during cycling [26]; a reversible dislocation motion helped by the back stress results in the higher β_E value. The irreversible dislocation motion during cycling is caused by several factors such as a large frictional stress, a cross slip and a cutting of dislocations. It is now well established that for b.c.c. metals the most important factor leading to the value of τ^* is the thermally activated motion of screw dislocations [27]. The large Peierls stress of a screw dislocation sheared along

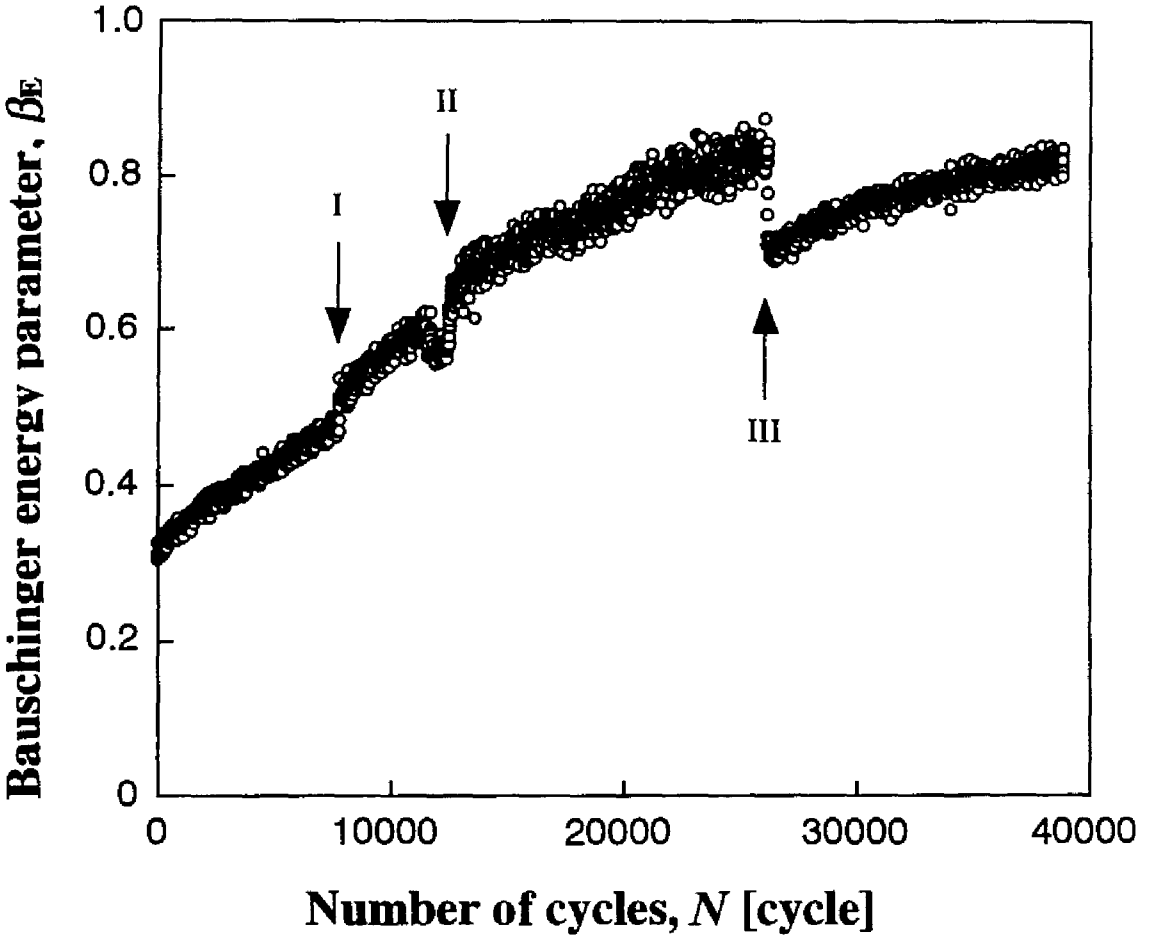

Fig.4-4 Change in the Bauschinger energy parameter β_E under ε_{pl} of 2×10^{-4}. Symbols of "I", "II" and "III" indicate the occurrences of rapid change in the β_E value.

{1 1 2} was also calculated using an atomic simulation [13]. Since the screw dislocations in b.c.c. metals show the cross slip and the higher frictional stress as referred in above, the recoverability of cyclic deformation presumably decrease with increasing relative contribution of the screw dislocations. Accordingly, the interpretation of the gradual increase in the β_E value can be done in terms of the decreasing relative contribution of screw dislocations to cyclic plastic deformation. This is compatible also with the gradual decrease in the stress asymmetry (Fig.4-3).

4.3.2 *Correlation of Changes in Each Parameter at Strain Burst*

In addition to the sudden reductions in the cyclic hardening curve (Fig.4-2), the β_E value changes rapidly as clearly seen in Fig.4-4. Such sudden changes imply the occurrence of discontinuous transition of internal deformation mechanism. The authors attempted to understand the change in the deformation mechanism accompanying the burst phenomena, with the help of the variations in the stress amplitude, the stress asymmetry and the Bauschinger energy parameter.

Figure 4-5 shows the correlation between individual sudden changes in the parameters, enlarging the vicinity of Position I (which is marked in Fig.4-4). The sudden increase in the β_E value coincides obviously with the reduction of the stress amplitude. After the huge burst at Position I, the specimen experienced a very rapid hardening stage and then the stress amplitude reverted to the previous value within a few hundred cycles. The rapid hardening after the burst was also seen in the previous literatures [2,5]. On the other hand, the β_E value remained higher than that before the burst. The stress asymmetry scattered largely after the burst, and an approximate value became lower. The appearances of new slip band at the strain burst were not recognized using the optical microscope unlike the αCu-Al [2] and αCu-Zn [6] alloys.

Let us consider the internal dislocation mechanism occurring at the Position I. The present specimen should contain the bundles of edge dislocations, which have been actually observed in cyclically-deformed Fe-13.6%Cr [21] and Fe-26%Cr alloy single crystals [9]. Such a stable dislocation configuration can grow into an obstacle against the motion of free dislocations, and surely contribute to the cyclic hardening. Neumann [1] has proposed that the huge strain burst is attributed to the dissociation of such stable dipoles. Also in the present study, the reduction in stress amplitude can be attributed to a rapid increase of mobile dislocations that were released by the local dissociations of the dipoles. This sudden increase in mobile dislocation density is supported also in αCu-Al alloy [2]. If the free edge dislocations are trapped

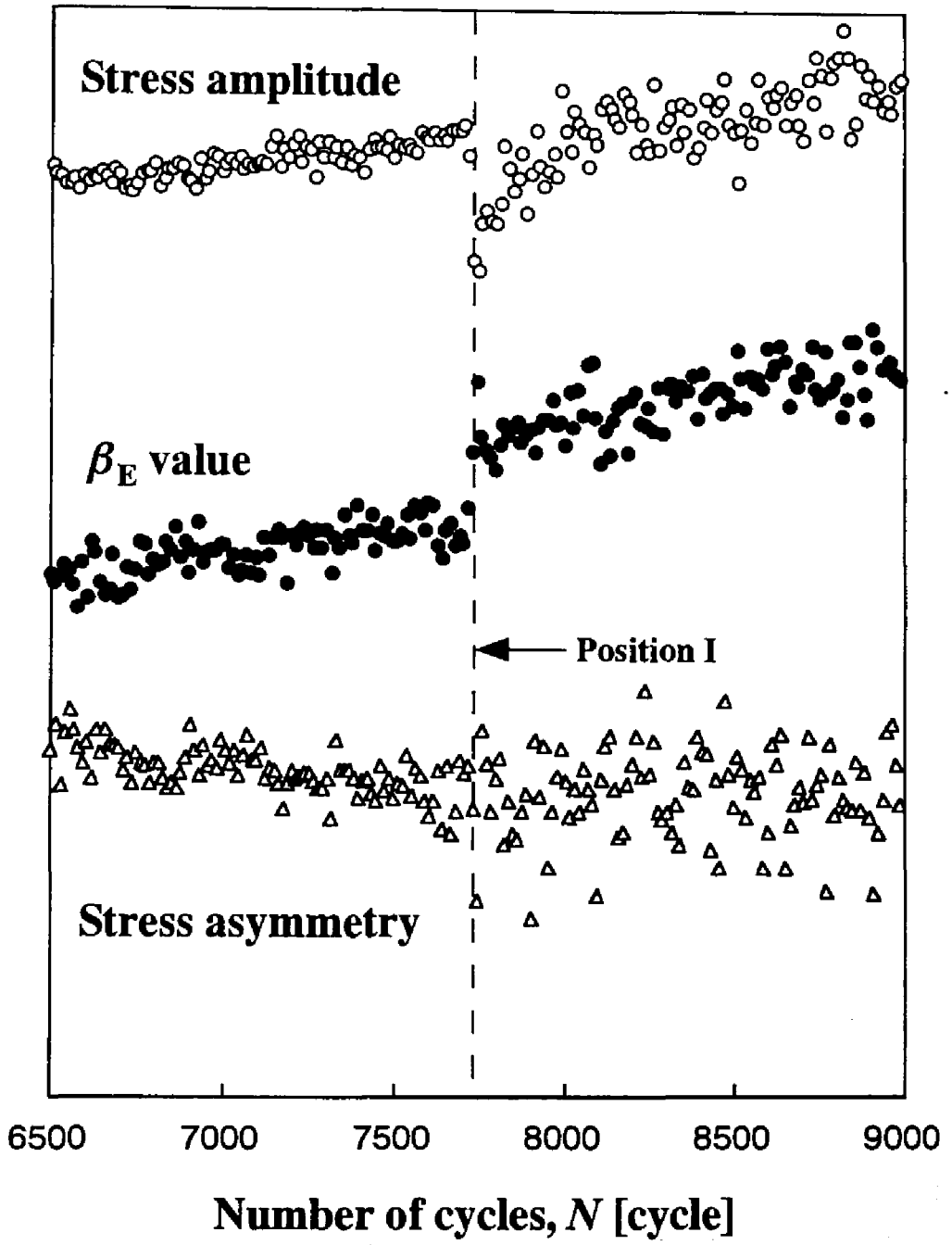

Fig.4-5 Details of the changes in each parameter at the Position I

resulting in the dipole formation, activities of the edge dislocations are relatively reduced. One can consider that the trapped edge dislocations are released by the occurrence of the strain burst; the movement of edge dislocations suddenly increases within a slip band where the burst occurs. This model of edge dislocation avalanche is compatible with the observed change in the stress asymmetry and in the β_E value at Position I. Both of the decreasing stress asymmetry and the increasing β_E value can be explained by the reduced movements of screw dislocations. This is because the screw dislocation motion on {1 1 2} plane should give rise to both the stress asymmetry and irreversible deformation process as referred above. The burst phenomenon at Position II is also understood in terms of the same dislocation mechanism.

After Position I, the scatters of the stress amplitude, the β_E value and the stress asymmetry became larger. The characteristic shape of cyclic hardening curve like "saw teeth" were locally observed as shown in Fig.4-6. The specimen sometimes hardened very rapidly during this period: its cyclic hardening rate reached up to 2.0×10^{-2} MPa/cycle as indicated in Fig.4-6 in comparison with an average hardening rate of 8.8×10^{-4} MPa/cycle. The change in the β_E value appears to have a certain correlation with that of the stress amplitude. The stress asymmetry scattered significantly, thus its correspondence to another parameter was unclear for the relatively small stress fluctuations shown in Fig.4-6 unlike the huge burst at Position I. The cyclic hardening curve of Fig.4-6 can be divided into short stages which are indicated by "A" to "E". The stress amplitude began to increase rapidly from Position A. On the other hand, the beginning of the decrease in the β_E value was found to be at Position B, even though the stress amplitude continued to increase. At Position C, the reduction in stress amplitude and the increase in β_E value occurred simultaneously. These changes are identical to those occurring at the Position I. Thereafter, similar process of these changes were repeated. The stress amplitude rapidly increased from Position C to E, again. The β_E value attained a local

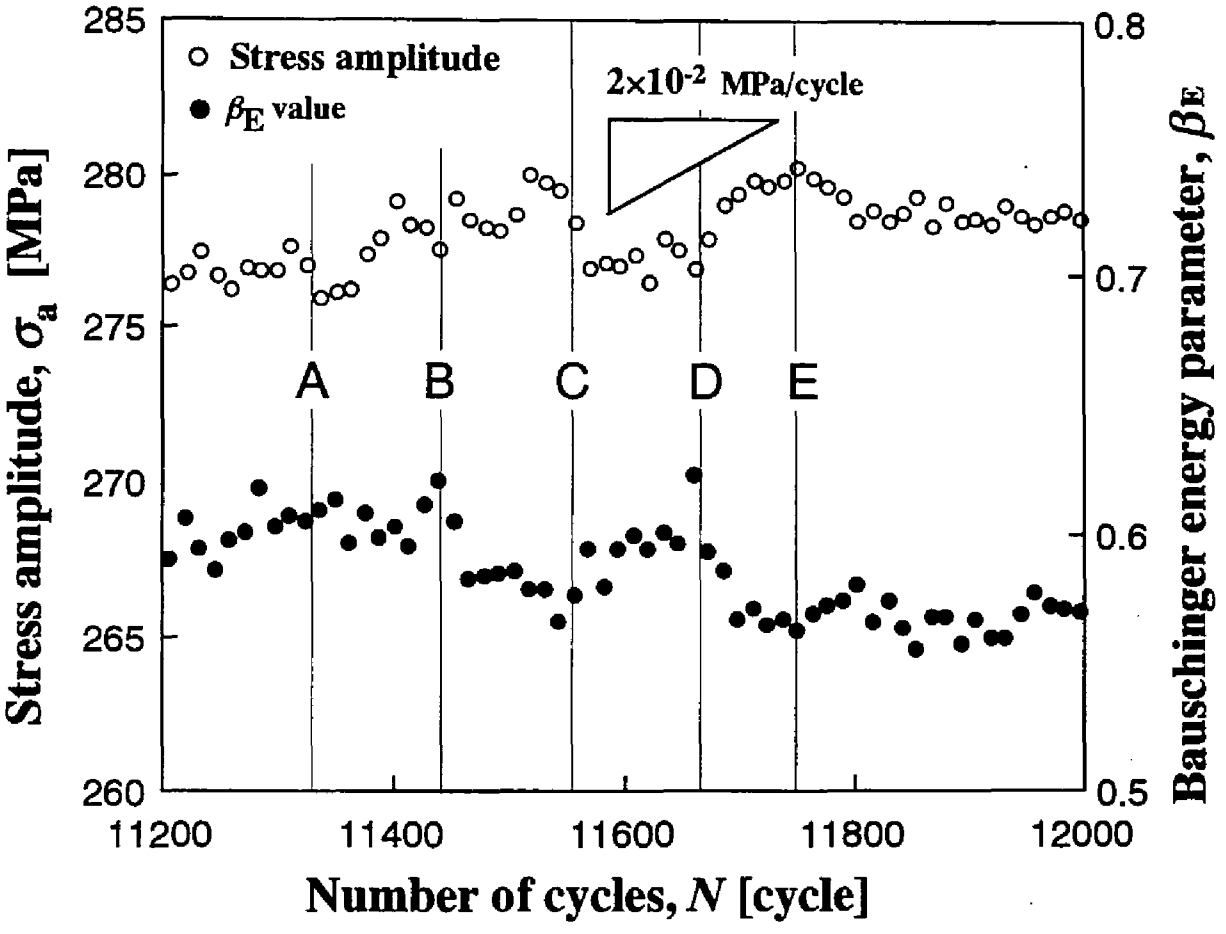

Fig.4-6 Observed fluctuations of stress amplitude and correspondent change in the β_E value.

maxima at Position D as well as that at the Position B.

Cyclic hardening behavior is usually ascribed to the development of dislocation substructure that gives the increase in dislocation density and/or the formation of strong obstacles against the dislocation motions. It is probable for the rapid hardening that the multipole or tangles of dislocations are formed on the path of mobile dislocations. It is worth to note that the β_E value began to decrease at Positions B and D while the specimen continued to harden. This fact supports the rapid hardening caused by the postulated obstruction against edge dislocation movements, because the compensational increase in screw dislocation motion can give rise to the reduction of the β_E value.

Position III showed different changes in stress amplitude and in the β_E value: the stress amplitude revealed steep increase and subsequent decrease, and the β_E value decreased rapidly as shown in Fig.4-7. The rapid cyclic hardening can be understood in the same manner which is discussed about Fig.4-6. The stress amplitude decreased not suddenly unlike the strain burst, but gradually within some hundred cycles. The β_E value also showed gradual transition. These slower transitions and the opposite change of the β_E value suggest that the rapid changes at Position III are not due to the sudden dissociations of the formed dipoles of edge dislocations. The β_E values just before Position III were very high, thus we pay attention to the hysteresis loop shape leading to such a high β_E value. Figure 4-8 shows the edge shapes of hysteresis loop before and after Position III. A difference in the edge shape is certainly visible between them, although their peak stresses are almost same. It is noticeable that before the Position III the hardening rate at the loop edge is comparable with elastic deformation at unloading: the specimen was deformed almost elastically at the loop edge. This should be responsible for the high β_E value before Position III mainly. This fact suggests that the dislocation movement including cross slip of screw dislocations were restricted at the loop edge, probably due to the formation of strong barriers against free dislocation and to a low density of mobile screw dislocations within the operative slip band. It

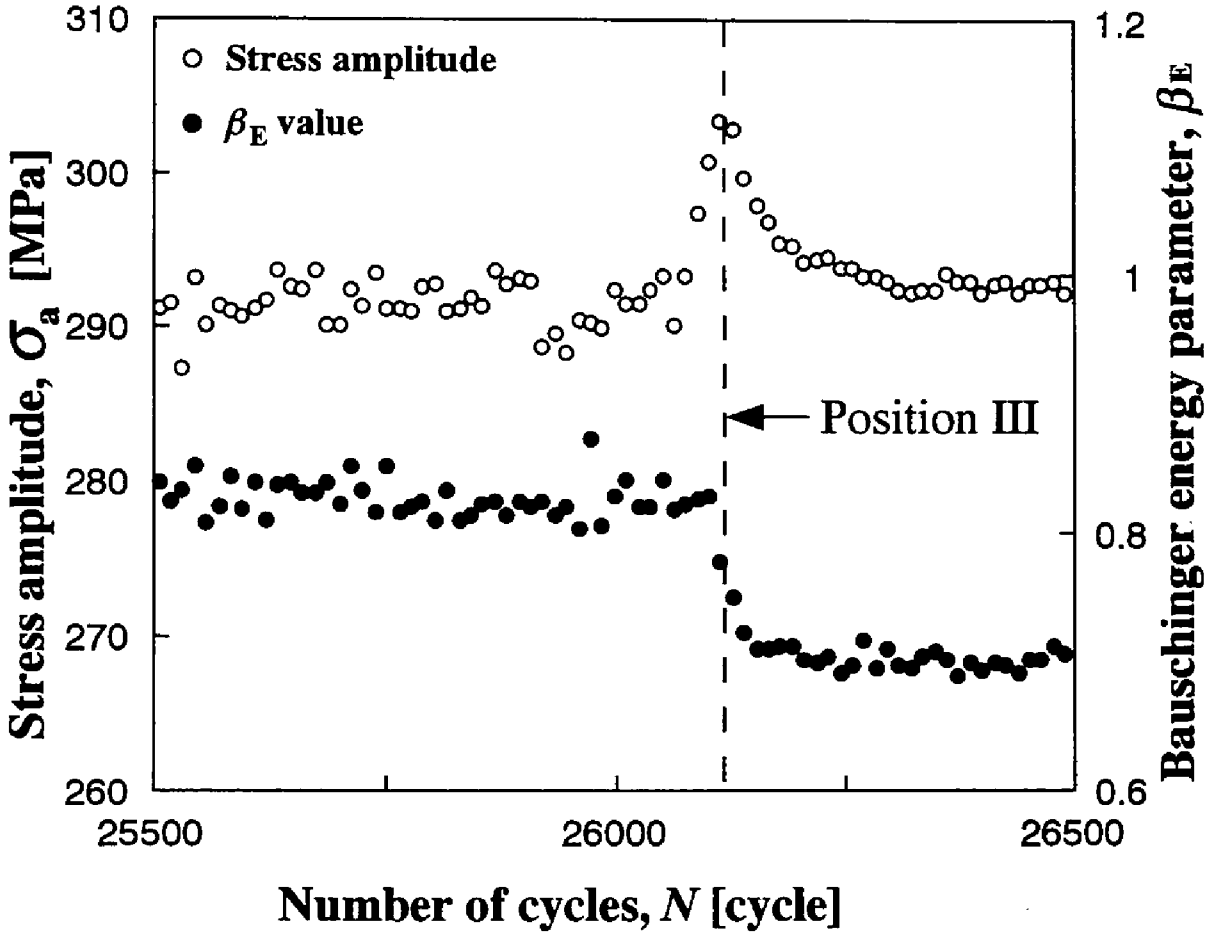

Fig.4-7 Details of changes in the stress amplitude and the β_E value at the Position III.

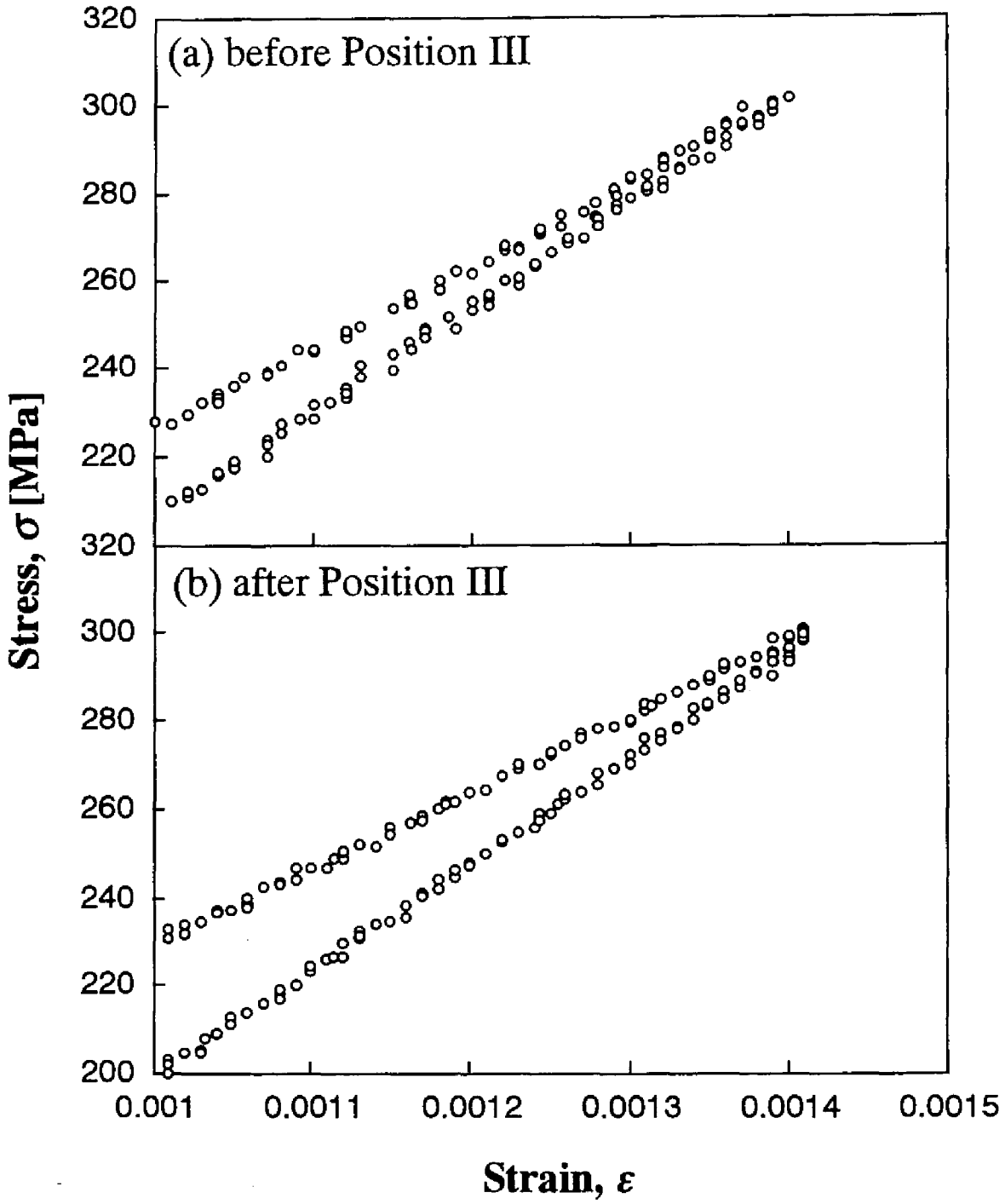

Fig.4-8 Edge shapes of hysteresis loops (a) before and (b) after the Position III.

is expected that partial cessation of the above dislocation mechanism causes the decrease in stress amplitude and in the β_E value at Position III. There are two possibilities leading to the drastic change in deformation mechanism at Position III. One is a breakdown of multipole or cell structure which is responsible for the high stress amplitude and β_E value, and the other possibility is the activation of new dislocation sources. If the release of the trapped edge dislocations is assumed, the β_E value should increase as observed at Positions I and II. In this sense, the breakdown of the strong multipoles can be eliminated from the possibilities. On the other hand, the model of the new source activation can successfully explain the change of cyclic response in the following manner. The significant increase in stress amplitude can enable the other dislocation sources to be activated. Dislocation density around the activated sources will gradually increase during subsequent cycles. Thus, it is speculated that a part of plastic strain accommodated previously by the hard slip bands is gradually replaced by the deformation of the newly activated sources. The reduction of the β_E value can also be interpretable, because the mobile-dislocation density around the newly-activated source is not enough to produce high reversibility and moreover the relative contribution of the hard slip band, which is associated with high reversibility, becomes reduced. However, the activation of new dislocation source is still doubtful, because we could not detect sudden appearances of conspicuous slip lines using the optical microscope unlike the f.c.c. single crystals [2,6]. But it was difficult to observe the development of the diffused slip lines throughout the experiment. There is a possibility that the observed surface aspect cannot reflect the local structural change in the present study correctly.

4.3.3 *Instability of Hysteresis Loop Shape*

With a careful observation of Fig.4-2, we can notice small fluctuations of stress amplitude at the middle stage of the experiment. These may be related to the frequent occurrences of small-scale strain bursts which were less conspicuous than those at Positions I and II as shown in Fig.4-5. Moreover, the magnitude of these fluctuations certainly changes with cycles. In order to estimate such a instability of hysteresis loop shape within relatively short period qualitatively, the standard deviations of stress amplitude s_σ were calculated for sequential nine cycles from Eq.4-2. Figure 4-9 shows the standard deviations normalized by the stress amplitude, indicating the presences of several stages. There are two sudden increases in the s_σ value at Positions I and II, and one sudden decrease at Position III. Since the fluctuations in Fig.4-2 are pronounced at the stage between the Positions II and III, it is likely that the large s_σ values are associated closely with the frequent occurrences of the small strain bursts. In the previous paper [14], we already described the factors that affect the magnitude of standard deviation caused by a measurement system and pointed out that these factors are unchanged during experiment. The s_σ value changed actually with cycles as shown in Fig.4-9, therefore the existence of several stages of the s_σ value should reflects the change in cyclic deformation process. As observed at Positions I and II, the decreased stress amplitude reverted to previous values within a few hundred cycles after the strain bursts. Thus, if we pay attention only to the stress amplitude like as a conventional research on the strain burst under strain control, the cyclic deformation process seems to recover completely from a structural state disordered by the strain burst. However, even after the recovery of stress amplitude, the instability of hysteresis loop shape was altered by the occurrences of the huge bursts as indicated obviously in Fig.4-9. It is apparent from Fig.4-9 that a different dislocation mechanism should govern the cyclic deformation after the huge bursts, being configurated through a reorganization of the avalanched

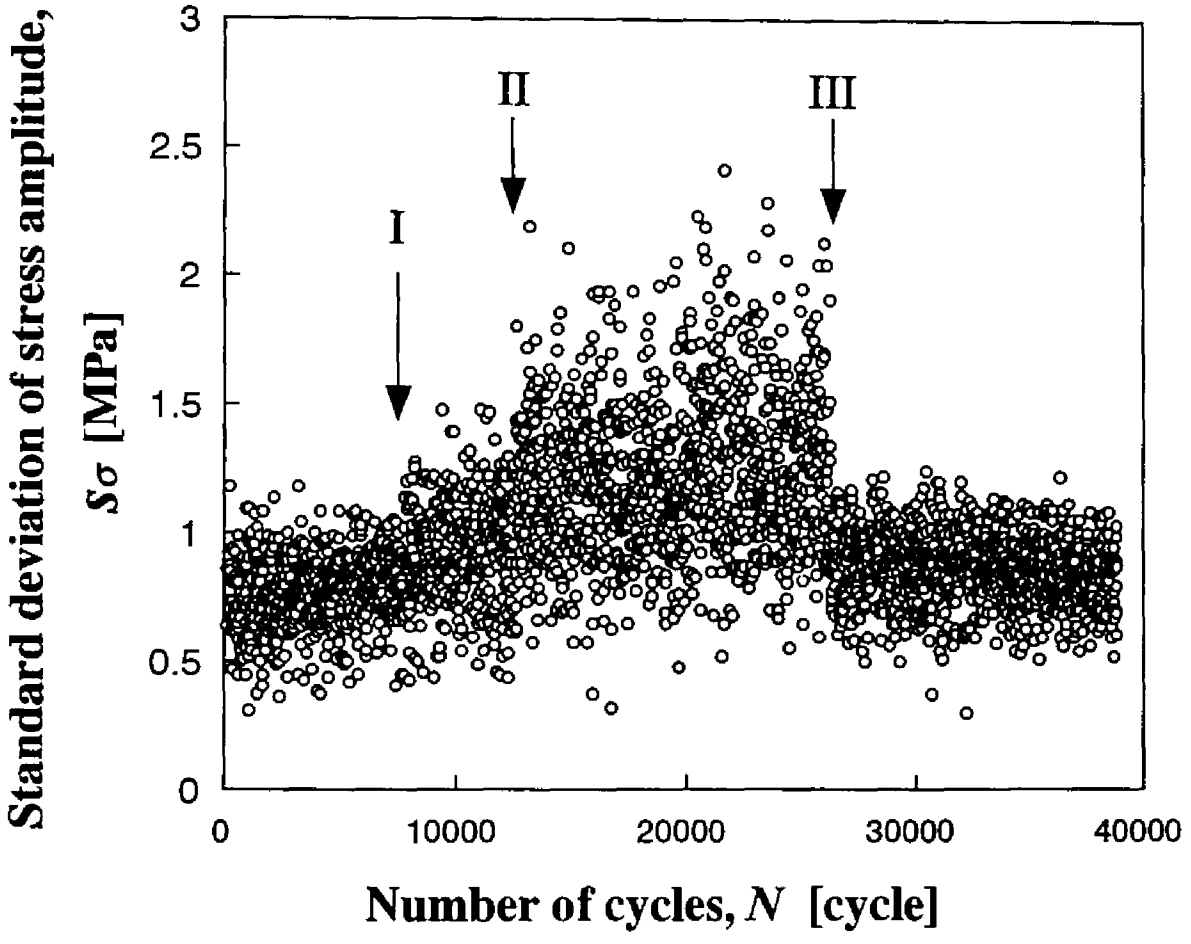

Fig.4-9 Standard deviations of stress amplitude, which are calculated for sequential nine cycles.

dislocation structure. The assumption of this structural change is supported also by the unrecoverable change in the β_E value at Positions I and II (Fig.4-4).

The distinct reasons for the sudden increases (Position I and II) and decrease (Position III) of the s_σ values are still unclear. However, one can expect the possible structural changes at each position, as described below. In the cyclically-deformed Fe-Cr [21] and Fe-Si [28] single crystals, the uniformly-distributed dislocation bundles have been observed. The huge strain bursts are probably induced by the breakdown of such a stable structure. Because the mentioned instability of hysteresis loop shape should comes from the local dissociation and reformation of multipoles, it is feasible that the reorganized structure after the huge burst contains weak dislocation bundles which can be dissociated easily. Accordingly, the huge strain burst may give rise to such an unstable dislocation distribution locally within an operative slip band. On the contrary, the stabilization of stress amplitude at the Position III can be understood by the reduced contribution of the slip bands which cause the small-scale strain bursts. This is consistent with the activation of new dislocation sources, which is argued in the Section 4.3.2.

4.4. CONCLUSIONS

From the investigation on the changes in several parameters during a cyclic deformation test, we have obtained following conclusions about the burst phenomena in Fe-30%Cr alloy single crystal oriented for the pronounced stress asymmetry.

1. Strain bursts detected as sudden reductions in stress amplitude were recognized in the Fe-30%Cr alloy single crystal.

2. At the occurrence of the huge strain burst, both of the increase in the Bauschinger energy parameter and the decrease in stress asymmetry were observed simultaneously. The changes of these parameters are consistent with the dissociation of edge dislocation dipoles, which has been proposed by Neumann.

3. In view of the permanent changes in the Bauschinger energy parameter and in the instability of stress amplitude even after the recovery of stress amplitude, it is likely that the huge strain burst can alter the internal dislocation distribution within an operative slip band.

References

1. P. Neumann, *Z. Metallkde.,* **59** (1968) 927.
2. S. I. Hong, C. Laird, *Mater. Sci. Eng.*, **A124** (1990) 183.
3. R. Neumann and P. Neumann, *Scripta Metall.*, **4** (1970) 645.
4. M. P. E. Desvaux, *Z.Metallkde.*, **61** (1970) 206.
5. A. Abel, M. Wilhelm and V. Gerold, *Z. Metallkde .*, **70** (1979) 577.
6. X. Hu, H. Margolin, X. Duan, S. Nourbakhsh, *Mater. Sci. Eng.*, **A157** (1992) 181.
7. T. Magnin and J. H. Driver, *Mater. Sci. Eng.*, **39** (1979) 175.
8. T. Magnin, A. Fourdeux and J. H. Driver, *Phys. Stat. Sol.* (a) **65** (1981) 301.
9. M. Anglada, B. Etemad, J. A. Planell and F. Guiu, *Scripta Metall.*, **14** (1980) 1319.
10. M. Anglada and F. Guiu, *Phil. Mag.* A, **44** (1981) 499.
11. M. Anglada and F. Guiu, *Phil. Mag.* A, **44** (1981) 523.
12. S. Takeuchi, E. Furubayashi and T. Taoka, *Acta Metall.*, **15** (1967) 1179.
13. V. Vitek, *Proc. R. Soc. Lond.* A, **352** (1976) 109.
14. Y. Kaneko and S. Hashimoto, *Mater. Sci. Eng.*, **A234-236** (1997), 386.
15. A. Abel, *Mater. Sci. Eng.*, **36** (1978) 117.
16. D. Hull; *Acta Metall.*, **8** (1960) 11.
17. R. Honda; *J. Phy. Soc. Japan,* **16** (1961) 1309.
18. R. M. Rose, D. P. Ferriss and J. Wulff; *Trans. Metall. Soc. AIME*, **224** (1962) 981.
19. P. Beardmore and D. Hull; *J. Less-Comm. Metals*, **9** (1965) 168.
20. H. Vehoff and P. Neumann, *Acta Metall.*, **28** (1980) 265.
21. B. Šesták, Z. Vicherková, V. Novák, S. Libovický and J. Brádler, *Phys. Stat. Sol.*, **(a)104** (1987) 79.

22. H. Mughrabi , K. Herz and X. Stark, *Acta Metall.*, **24** (1976) 659.
23. E. Furubayashi, *J. Phys. Soc. Japan*, **27** (1969) 130.
24. D. Vesely, *J. Microscopy*, **97** (1973) 191.
25. A. Seeger, *Phil. Mag.*, Ser.7, **45** (1954) 771.
26. A. Abel, *Mater. Forum*, **10** (1987) 11.
27. A. Seeger and B. Šesták, *Scripta Metall.*, **5** (1971) 875.
28. B. Šesták, V. Novák, S. Libovický, *Phil. Mag. A*, **57** (1988) 353.

Chapter V

Bicrystals Study on Effect of Grain Boundaries on Fatigue Crack Propagation Behavior

5.1. INTRODUCTION

In usual polycrystalline materials subjected to cyclic loading, a fatigue crack can be nucleated and frequently propagates along the GBs. Such an intergranular cracking sometimes plays a serious role on the fatigue strength. However, the intergranular fatigue cracking should involve many factors such as GB stucture, elastic anisotropy, plastic strain imcompatibility etc. Thus, the factors affecting the property of the intergranular crack are still ambiguous. It has been reported in nickel polycrystals [1] and copper bicrystals [2,3] that one of the criteria is the GB character which is determined by a misorientation between the neighboring crystals. A local GB oxidation that may be sensitive to the GB structure has been proposed as a dominant mechanism of the intergranular fatigue cracking [4,5].

However, it appears that the above GB damage under air environment is not so dominant to induce the intergranular fatigue cracking in a material showing high corrosion resistance. In such an environmental and material conditions, a certain criterion probably governs the occurrence of the intergranular fatigue cracking. In addition to the GB character distribution [6], another criterion should be taken into account in designing the GB possessing a high fatigue durability.

On the other hand, the GB can act as a barrier against intragranular fatigue cracking. It has been reported that an intragranular fatigue crack is grown by the processes of shear decohesion of a slip band [7 -9] or alternate slip activities of two different slip systems at the crack tip [10]. Such a propagating intragranular crack must encounter a grain boundary (GB) in a usual polycrystalline material. Retardation of the intragranular cracking has been found out in the vicinity of the GB on the coarse-grained specimen [11] and the bicrystal specimens [12,13]. This deceleration of the crack growth rate is probably related to the continuity of slip deformation between adjoining crystals at GB.

When the primary slip directions are common between the adjoining grains and are lying in the GB plane, the GB shows high frequency of

the slip continuity in comparison with an orientation relationship where the primary slip directions of the adjoining grains are not common. Lim and Raj [14] clearly showed that Σ3(111) twin boundary possessed high slip continuity in the strained nickel bicrystals having several <110> tilt boundaries. Likewise, such a high slip continuity in b.c.c. metals is expected at Σ3(112) twin boundary because this orientation relation gives a primary slip vector and a slip plane which are common between two grains. The Σ3(112) boundary has been calculated to have lower interfacial energy [15] and was contained most next to small angle boundaries in the annealed Fe-6.5%Si alloy [16]. Moreover, the mechanical twinning —— which gives rise to two Σ3(112) twin boundary between twinned region and matrix ——sometimes observed in the ferritic stainless steels [17,18].

Because an operative slip system changes with a tensile axis, an ability of the slip transfer between the grains should be sensitive to the tensile axes of two adjoining grains even at the same relative orientation relationship: there is a tensile axis where the slip system common between the grains is no longer the primary system. The purpose of the present chapter is to investigate the dependence of the operative slip vector on the crack growth retardation near the Σ3 (112) boundary. The author attempts to clarify an effect of the slip continuity on the fatigue crack growth near the GB using bicrystal specimens. Because an operative slip system changes with a tensile axis, an ability of the slip transfer between the grains should be sensitive to the tensile axes of two adjoining grains even at the same relative orientation relationship: there is a tensile axis where the slip system common between the grains is no longer the primary system

In the present study, a criterion for the occurrence of intergranular fatigue crack propagation has been investigated using two kinds of Fe-30%Cr alloy bicrystals which have the GBs almost perpendicular to loading axis. We paid attention to geometrical relationships between the preferential growth directions of intragranular cracking in adjoining grains. In order to diminish the effect of the GB structure, the GBs of

these two specimens were set to be exactly the same. Moreover, another purpose of the present chapter is to investigate the dependence of the operative slip vector on the crack growth retardation near the Σ3 (112) boundary. The author attempt to clarify an effect of the slip continuity on the fatigue crack growth near the GB using bicrystal specimens.

5.2. EXPERIMENTAL PROCEDURE

Single crystals of Fe-30wt.%Cr alloy were grown by the Bridgman method in argon using the alumina molds. Bicrystals were produced by the diffusion bonding under an appropriate compressive pressure using the single crystals with a flat and smooth bonding plane. The diffusion bonding was done in vacuum at 1373K for 200 hours. We could obtain the bicrystals with very flat GBs. We produced two kinds of the bicrystals having [1 1 0] symmetrical tilt boundaries. The angle between the [0 0 1] directions of constituent grains was about 22° and 70°, respectively.

Two kinds of the CT specimens (Bicrystals A and B) were shaped from the bicrystal of the 22° by a spark cutter. These specimens had same grain boundary. Figure 5-1 shows schematic illustrations of the bicrystal specimens and the stereographic projections of their constituent grains. The loading axes of the constituent grains were different between these specimens, but the GBs contained in them were quietly the same. Broad surfaces of both the specimens were fixed to (1 1 0) plane. Each specimen has the following crystallographic and geometrical features. (A) Both constituent grains of Bicrystal A have equivalent tensile axes of $<1\,4\,4>$. The GB plane of Bicrystal A was located normal to the tensile axis. A notch was introduced in Grain 2_A parallel to the GB. (B) Grains 1_B and 2_B of Bicrystal B were oriented to $<1\,1\,1>$ and $<1\,4\,4>$, respectively. The normal of the GB plane was inclined to the tensile axis at 22° in Bicrystal B. The notch was produced at Grain 1_B. For the comparative purpose, the single crystal specimens having [1 $\bar{1}$ 1] and [4 $\bar{4}$ 1] tensile axes were also prepared.

Two kinds of the bicrystal specimens (Bicrystals C and D) were also prepared from the bicrystal of 70°. The stereographic projection of the produced bicrystal specimens (Bicrystal C and D) are shown in Fig.5-2. According to the Brandon's criterion for the coincide site lattice (CSL) [19], the present GBs are regarded as the CSL boundary.

These bicrystals had an orientation relationship of the Σ3(112) twin boundary. The neighboring grains of the Σ3 relation have one common <111> direction, which is the slip vector of b.c.c. metals and alloys. The bicrystals were shape to compact tension (CT) specimens ($20\times 20\times 1.5mm^3$) with a spark cutter. The GB planes of both specimens are located parallel to loading axes. The <111> primary slip vectors in the Bicrystal C are common between Grains 1_C and 2_C and are lying in the GB plane as shown in Fig.5-2. The loading axes of constituent grains were controlled to be in a center of stereographic triangle. In Bicrystal D, the <111> direction common between both grains was directed to the tensile axis. Hence, the slip deformation would not occur towards the common <111> direction. In Bicrystal C, a notch was introduced along a maximum-resolved-shear-stressed plane (mrssp). Since many equivalent slip systems would be activated in Bicrystal D, the notch was introduced normal to the tensile axis.

The shaped specimens were annealed in vacuum at 1373K and then quenched in water. Prior to the fatigue test, the specimen surfaces were polished mechanically and electrolytically. In order to measure crack length, fiducial lines at surface were drawn parallel to the loading axis at a regular interval of 0.1 mm. The crack growth rate was calculated length projected to x-axis shown in Fig.5-2. The fatigue crack propagation tests were carried out in air at room temperature in a servo-hydraulic machine. Triangular cyclic load wave was applied at a frequency of 10 Hz at a load ratio of 0.1 ($=P_{min}/P_{max}$). For Bicrystals A and B, the load amplitude was gradually reduced in order to maintain a constant crack growth rate of about 10^{-8} m/cycle during the fatigue crack propagation tests. On the other hand, the load amplitudes for Bicrystals C and D were kept constant after fatigue crack initiation. The propagating fatigue cracks were observed with an optical microscope.

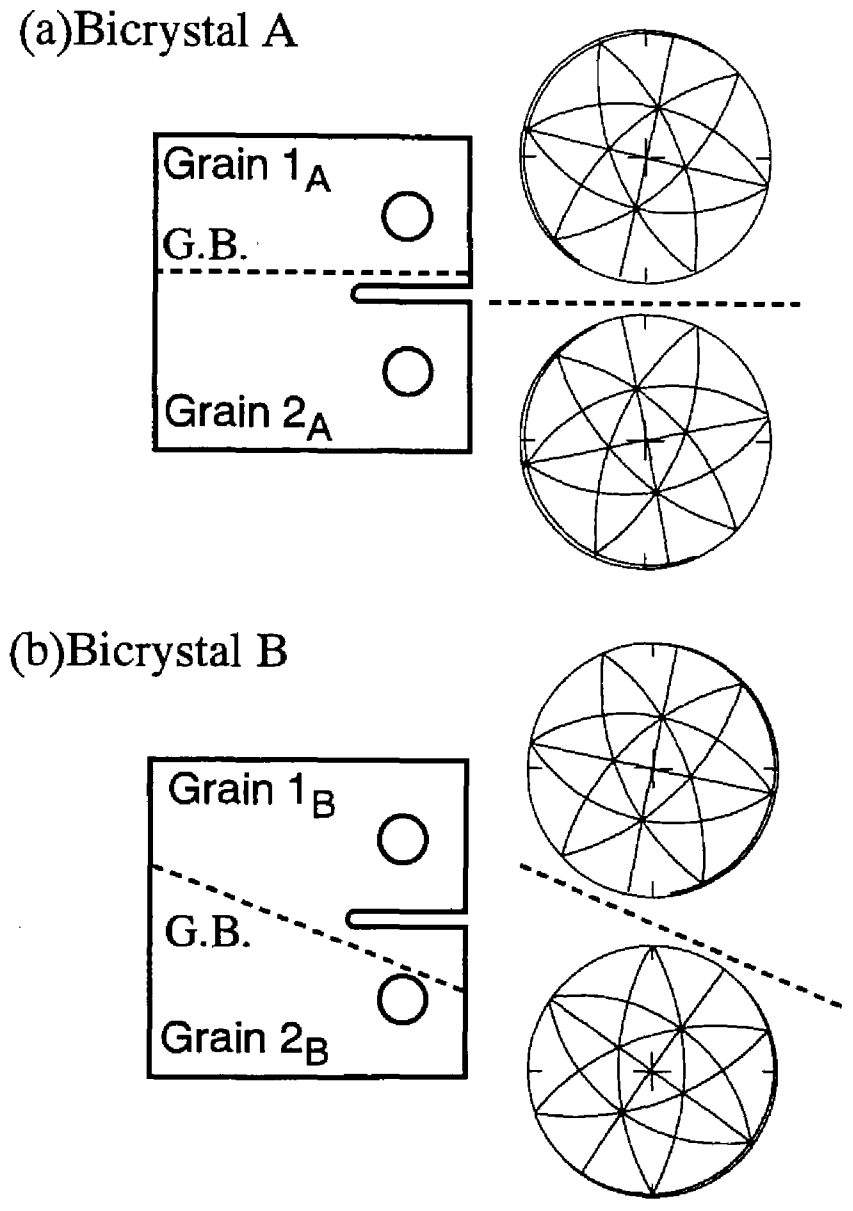

Fig.5-1 Schematic illustrations showing locations of grain boundaries and stereographic projections of constituent grains in (a) Bicrystal A and (b) Bicrystal B. Both of bicrystal specimens have the same grain boundary.

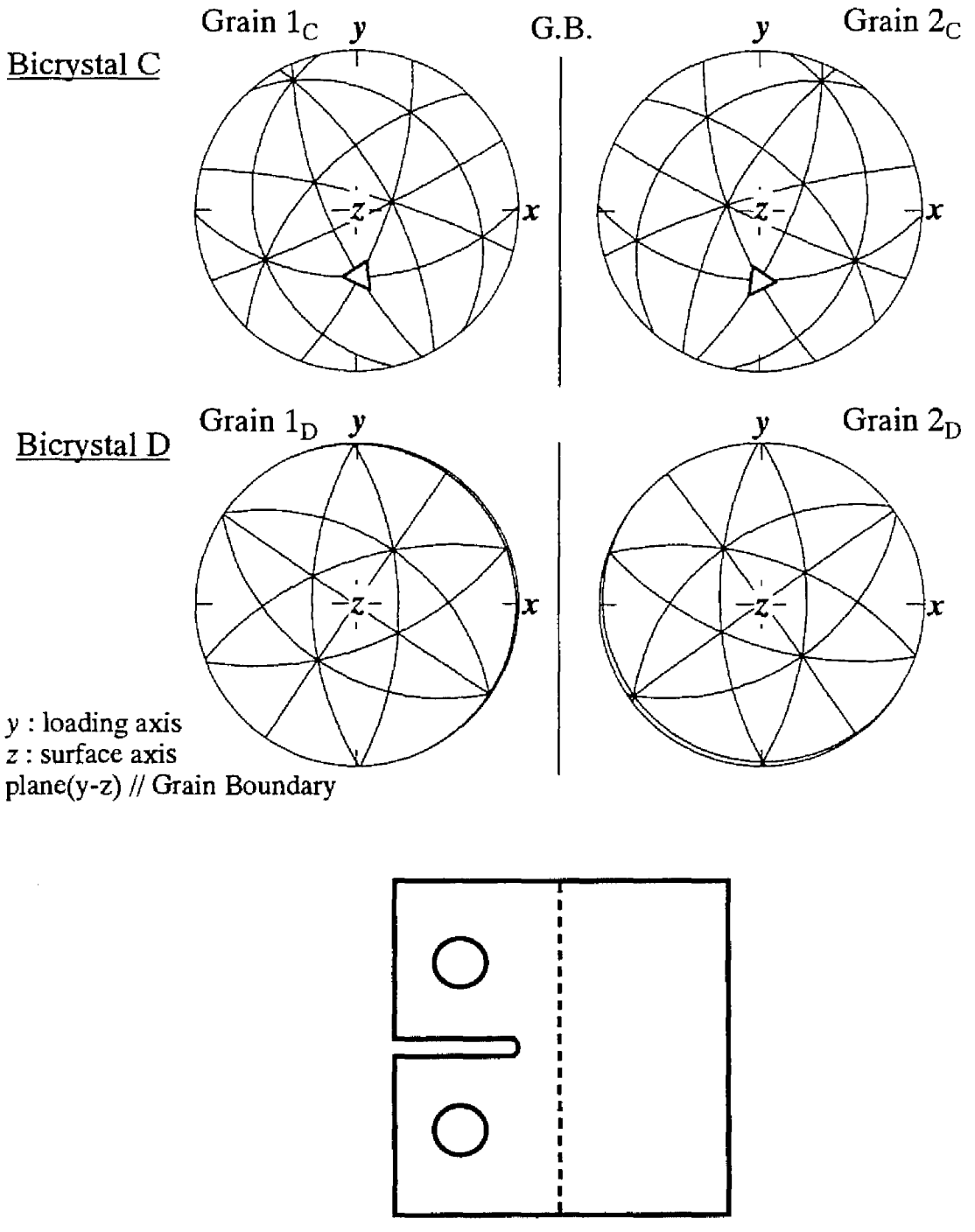

Fig.5-2. Stereographic projections of orientation and shape of Bicrytstals C and D. Open triangles in the stereographs indicate common <1 1 1> slip direction.

5.3. RESULTS AND DISCUSSION

5.3.1 *A Simple Criterion for Occurrence of Intergranular Fatigue Crack Propagation*

Figure 5-3 shows the propagating fatigue cracks in the single crystal specimens. It has been found that the intragranular fatigue in the Fe-30%Cr alloy crystals was grown along slip planes as described in Chapter 2; the shear decohesion of the slip plane was the nature of the intragranular fatigue crack growth for this material. Likewise, the present fatigue cracks in the single crystals were grown along several slip planes. We can notice that these intragranular fatigue cracks tended to propagate towards certain directions. The [1 $\bar{1}$ $\bar{1}$] cracking direction was most preferred for the [4 $\bar{4}$ 1] single crystal. The fatigue crack in the [1 $\bar{1}$ 1] single crystal was oriented to directions from [1 $\bar{1}$ $\bar{1}$] to [1 $\bar{1}$ $\bar{2}$]. This preferential direction should be determined by the geometrical relationship between the slip plane and the specimen surface, because the observed fatigue crack corresponds to an intersection of the slip plane with the broad surface.

Fatigue cracks propagated in Bicrystals A and B are presented in Fig.5-4. The intragranular fatigue cracks were initiated and propagated from the notch tips in Grains 2_A and Grain 1_B, respectively. The trace analyses of the specimens surface provide the following crystallographic features of the fatigue cracks. The fatigue crack in Grain 2_A was grown along (1 $\bar{1}$ 2) slip plane towards the [1 $\bar{1}$ 1] direction. In the same way, the (1 $\bar{1}$ $\bar{2}$)[$\bar{1}$ 1 $\bar{1}$] crack system appears to be operated in Grain 1_B, whereas a kink of the crack is locally seen. This tendency in each constituent grain agrees well with the previous results of the single crystal with the [4 $\bar{4}$ 1] tensile axis. There is no significant effect of the GBs on the cracking path in the region distant from the GBs. The Schmid factor of [1 $\bar{1}$ $\bar{1}$](1 $\bar{1}$ 2) slip system of the [4 $\bar{4}$ 1] tensile axis is almost 0.5, thus the slip bands are easy to be developed

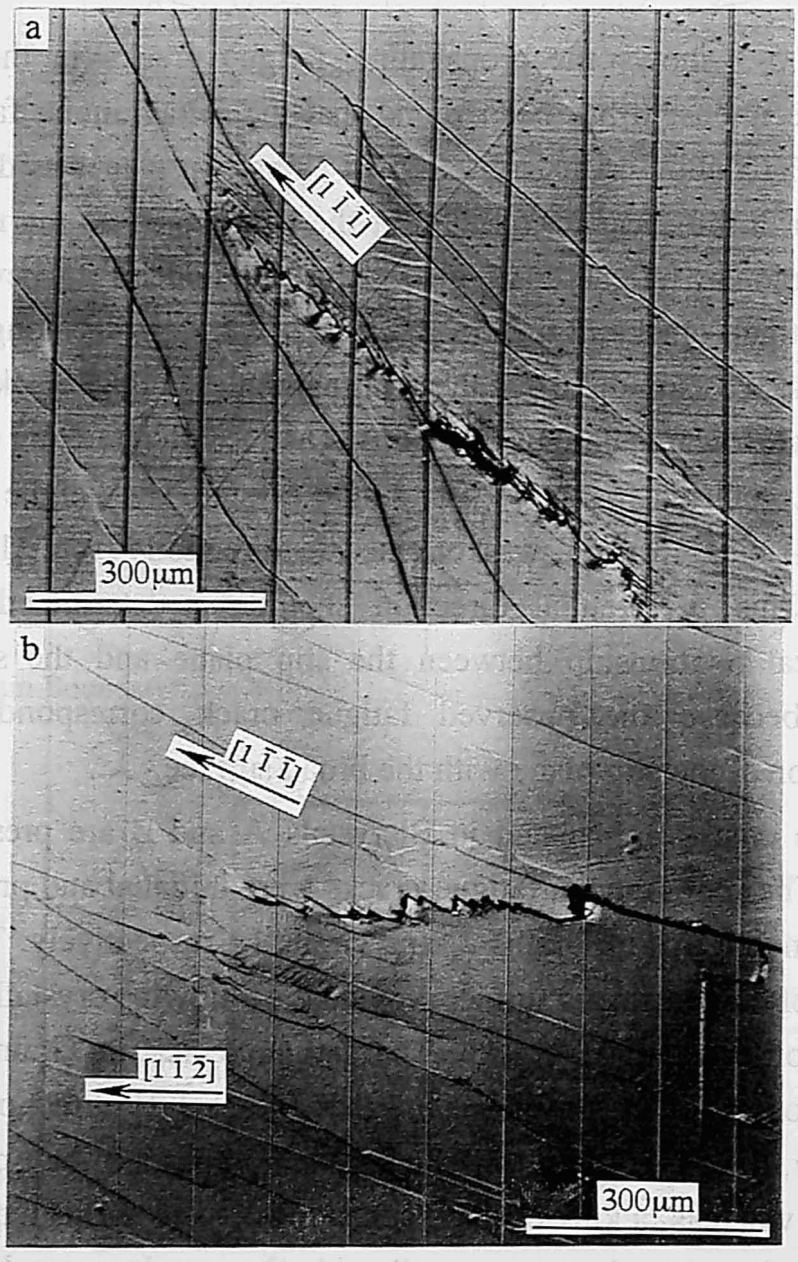

Fig.5-3 In-situ optical observation of fatigue crack propagation in the single crystals of (a) [4 $\bar{4}$ 1] and (b) [1 $\bar{1}$ 1] tensile axes.

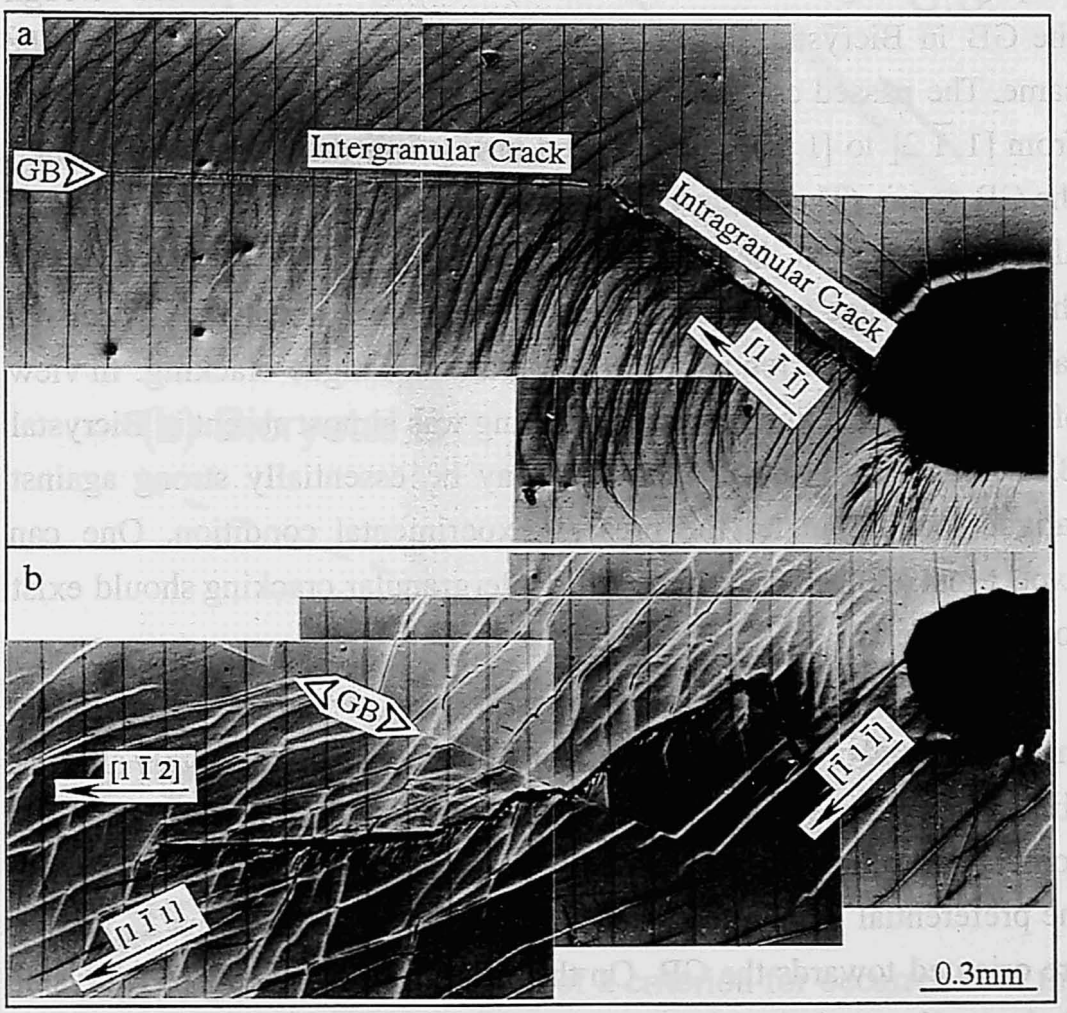

Fig.5-4 Photographs showing the fatigue cracks in (a) Bicrystal A and (b) Bicrystal B. The intergranular fatigue crack propagation was observed in Bicrystal A. On the other hand, the fatigue crack passed through the GB in Bicrystal B.

along it. Developed slip bands of this kind would be a preferred path of the fatigue crack.

In the further load cycling, these intragranular cracks reached the GBs. The behavior of the fatigue crack encountering the GBs was completely different between Bicrystals A and B. The fatigue crack in Bicrystal A was captured by the GB and subsequently continued to propagate along it. On the other hand, the fatigue crack passed through the GB in Bicrystal B, although the GBs of both bicrystals are the same. The passed crack propagated within Grain 2_B towards directions from [1 $\bar{1}$ 2] to [1 $\bar{1}$ 1] as indicated in Fig.5-4, thus never approached the GB again. (The observed crack growth directions in Grain 2_B were almost identical to that obtained in the single crystal.) This result of the crack passage suggests that the GB structure is not always a decisive factor for the occurrence of the intergranular fatigue cracking. In view of the fact that the intergranular cracking was almost absent in Bicrystal B, a structure of the present GB may be essentially strong against fatigue loading under the present experimental condition. One can expect that another criterion for the intergranular cracking should exist for this material.

It was recognized in the single crystal specimens that each grain has the preferential crack growth direction associated with the highly sheared slip system. These preferential crack propagation directions of the constituent grains are schematically shown in Fig.5-5. In Bicrystal A, the preferential crack propagation directions of both Grains 1_A and 2_A are oriented towards the GB. On the other hand, Grain 2_B of Bicrystal B shows the preferential crack propagation which is directed out of the GB, while the preferential direction in Grain 1_B is still oriented towards the GB. According to Fig.5-5, it is easy to understand that the fatigue cracks initiated in Grains 2_A and 1_B propagated towards the GB. Now we consider the intergranular fatigue cracking along the present GB. The shear decohesion of the GB plane —— which was found at Σ3(112) twin boundary [20] and will be reported in Chapter 6 ——can not be a cause of the intergranular cracking because the GB

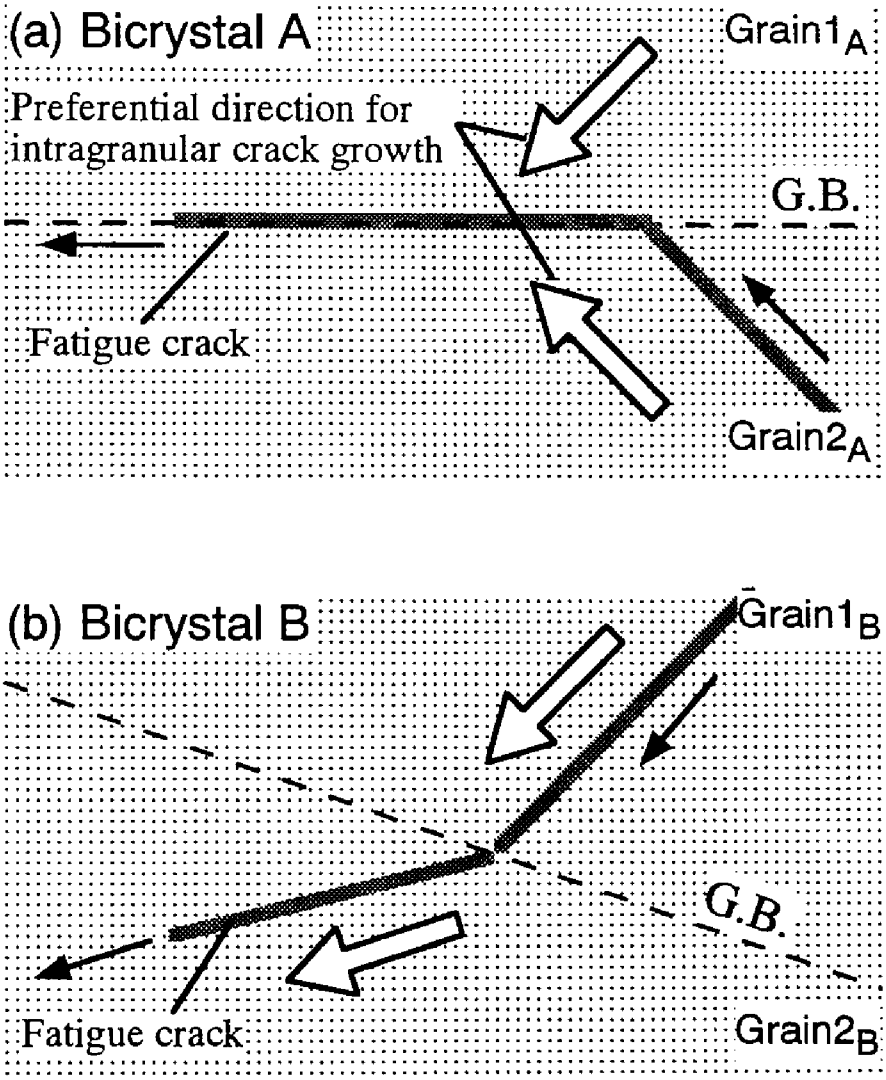

Fig.5-5 Schematic illustration of a criterion for occurrence of the intergranular fatigue crack growth ((a) intergranular crack growth and (b) crack passage through grain boundary.) Open arrows indicate the preferential crack propagation direction measured in the single crystal specimens. The microscopic crack directions of the bicrystal specimens are from right to left.

plane is approximately {1 4 4}. It has been reported that a local GB oxidation due to air environment is required for the intergranular fatigue crack growth in Fe-Si alloy bicrystals fatigued at elevated temperature [4]. However, it can be assumed for a stainless steel that the local GB damage of this kind at room temperature is minor enough to induce the GB cracking. For this reason, the passage through the GB in Bicrystal B can be interpreted. On the other hand, the fatigue crack was grown along the GB in Bicrystal A, whereas the extent of its GB damage is expected identical to that of Bicrystal B because of the same GB structure. Such a crack propagation along the GB should be understood in the following manner. As illustrated in Fig.5-5a, the slip band in Grain 1_A does not form such that the fatigue crack leaves the GB: the fatigue crack captured by GB can not leave the GB when the preferential crack directions of the neighboring grains are oriented towards the GB. The intergranular crack in Bicrystal A contained short intragranular cracks actually, but such an intragranular crack easily reverted to the GB.

5.3.2 *Relationship between Crack Propagation and Slip Continuity at the Σ3(112) Twin Boundaries.*

With increasing load amplitude, slip lines began to appear around the notch tip. Fatigue cracks were nucleated at the developed slip band. Figure 5-6 presents the fatigue cracks observed at specimen surface during the experiments. The surface observation after the fatigue experiments revealed that the fatigue cracks were grown in the manner of shear decohesion of the slip band. The fatigue crack in Grain 1 of Bicrystal C propagated along {123} plane. After the passage through the GB, the fatigue crack propagated along {123} plane of Grain 2. In Bicrystal D, the fatigue crack propagated along {112} and {123} planes with frequent changes of the cracking path.

Figure 5-7 shows relationship between crack growth rate and crack length in Bicrystals C and D. The crack growth rate in Bicrystal C increased monotonically with increasing crack length in both grains. This is consistent with the increasing stress intensity factor. Hence, it can be said that Bicrystal B showed no significant effect of the GB on the crack growth rate. In Bicrystal D, the crack growth rate also increased with the crack length on the whole. However, a local reduction of the crack growth rate was observed in the vicinity of the GB.

Due to high stress concentration at the crack tip, the fatigue crack propagation involved formation of slip lines. A general GB usually acts as a barrier against the development of such a slip line. Figure 5-8 shows the slip lines at the GBs in Bicrystals C and D. In the vicinity of the GB of Bicrystal C, many slip lines which are continuous between two grains were observed as seen in Fig.5-8. On the other hand, the slip lines in Bicrystal D were terminated at the GB. It is likely that dislocations readily passed through the GB owing to the common primary slip vectors of the constituent grains in Bicrystal C (Fig.5-2).

The intragranular fatigue cracking of the shear decohesion is assumed to involve dislocation emission from crack tip, formation of

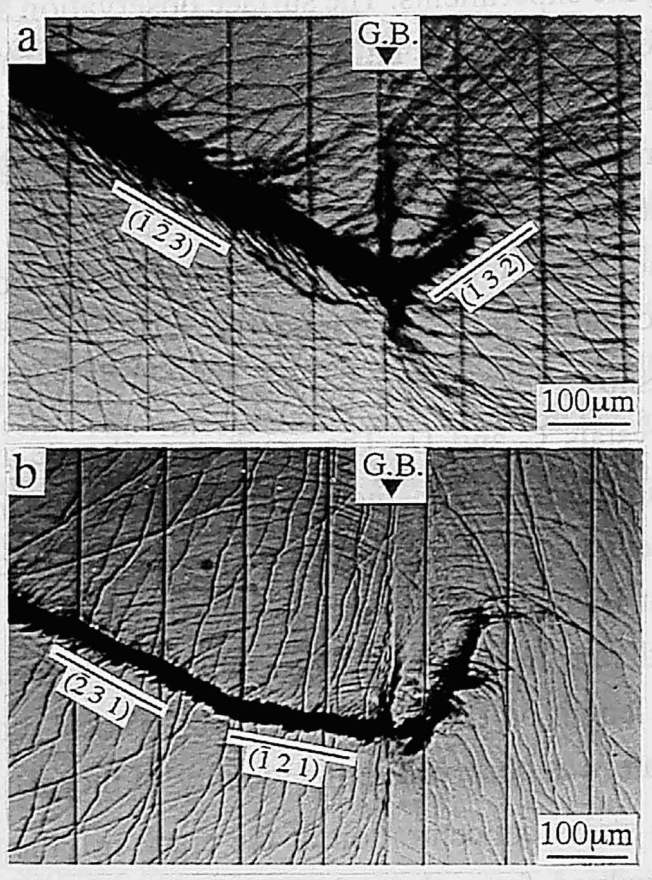

Fig.5-6. In-situ optical micrographs showing fatigue cracks traversed the grain boundary on (a) Bicrystal C and (b) Bicrystal D.

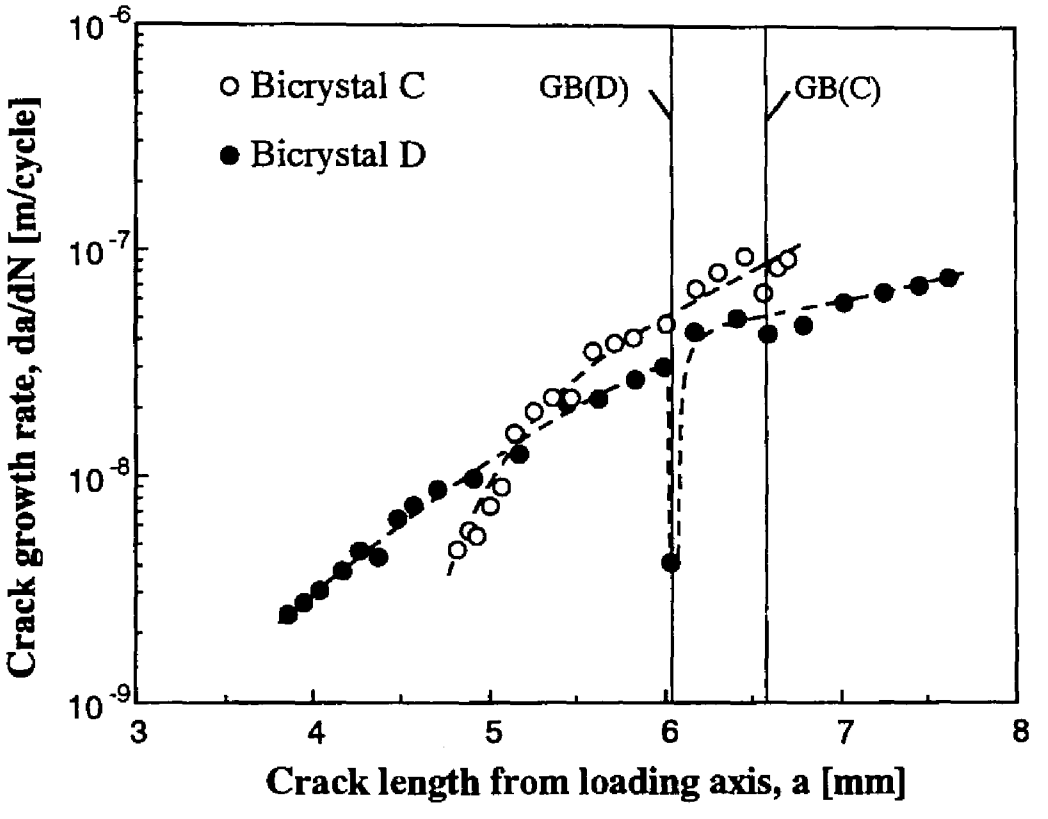

Fig.5-7 Relationships between crack growth rate and crack length in Bicrystals C and D.

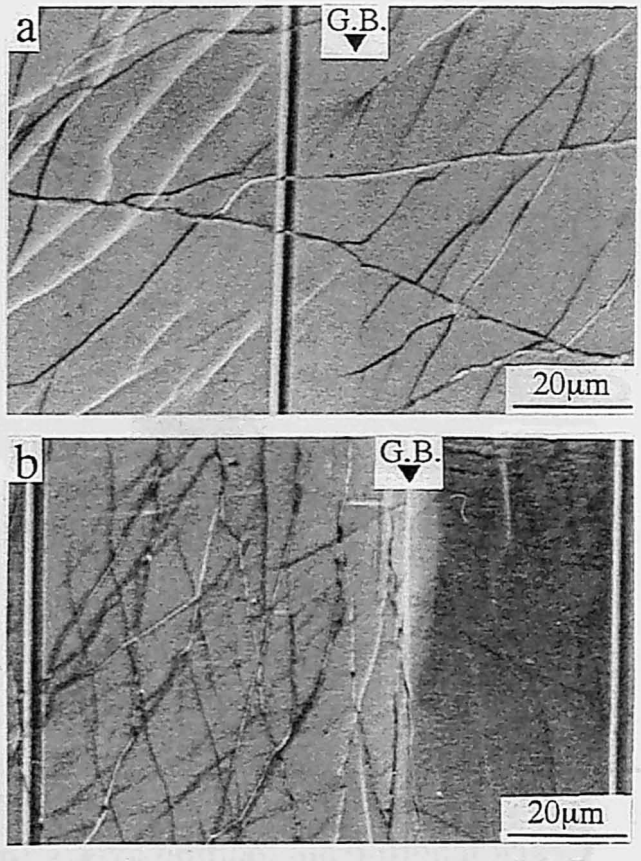

Fig.5-8 Slip lines at the grain boundary in the vicinity of the primary crack on (a) Bicrystal C and (b) Bicrystal D. A fiducial line can be seen in the figure from top to bottom.

slip band and subsequent separation of the slip band [21]. It is probable that the primary dislocations emitted from the propagating crack in Grain 1 could readily pass the GB, resulting in the formation of the slip band which is continuous between two grains. This slip band formation across the GB is supported by Fig.5-8a. The absence of the GB influence on the crack growth rate in Bicrystal C is attributable to the slip band formation which would be the preferential path of the intragranular cracking. On the other hand, because the operative dislocations can not pass through the GB, no continuous slip bands across the GB are produced. At such an incompatible GB, the fatigue crack propagation is retarded probably until another slip band is developed sufficiently. The present results strongly support that the GBs contribute to the resistance to fatigue crack growth.

5.4. CONCLUSIONS

From the investigation on the path of the fatigue crack at the GB of the bicrystals CT specimen (Bicrystals A and B), following conclusions could be obtained.

1. A bicrystal specimen in which both grains are oriented to <1 4 4> tensile axis showed that the fatigue crack encountering the GB began to propagate along that GB. On the other hand, when one of the constituent grains had a <1 1 1> tensile axis, the fatigue crack passed through the GB.

2. Such a different crack behavior at the GB can be understood in terms of the geometrical relationship between the GB and preferential crack growth directions of the constituent grains.

From the investigation on the crack growth retardation at the GB of the bicrystals CT specimens (Bicrystals C and D) having the GBs parallel to the tensile axis, following conclusions could be obtained.

3. At the GB where the operative slip vectors of the adjoining grains were common, no significant reduction in the crack growth rate was observed. On the other hand, the retardation of fatigue crack growth was observed locally at the GB where the operative slip vectors were not common between the adjoining grains.

4. It was experimentally recognized that the crack retardation at the GB is associated closely with the slip continuity between adjoining grains. The present results strongly support that the GBs contribute to the resistance to fatigue crack growth.

References

1. L.C.Lim, *Acta Metall.*, **35** (1987), 1653.
2. A.Vinogradov, S.Hashimoto and S.Miura, *Scripta Metall.*, **32** (1995), 427.
3. A.Vinogradov, S.Hashimoto and S.Miura, *Scripta Metall.*, **34** (1996), 775.
4. R.Lombard, H.Vehoff and P.Neumann, *Z.Metallkd*, **83** (1992), 463.
5. A.Vinogradov, T.Mimaki and S.Hashimoto, *Meter.Sci.Eng.*, **A216** (1996), 30.
6. T.Watanabe, *Mater.Sci.Eng.*, **A176** (1994), 39.
7. Z.S.Basinski and S.J.Basinski, *Scripta Metall.*, **18**(1984), 851.
8. A.Hunsch and P.Neumann, *Acta Metall.*, **34**(1986), 207.
9. Bao-Tong Ma and C.Laird, *Acta Metall.*, **37**(1989), 325.
10. P.Neumann, *Acta Metall.*, **22**(1974), 1155.
11. Qi Chen and H.W.Liu: *Scripta Metall.*, **28**(1993), 849.
12. C.Li and T.Bretheau, *Acta Metall.*, **37**(1989), 2645.
13. C.Li, *Metall.Trans*. A, **23A**(1992), 3293.
14. L.C.Lim and R.Raj, *Acta Metall.*, **33**(1985), 1577.
15. D.Wolf, *Phil.Mag.A*, **62**(1990), 447.
16. T.Watanabe, K.Arai, K.Yoshimi and H.Oikawa, *Phil.Mag.Lett.*, **59**(1989), 47.
17. T.Magnin and F.Moret, *Scripta Metall.*, **16**(1982), 1225.
18. M.Anglada, M.Nasarre and J.A.Planell, *Scripta Metall.*, **21** (1987), 931.
19. D.G. Brandon, *Acta Metall.*, **14** (1966), 1479.
20. H.Mori, R. Itoh, T.Kozakai and T.Miyazaki, *Scripta Metall.*, **14** (1980), 929.
21. K.Tanaka and T.Mura, *Acta Metall.*, **32**(1984), 1741.

Chapter VI

Interfacial Fatigue Cracking along Mechanical Twin Boundaries

6.1. INTRODUCTION

It is well known that b.c.c. metals and alloys can be deformed by mechanical twinning. On ferritic stainless steels, such a mechanical twinning occurs frequently even at room temperature [1-4]. In view of the coincidence-site lattice model, the grain boundary (GB) between the twinned region and matrix is regarded as Σ3(112) twin boundary, where the Miller index (112) indicates the boundary plane. Thus, the generated twin bands are interposed between two Σ3(112) twin boundaries. The GB structure of the Σ3(112) twin boundary has been calculated to be stable and have lower GB energy than the other large-angle GBs [5]. The monotonic tensile tests on molybdenum bicrystals have shown that the Σ3(112) twin boundary possesses higher fracture resistance against the normal stress to the boundary plane, clearly indicating good correlation of fracture strength with the GB energy. [6, 7]

The Σ3(111) coherent twin boundary is one of this kind of special boundaries for f.c.c. metals and alloys. It is also well known that annealing twin boundaries in f.c.c. metals and alloys possess stable boundary structures and low interfacial energies. Investigations of the intergranular corrosion in Al [8] and in Cu and Cu-9at.%Al [9], on stress-corrosion cracking in Cu-9at.%Al [10], on liquid-metal embrittlement [11,12] and on grain boundary sliding [13], revealed that the twin boundaries showed much higher resistance than the other high-angle grain boundaries against such chemically assisted phenomena in which the materials undergo no or a small deformation.

In contrast with these findings, Boettner et al [14] reported that the cracks were formed preferentially along annealing twin boundaries in fatigued copper polycrystals. This kind of preferred fatigue cracking at the Σ3(111) twin boundary has been found in copper and α-brass [15], austenitic stainless steel [16] and α-brass [17].

The twin boundary planes, Σ3(111), in f.c.c. structures can be

parallel to operative slip planes by plastic deformation. Heinz and Neumann [16] studied twin boundary cracking in austenitic stainless-steel polycrystals and proposed that the elastic anisotropy of crystals can induce an additional shear stress near the twin boundaries, and that the plastic strain due to the stress could be localized at the twin boundaries near the fatigue limit. The validity of their model was examined by Waltersdorf and Vehoff [18] on Fe-Si bicrystals with slip planes parallel to the boundary planes. Peralta et al [19] also reported that the twin boundaries can act as stress concentrators due to elastic strain incompatibility. Llanes and Laird [20] have shown using transmission electron microscopy that regions adjacent to the twins are preferred sites for the earlier formation of persistent slip bands in polycrystalline copper.

On the basis of the crack initiation at annealing twin boundaries in f.c.c. metals, a fatigue crack in the b.c.c. metal is possible to be initiated preferentially at the mentioned mechanical twin boundary in spite of the fact that the $\Sigma 3(112)$ boundary possesses the high fracture resistance. This is because the (112) twinning plane can be an operative slip plane and many b.c.c. crystals have the elastic anisotropy as well as the f.c.c. crytals.

In the present study, fatigue experiments were carried out on the twinned specimen with a sheet shape and the CT specimens. Fatigue crack initiation at twin boundaries and propagation along these throughout the specimen thickness are investigated.

6.2. EXPERIMENTAL PROCEDURE

The single crystals used in this study were grown by the Bridgman method from a Fe-30mass%Cr alloy. Two kinds of specimens were cut from the single crystals. One is for the investigation of crack initiation at the twin boundaries, having a gauge shape of square cross section of 1.5x1.5 mm^2 and length of 4 mm (sheet specimen). The other kind is a compact tension (CT) specimen (20×20×1.5 mm^3) for monitoring crack propagation along the twin boundaries. We prepared two CT specimens (CT#1 and CT#2). After the cutting by spark erosion, the specimens were annealed at 1100°C in vacuum and then quenched in water.

A schematic illustration and stereographic projection of the sheet specimen is shown in Fig.6-1. The [111] primary slip vector of the sheet specimen was inclined to the tensile axis at 45°, lying in the plane that contains the tensile and surface axes. The plane of maximum resolved shear stress was $(1\ 1\ \bar{2})$. The Schmid factor of $[1\ 1\ 1](1\ 1\ \bar{2})$ system was almost 0.5. Compressive load applied to the sheet specimen can induce the mechanical twinning of $[1\ 1\ 1](1\ 1\ \bar{2})$ system. In order to introduce $(1\ 1\ \bar{2})$ twin boundaries without little plastic deformation, the sheet specimen was compressed in liquid nitrogen until mechanical twinning occurred. Thereafter, surface of the sheet specimen was polished for elimination of the surface steps due to the mechanical twinning. Symmetrical tension-compression test was performed under load control on the sheet specimen containing the twin boundaries. Stress amplitude was raised stepwise at a rate of approximate 10MPa/5000cycle until fatigue crack initiation was detected.

A schematic illustration and stereographic projection of the sheet specimen is shown in Fig.6-1. CT#1 and CT#2 had a loading axis close to $[\bar{3}\ 3\ 1]$ and a surface plane of (1 1 0). CT#1 was cyclically loaded at a load ratio ($=P_{min}/P_{max}$) of 0.1. CT#2 was cyclically deformed under a constant displacement amplitude at the loading point.

All of the fatigue tests were carried out in air at room temperature in a servo hydraulic machine. During fatigue experiments, the surface of the specimens were observed using an optical microscope with nomarski interferometer.

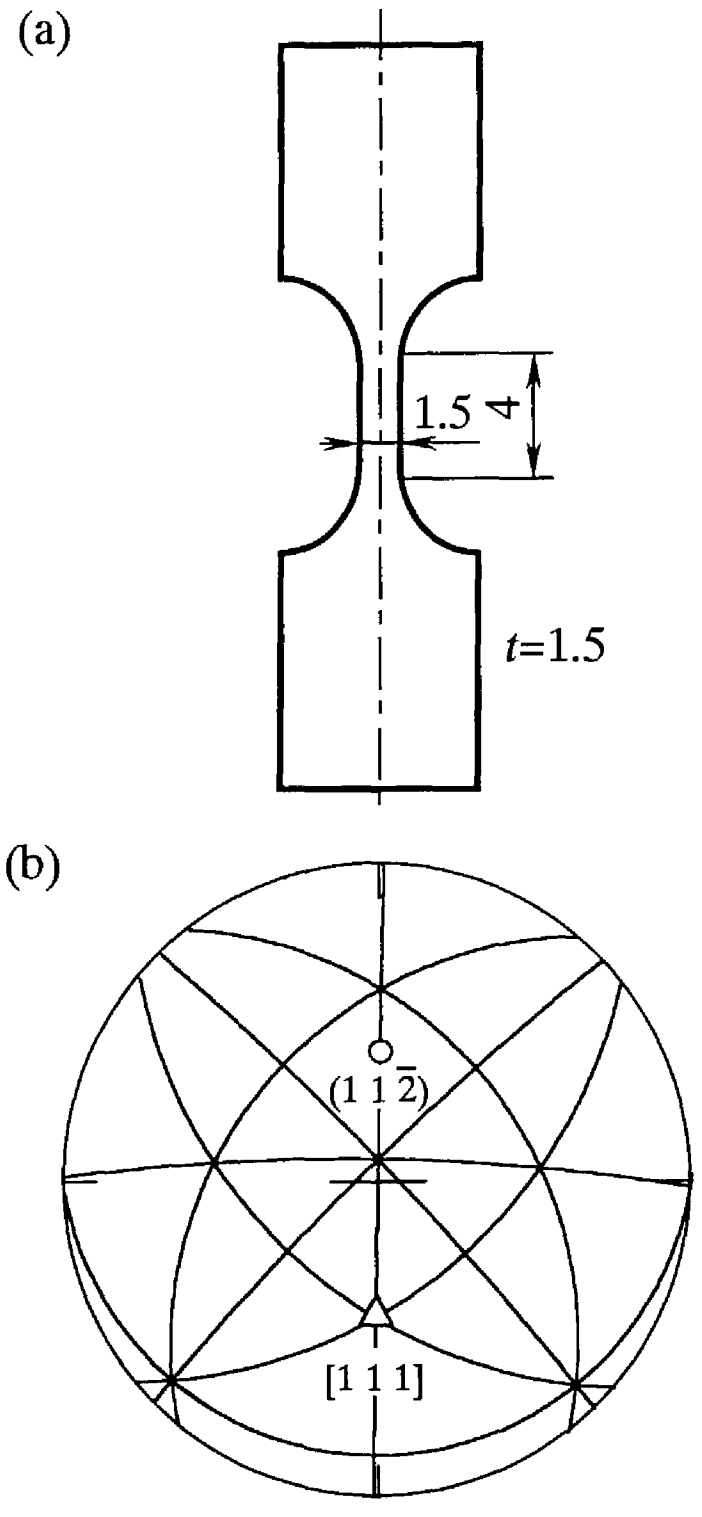

Fig.6-1 Schematic illustration of the single crystal sheet specimen and the stereographic projection of crystallographic orientation.

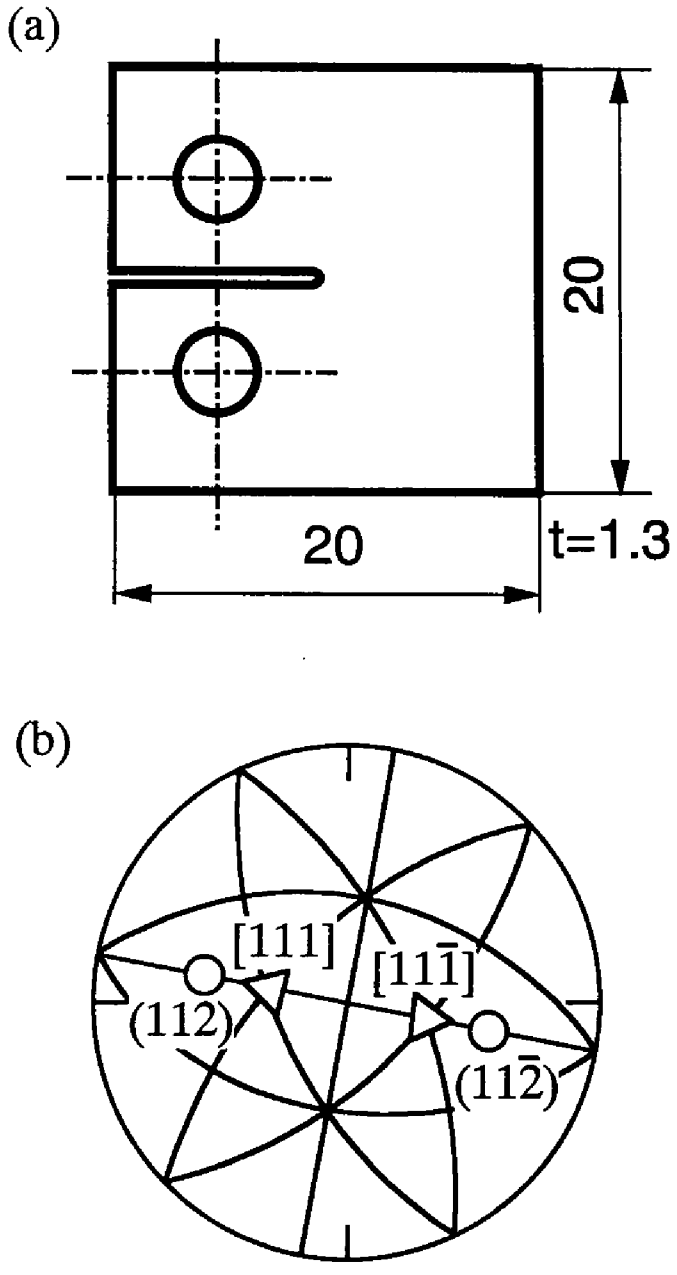

Fig.6-2 Schematic illustration of the single crystal CT specimen and stereographic projection of the crystallographic orientaion.

6.3 RESULTS AND DISCUSSION

6.3.1. *Slip localization and Fatigue Crack Initiation at Mechanical Twin Boundaries*

The sheet specimen was monotonically compressed in liquid nitrogen at a cross head speed of 0.1mm/min. Mechanical twinning occurred at 537MPa with a sudden reduction in compressive stress. From the stress-strain curve of the compressive test, little slip deformation was noticeable. The specimen was unloaded after the occurrence of the mechanical twinning. Figure 6-3a shows a part of the specimen surface with the mechanical twins generated. Thick black traces normal to the tensile axis corresponded to the mechanical twins since these bands possessed a certain thickness. However, it was difficult to know whether thin traces corresponded to the mechanical twins or slip steps. The surface observation after the compressive test indicated that the number of the $(1\ 1\ \bar{2})$ twin bands was at least ten.

In the tensile-compressive fatigue test on the sheet specimen containing the twin bands, slip lines appeared on the specimen surface first at a stress amplitude of 70MPa. Most of the slip lines were operated along $(1\ 1\ \bar{2})$ plane. Further increasing in stress amplitude intensified the development of the slip lines. When the stress amplitude was raised to 170MPa, the fatigue crack initiation was detected from in-situ surface observation with an optical microscope. This value of stress amplitude was lower than the yield stress (≒200MPa) of the single crystal having the same orientation. Figure 6-3b shows the aspect of the slip lines after the fatigue test, being the same area of Fig.6-3a. Figures 6-3a and 6-3b clearly indicate that the location where the slip deformation was activated was coincident exactly to the twin bands. No any intense slip lines could be found in the region distant from the twin bands. Results of SEM observation after the tensile-compressive test are shown in Fig.6-4. Figure 6-4a clearly shows the

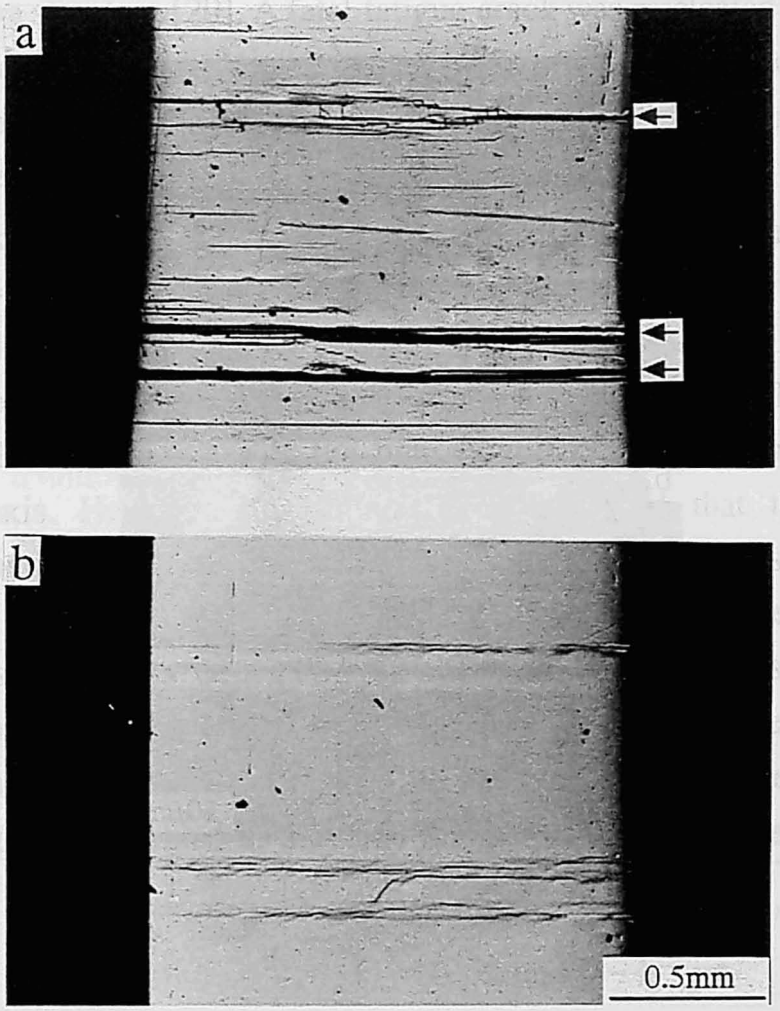

Fig.6-3 Optical photographs showing the surface aspects of the sheet specimen. Arrows indicate the twin bands.

(a) After the occurence of mechanical twinning in the monotonic compression test.

(b) After the fatigue test

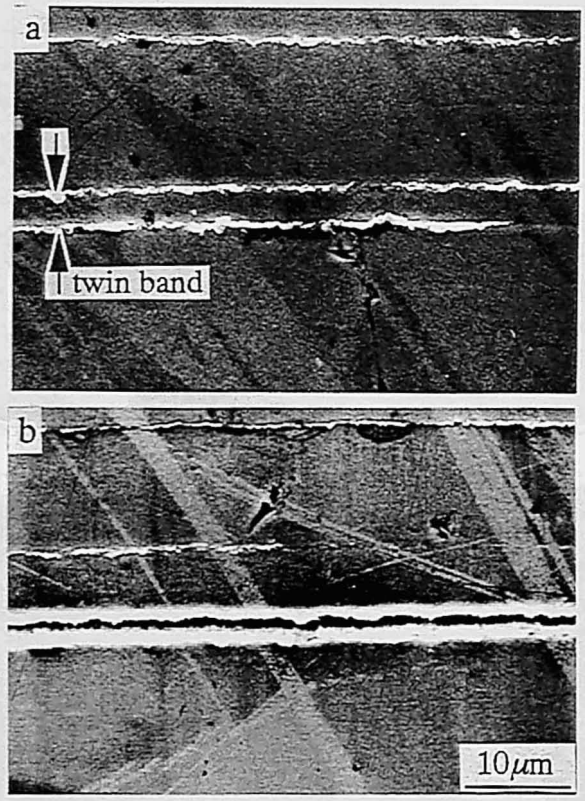

Fig.6-4 SEM photographs showing (a) PSBs localized at the twin boundaries and (b) interfacial cracking along the twin boundary in the sheet specimen.

formations of the slip bands locally at the twin boundaries. The developed slip bands seemed to be the PSBs because the visible extrusions at the twin boundaries are peculiar to the PSBs. Such a PSB just adjacent to a twin boundary has actually been seen using TEM in fatigued copper polycrystal, being detected as the ladder-like dislocation structure [20]. A fatal fatigue crack was nucleated favorably at such a damaged twin boundary as shown in Fig.6-4b. It is concluded that the mechanical twin boundary is one of the preferred nucleation site in the ferritic stainless steel under fatigue deformation.

Crack formation at every other twin boundary have been reported in Cu [14] and austenitic stainless-steel polycrystals [16]. Stacks of the lamellar twins are composed of alternate crystals with the same orientations. The twin boundaries included in these stacks can be classified into two types if the twin boundaries are inclined to the tensile axis. Heinz and Neumann [16] proposed that the elastic anisotropy induces additional inhomogeneous shear stresses acting on the twin boundaries near the surface, in and out of phase with the applied shear stress depending on the twin boundaries, so that the additional in-phase shear stress causes crack formation at every other twin boundary. The present cracking features at a distance from the notch may be explained in the same manner as in their model.

6.3.2. *Fatigue Crack Propagation along Mechanical Twin Boundaries*

In the fatigue experiment on CT#1, the intragranular fatigue cracks were nucleated at the notch tip and propagated along slip planes. After short intragranular propagation, mechanical twins were generated ahead of the crack tip. Their twinning planes were inclined to the loading axis. The fatigue crack encountered the mechanical twin during further cycling. When the crack was intersecting the mechanical twin, the mode of crack propagation was frequently changed from the intragranular cracking to the twin boundary cracking. Thereafter, the twin boundary cracks reverted to intragranular cracking again.

During the intragranular crack propagation occurred, another mechanical twin was newly generated ahead of the crack tip. A unit of fatigue cracking process consisted of the above intragranular cracking, the occurrence of mechanical twinning and the twin boundary cracking. The cracking process was repeated during the fatigue test. Finally, CT#1 was fractured by cleavage along the (001) plane. Figures 6-5 and 6-6 shows the fractographic feature of the fatigue cracking along the twin boundaries. Three flat parts of fracture surfaces of the twin boundary cracking are notable. The twin boundary cracking in CT#1 penetrated almost throughout the specimen thickness. Specimen B2 similarly showed the fatigue crack growth along the twin boundaries. However, no mechanical twinning followed after the first simultaneous generation of several mechanical twins. This result strongly suggested that the inclined twin boundary to the loading axis were very susceptible to fatigue deformation and could become a cracking path.

A fatigue crack in CT#2 was initiated at the notch and propagated as well as CT#1. The simultaneous occurrence of eleven mechanical twins was observed when the crack attained a length of about 2 mm, measured from the notch. The formation of the mechanical twins was limited to the front of the crack tip at distances from 0.1 to 1.9mm. The widths of the twin bands were estimated to be from 2 to 8 μm. However, no any mechanical twins were generated during the

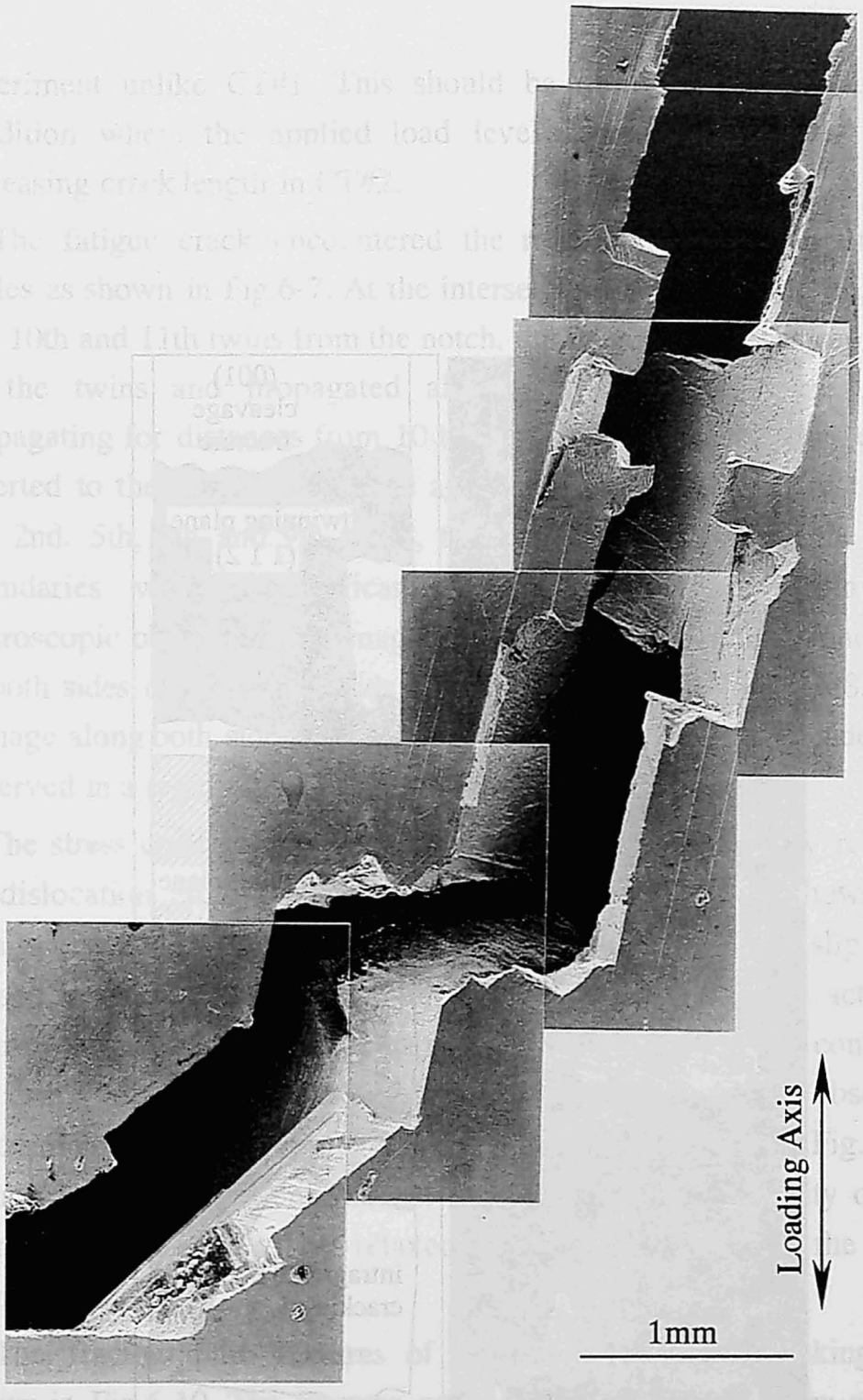

Fig.6-5 A primary fatigue crack observed from the surface direction in CT #1.

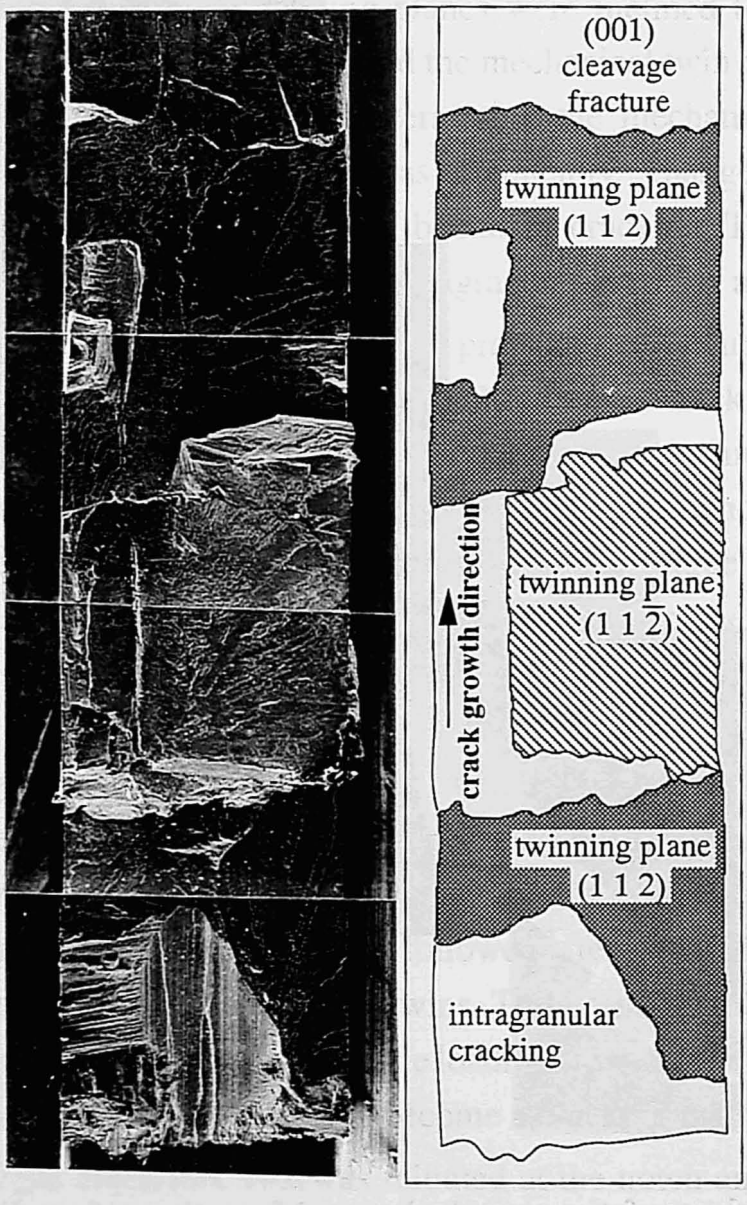

Fig.6-6 Fracture surface of the twin boundary cracking observed in CT#1.

experiment unlike CT#1. This should be due to the experimental condition where the applied load level decreased gradually with increasing crack length in CT#2.

The fatigue crack encountered the mechanical twins in further cycles as shown in Fig.6-7. At the intersections with the 3rd, 4th, 6th, 8th, 10th and 11th twins from the notch, the fatigue crack was captured by the twins and propagated along the twin boundaries. After propagating for distances from 10 to 500μm, the twin boundary crack reverted to the intragranular one again. At the intersections with the 1st, 2nd, 5th, 7th and 9th twins, the crack passed through the twin boundaries without significant interfacial cracking. From the microscopic observation, damaged regions and cracks along one side or both sides of the twin bands were found as shown in Fig.6-8. The damage along both sides was predominant and that along one side was observed in a region distant from the main crack.

The stress concentration at a crack tip in metals is usually relaxed by dislocation emissions from the crack tip. Figure 6-9 shows the details of the crack wakes at the 1st and 11th twins. Many slip lines caused by such dislocation activity near the 1st twin were actually seen in the wake of the crack as shown in Fig.6-9a. On the contrary, the slip localization along the twin boundary was observed predominantly in the vicinities of the 11th twin as shown in Fig.6-9b. Hence, the stress concentration at the crack tip in the vicinity of the twins is considered to be relaxed by slip activity along the twin boundaries.

The fractographic features of the twin boundary cracking are shown in Fig.6-10. The fracture surfaces of the twin boundary cracks were smoother than those of the intragranular ones. The cracks along twin boundaries were limited to be near the specimen surface unlike CT#2. As can be seen in Fig.6-10, the depths of the crack penetrations along the twin boundaries into the inner sites decreased with increasing distance from the notch at the specimen surface. The twin boundary cracks at 3rd, 4th and 11th twin bands had the penetrating depths of

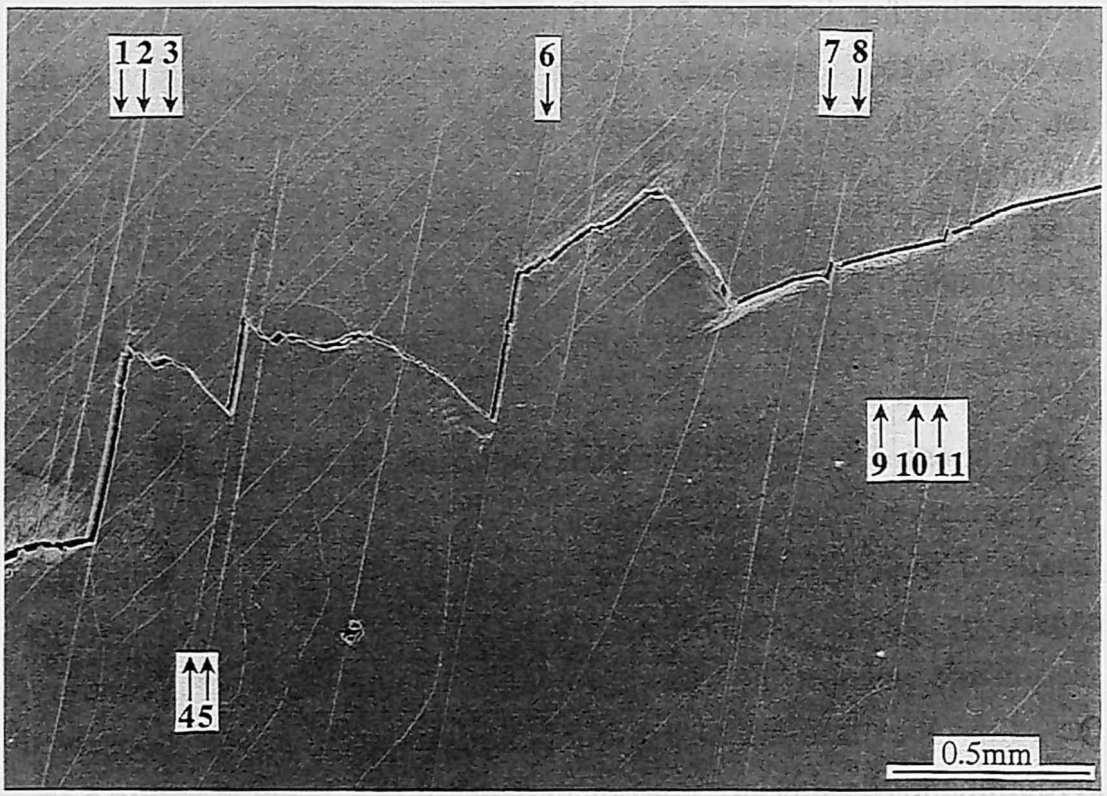

Fig.6-7 SEM photograph showing fatigue cracking in CT#2, where the numbers 1 to 11 show the twin bands.

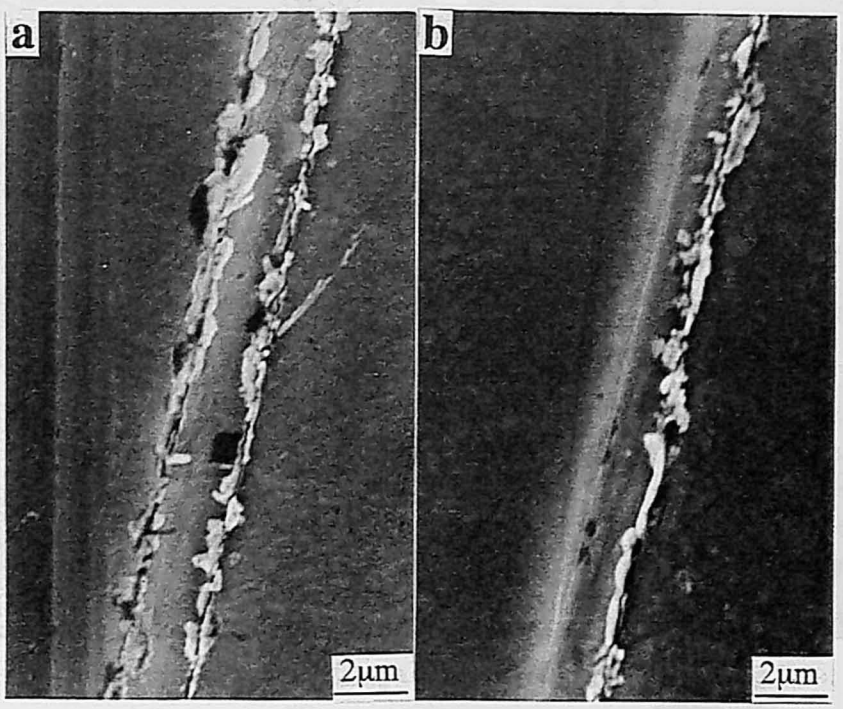

Fig.6-8 Twin bands observed at the surface of CT#2, having the slip band along (a) both and (b) one side of the twin boudary.

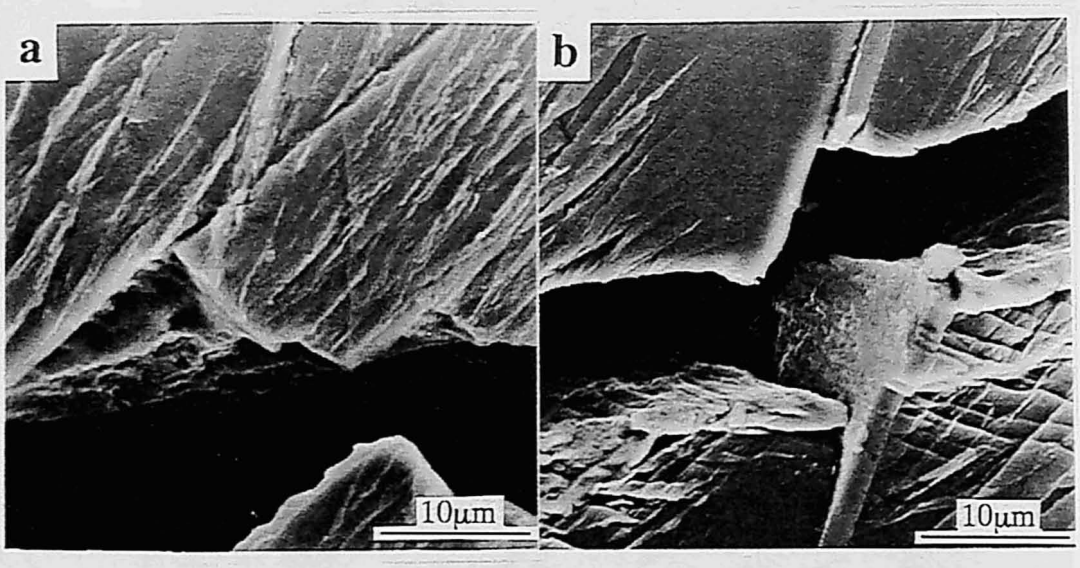

Fig.6-9 SEM photograph showing the intersection of the fatigue crack at (a) the irst twin band and (b) the eleventh twin band. At eleventh twin band, the slip along the twin boundary is predominant and the resultant twin boundary cracking is significant.

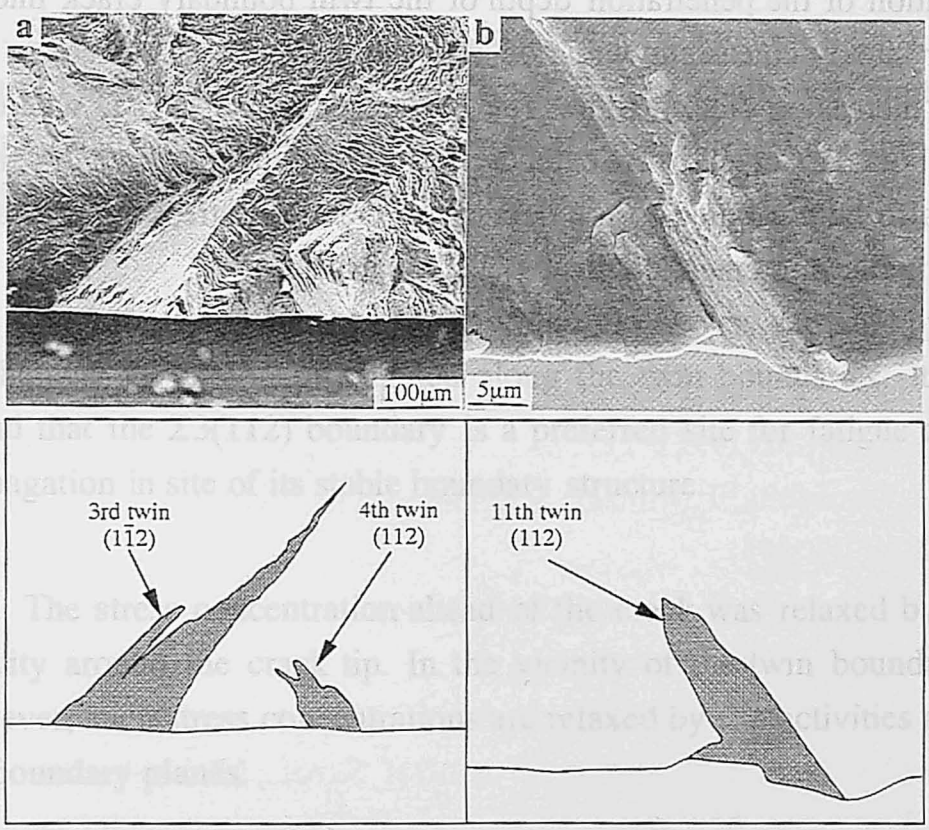

Fig.6-10 Fracture surface of the twin boundary cracking (a) at the third and fourth twin bands and (b) at the eleventh twin band. The magnification of (b) is higher than that of (a) by a factor of 15.

about 300, 85 and 30 μm, respectively. On a crack growth test under a constant displacement amplitude at a loading point, a stress concentration at a crack tip is commonly decreased with increasing crack length. The extent of an incompatible stress and the resultant damage along the twin boundaries at a specimen surface should be proportional to the extent of the stresses in the vicinity of a twin. The variation of the penetration depth of the twin boundary crack into the inner site is consistent with the decrease of the energy release rate with increasing crack length. The discrepancy from CT#1, where the twin boundary cracks were extended throughout the specimen thickness, can also be attributed to the decreasing crack tip stress concentration with increasing crack length.

6.4 CONCLUSIONS

The results of this investigation on fatigue crack propagation in a ferritic stainless steel crystal including mechanical twins are summarized as follows.

1. Slip deformation in the specimen with a square cross section occurred preferentially at the twin bands. Fatigue cracks were initiated at the mechanical twin boundaries where the slip deformation was localized.

2. The fatigue crack propagating within grains was captured by the mechanical twins and propagated along the twin boundaries. It was found that the $\Sigma 3(112)$ boundary is a preferred site for fatigue crack propagation in site of its stable boundary structure.

3. The stress concentration ahead of the crack was relaxed by slip activity around the crack tip. In the vicinity of the twin boundaries, however, such stress concentrations are relaxed by slip activities along the boundary planes.

References

1. T.Magnin and F.Moret, *Scripta Metall.*, **16** (1982), 1225.
2. T.Magnin, L.Coudreuse and A.Fourdeux, *Mater.Sci.Eng.*, **63** (1984), L5.
3. M.Anglada, M.Nasarre and J.A.Planell, *Scripta Metall.*, **21**(1987), 931.
4. I.M.Wolff and A.Ball, *Acta Metal.Mater.*, **39**(1991), 2771.
5. D.Wolf, *Phil.Mag.A*, **62**(1990), 447.
6. J.B.Brosse, R.Fillit and M.Biscondi, *Scripta Metall.*, **15**(1981), 619.
7. H.Kurishita, A.Ohishi, H.Kubo and H.Yoshinaga, *Trans.JIM*, **26**(1985), 345.
8. G.Hasson, J.-Y.Boos, I.Herbeuval, M.Biscondi and C.Goux, *Surf.Sci.*, **31**(1972), 115.
9. M.Yamashita, T.Mimaki, S.Hashimoto and S.Miura, *Phil.Mag.A*, **63**(1991), 695.
10. M.Yamashita, T.Mimaki, S.Hashimoto and S.Miura, *Phil.Mag.A*, **63**(1991), 707.
11. J.A.Kargol and D.L.Albright, *Metall.Trans.A*, **8**(1977), 27.
12. A.Ohtsuki and M.Mizuno, *Trans.JIM, Suppl.*, **27**(1986), 789.
13. T.Watanabe, M.Yamada, S.Shima and S.Karashima, *Phil.Mag.A*, **40**(1979), 667.
14. R.C.Boettner, A.J.McEvily, Jr. and Y.C.Liu, *Phil.Mag.*, **10**(1964), 95.
15. A.W.Thompson, *Acta Metall.*, **20**(1972), 1085.
16. A.Heinz and P.Neumann, *Acta Metal.Mater.*, **38**(1990), 1933.
17. P.Gopalan and H.Margolin, *Mater.Sci.Eng.*, **A142**(1991), 11.
18. J.Waltersdorf and H.Vehoff, *Z.Metallkde.*, **81** (1990), 702.
19. P.Peralta, L.Llanes, J.Bassani, and C.Laird, *Phil.Mag.A*, **70** (1994), 219.
20. L.Llane and C.Laird, *Mater.Sci.Eng.*, **A157**(1992), 21.

Chapter VII

Summary

The purpose of the present thesis is to investigate the fundamental aspects concerning fatigue of the ferritic stainless steel. This material containing the b.c.c. lattice is expected to show wide variety of deformation and fracture property from the accumulated knowledge about the deformed b.c.c. metals and alloys. In order to simplify the deformation and fracture behavior of the material, the author prepared the single and bicrystals using the Bridgman method. In the series of the monotonic and fatigue experiments reported in the present thesis, the following summaries could be obtained.

The orientation dependence of both tensile deformation (sheet specimen) and fatigue crack propagation (CT specimen) in the single crystals where the loading axes were oriented from [0 0 1] to [1 $\bar{1}$ 0] via [1 $\bar{1}$ 1] was examined. Under the monotonic tensile deformation, a specimen with [1 $\bar{1}$ 1] tensile axis possessed the highest yield stress and ultimate tensile strength as predicted by the Schmid's law and by multiple slip orientation. On the other hand, the resistance to fatigue crack propagation increased as the loading axis was oriented to [1 $\bar{1}$ 0] direction, unlike the tensile deformation. The morphology of the fatigue cracks on the surfaces were classified into two kinds, which are associated with the geometrical relationship between a glide direction of responsible slip and broad surface of the specimen. Predominant cracking kind in a fatigued specimen varied depending on the loading axes. It is suggested that the orientation dependence of crack growth resistance can be understood by the variation in the predominant cracking kind

The sheet single crystals having a {1 1 2} primary slip plane were cyclically deformed under plastic strain control. The changes in cyclic stress–strain response —— which can reflect the internal dislocation process —— were investigated at several amplitude: in addition to cyclic hardening behavior, the Bauschinger energy parameter β_E and in the stress amplitude asymmetry between tensile and compressive straining, which is often observed in b.c.c. single crystals, were measured in order to obtain informations about the cyclic

deformation state. Operative dislocation mechanism and its dependence on strain amplitude were discussed by comparing the individual changes in the stress amplitude, the Bauschinger energy parameter and the stress asymmetry. The change in the Bauschinger energy parameter β_E during the experiments depended strongly on the plastic strain amplitude, although the shapes of the cyclic hardening curves were almost the same. The β_E value continued to increase until a cumulative plastic strain of at $\varepsilon_{pl} = 2 \times 10^{-4}$ and 5×10^{-4}. On the other hand, the specimen cycled at $\varepsilon_{pl} = 1.2 \times 10^{-3}$ showed a local maximum of the β_E value; this phenomenon is similar to that observed in a copper single crystal containing PSBs. The developed extrusions and the fatigue crack initiation along these were found in the specimen at $\varepsilon_{pl} = 1.2 \times 10^{-3}$. Since the β_E maximum probably coincides with the beginning of the PSB nucleation, the prediction of fatigue crack initiation is expected to be practicable by measuring the β_E value in the present material.

Significant change in cyclic stress-strain response occurring at strain burst have been investigated also by measuring the stress amplitude, the Bauschinger energy parameter, stress asymmetry and instability of stress amplitude. Under a plastic strain amplitude of 2×10^{-4}, occurrences of two strain bursts were recognized as sudden huge reductions in stress amplitude. Such huge bursts were accompanied by sudden increase in the Bauschinger energy parameter and decrease in stress asymmetry that is peculiar to the b.c.c. crystals with the {1 1 2} primary slip plane. According to the obtained changes in the cyclic response the changes in the activities of the screw and edge dislocations could be drawn. This dislocation mechanism can be understood by the dissociation of dislocation dipoles, which has been proposed by Neumann.

Fatigue crack propagation tests have been carried out in bicrystal CT specimens. A geometrical criterion for the occurrence of intergranular crack propagation was investigated. A bicrystal having a symmetrical tilt boundary (θ=22°) was prepared by a diffusion bonding. Two kinds of the CT specimens cut from the same bicrystal differs in

tensile orientations of constituent grains. A bicrystal specimen in which both grains are oriented to < 1 4 4 > tensile axis showed that the fatigue crack encountering the GB began to propagate along that GB. On the other hand, when one of the constituent grains had a < 1 1 1 > tensile axis, the fatigue crack passed through the GB. This difference in the crack behavior around the GB can be understood in terms of the geometrical relationship between the GB and preferential crack growth directions of the constituent grains. This results suggest that the GB structure is not always a decisive factor determining whether a fatigue crack propagates along a GB or not.

In order to understand the contribution of grain boundary to crack growth resistance, retardations of intragranular fatigue crack growth at Σ3(112) twin boundaries have been investigated using the bicrystal CT specimens which have a grain boundary parallel to loading axis. Two kinds of the specimens that differed in a loading axis were prepared from the same bicrystal. In the specimen which possessed a common primary slip vector between constituent crystals, no any influences of grain boundary on crack growth rate was found. On the other hand, a pronounced retardation effect of crack growth was revealed in the specimen having none of common operative slip vectors. These results were consistent with the surface observation that slip lines were continuously transmitted through the grain boundary in the specimen having the common slip vector, since the crack growth was due to shear decohesion of slip plane. It is suggested that the retardation of crack growth is associated closely with the slip continuity between neighboring grains.

The slip localization at mechanical twin boundaries and the resultant interfacial fatigue cracking along these boundaries were investigated. Fatigue tests were performed on the twinned specimen with a square cross section to monitor crack initiation and on the compact tension specimens for crack propagation. The fatigue test for the crack initiation showed that slips were operated preferentially at twin bands and fatigue cracks were initiated at the twin boundaries. The fatigue crack in the

compact tension specimen frequently propagated along the twin boundaries throughout the specimen thickness. These results strongly suggest that the Σ3(112) twin boundary ——which possesses a stable interfacial structure ——is very weak against the fatigue deformation. It can be proposed that we should avoid to use the materials containing the deformation twins which can be induced at low-temperature deformation and/or at high strain-rate deformation.

List of Publications Concerning This Thesis

Chapter II

1. Y. Kaneko, S. Hashimoto, T. Mimaki and S. Miura, "Dependence of Crystallographic Orientation on Fatigue Crack Growth of Fe-30%Cr Alloy Single Crystals", *Strength of Materials*, (1994), pp.513-516.

Chapter III

2. Y. Kaneko, T. Mimaki and S. Hashimoto, "Cyclic Response of Fe-30%Cr Alloy Single Crystals Having (112) Primary Slip Plane", *Acta Materialia*, in printing.

Chapter IV

3. Y. Kaneko, T. Mimaki and S. Hashimoto, "Cyclic Response and Burst Phenomena in Cyclically Deformed Single Crystals of a Ferritic Stainless Steel", *Materials Science & Engineering*, **A245** (1998) , pp.233-241.

Chapter V

4. Y. Kaneko and S. Hashimoto, "Relationship between Crack Propagation and Slip Continuity at the Σ3(112) Twin Boundary in Fe-30%Cr Alloy", *J.Japan Inst.Metals*, **60** (1996), pp.345-346.

5. S. Hashimoto and Y. Kaneko, "A Simple Criterion for Occurrence of Intergranular Fatigue Crack Propagation in a Ferritic Stainless Steel", *Materials Science Forum*, in printing.

Chapter VI

6. Y. Kaneko, S. Hashimoto and S. Miura, "Cracking along Mechanical Twin Boundaries during Fatigue Deformation in Ferritic Stainless Steel Crystal", *Philosophical Magazine Letters*, **72** (1995), pp.297-301.

7. S. Hashimoto and Y. Kaneko, "Interfacial Fatigue Cracking along Mechanical Twin Boundaries in Fe-30%Cr Alloy", *Interface Science and Materials Interconnection, Proceeding of JIMIS-8* (1996), pp.471-474.

Acknowledgments

The author would like to express his sincere gratitude to Associate Professor Satoshi Hashimoto, Department of Engineering Physics and Mechanics, Kyoto University, for his excellent guidances throughout the doctor's degree program.

He would like to express his grateful appreciation to Professor Ryuichi Ohtani and Professor Shojiro Ochiai, Department of Engineering Physics and Mechanics, Kyoto University, for their fruitful suggestions and discussion.

He wishes to thank to Professor Toshinobu Shibata, Department of Mechanical Engineering, Kyoto University and Professor Toshiro Makino, Department of Engineering Physics and Mechanics, Kyoto University, for their interests and encouragement.

He gratefully thanks to Professor Emeritus Sei Miura, Kyoto University (now at Kumamoto Institute of Technology), Professor Takuro Mimaki of Doshisha University and Professor Kazuo Kitagawa of Kanazawa University for their supports and encouragement throughout this work.

Many thanks are due to Associate Professor Susumu Onaka of Tokyo Institute of Technology, Associate Professor Alexei Vinogradov of Kanazawa University and Dr. Hiroyuki Kato of Kyoto University, for their fruitful suggestions and discussion concerning this work.

Mr. Koji Amano and Mr. Tsuyoshi Kitaoka (Doshisha University), Mrs. Yoko Morita-Inoue and Mr. Hideaki Ikehata (Kyoto University) are especially acknowledged for helping parts of the experiments.

Finally, the author sincerely thanks to my parents for their valuable supports to accomplish this research.